Formin-nucleated F-actin cables associate with mitotic spindles in the intact epithelium of *Xenopus laevis*

By

Angela M. Kita

A dissertation submitted in partial fulfillment of

the requirements for the degree of

Doctor of Philosophy

(Cellular & Molecular Biology)

at the

UNIVERSITY OF WISCONSIN-MADISON

2014

Date of final oral examination: August 22, 2014

The dissertation is approved by the following members of the Final Oral Committee:

William M. Bement, Professor, Zoology
Erik Dent, Associate Professor, Neuroscience
Timothy Gomez, Professor, Neuroscience
Yevgenya Grinblat, Associate Professor, Zoology
Mary Halloran, Professor, Zoology

Table of Contents

Acknowledgements

I have relied on many people through my graduate career, for advice and guidance, for a needed push, and for a chance to unwind. As an advisor, Bill Bement has managed to fill all those roles. He was always around to answer, or ask, the necessary questions, and helped keep me on the path even when nothing seemed to be going right. I am also (mostly!) thankful for his humor, which kept me entertained, and for his lab tradition of Spirit Week. Thanks, Bill.

I would also like to thank my fellow lab members, past and present. Brian Burkel helped me get started in the lab and also helped me put out the (small) fire I started on my bench a handful of days into my tenure. Ann Miller was always willing to answer questions and is my science superhero. Thanks to Emily Vaughan for providing music in the lab and a listening ear in our office. I learned a lot from Josh Sandquist and his general goofiness has been missed. Kevin Sonnemann showed me the wonders of statistics and was always available to answer questions when a hand was raised. Thanks to Nick Davenport for the science advice, conversation, and coffee-runs/lab-escapes. Matt Larson has been an excellent partner-in-crime, both in embryo endeavors and hole-punch escapades. Alison “1L” Moe is a wonderful benchmate and I’ve enjoyed our conversations, science-related and the not-so-much ones. Adriana Golding has brought renewed enthusiasm to the lab; I look forward to her future successes.

Many friends have moved on, as is the nature of this science business. I would like to especially thank a few whose influence was dear to me: Brian Teague, for being a steadfast friend and for Choral Union; Sarah Hanson for much needed cat-time and Rock; and Stephanie Maiden for her friendship, camaraderie, and support, which she gave equally through happy and challenging times. Thank you to Stacey Kigar, who showed me the excellence of many things, like dance parties (in lab an out), the east side of town, and delicious food. I would also like to thank Celeste Eno and Allison Lynch

for our regular unwinding meetings, and to Allison especially for her proofing and knitting skills. There are many others who have been a part of my life over the last several years, who have made my life better in countless ways. I am grateful for your friendships.

I would like to thank my family, whose support allowed me to reach this point: my mother Sally and sister Caroline, Carol and Darryl, and the families who have adopted me over the years. I would also like to thank my family that has passed. You are missed.

Finally, I would like to thank Will. You have filled my life with color and music, and you brought Penny into our lives. I am thankful for your warmth, your ridiculousness, and all the ways you make me happy, large and small.

Formin-nucleated F-actin cables associate with mitotic spindles in the intact epithelium of *Xenopus laevis*

Angela M. Kita

Under the supervision of Professor William M. Bement

At the University of Wisconsin-Madison

Mitotic spindles are elaborate, captivating structures that segregate condensed chromosomes through the coordinated activity of microtubules and force generating motor proteins. Study of mitotic spindles is therefore centered almost entirely on microtubule-based activities. In contrast, the textbook view of the mitotic actin cytoskeleton has relegated actin filaments to cortical interactions at the cell edges, far from the mitotic spindle. However, it is likely that cytoplasmic arrays of filamentous actin (F-actin) may have been overlooked due in large part to the difficulty of preserving and visualizing fine actin networks. My work characterizes a novel population of actin structures at the mitotic spindle in the intact epithelium of a vertebrate system. In Chapter 1, examination of endogenous F-actin localization revealed actin cables that spanned between spindle poles and the cortex, and reached from poles inward along the spindle body. These structures altered over the course of mitosis and live imaging experiments showed they moved dynamically with the spindle. In Chapter 2, I employed chemical inhibitors of actin polymerization, actin nucleation activity, and microtubule polymerization to determine the function of spindle F-actin. The results of these manipulations indicated regulation of actin at the spindle by one or more formin proteins, which generate new actin filaments, and further pointed to potential actin:microtubule crosstalk activity. In Chapter 3, I conducted a candidate screen of formin localization during mitosis. I identified the *Xenopus* formin, inverted formin 2 like (IFL2) as a regulator of spindle-associated F-actin. Knockdown of IFL2 resulted in a decrease of

actin at the spindle, and overexpression or dominant negative IFL2 expression caused aberrations in both spindle F-actin structures and the spindle. Collectively, these results describe the localization of F-actin to the mitotic spindle and suggest a potential direct role for actin at the spindle during mitosis.

Introduction

Eukaryotic cells take on an array of forms that are important for their specific functions within an organism. For example, neuronal cells form long, slender projections that function in cell-to-cell communication across long distances, while specialized epithelial cells within the auditory system build highly structured stereocilia that allow for sound waves to be transduced into cell signals. Additionally, sheets of cells can participate in coordinated movements that drive morphological shape changes. Individual cells can rapidly change shape, as in axon growth cone movement in response to external cues, or build internal structures to compete specific tasks, as in mitotic spindle formation, which drives the precise segregation of chromosomes prior to cytokinesis. All of these shapes and movements represent changes in one or more cytoskeletal systems, which can be assembled and disassembled by cellular signaling.

Two of the most well characterized cytoskeletal systems are the actin and microtubule cytoskeletons. Actin monomers (G-actin) are polymerized into helical filaments (F-actin), which can function dynamically in processes like cell motility via cell crawling or serve as more stable tracks for cargo transport. Actin filaments can also be built into large arrays used to generate force, as in muscle cell contraction or cell division. Although microtubules participate in similar processes, they are structurally distinct from actin filaments. Microtubule α and β subunits are maintained in a dimer that is assembled into tubes made up of 13-15 linear protofilaments. Unlike actin polymerization, which can occur rapidly, microtubule assembly is slow. Cells employ microtubules to complete tasks such as long-range vesicle transportation (e.g. along neuronal projections) and cell movements via flagellar motor activity.

In addition to performing distinct functions within the cell, the actin and microtubule cytoskeletons are known to coordinate their activities in several processes. During neuronal growth cone guidance, microtubule dynamics drive the forward

movement of the growth cone while the actin cytoskeleton mediates the direction sensing necessary to guide the entire structure.

The textbook model of actin and microtubules during mitosis is that microtubules make up the mitotic spindle while F-actin remains at the cell periphery in the cortex. The majority of mitotic events are thus attributed to microtubules that perform various functions during mitosis: separation of the nascent spindle poles through cortical dynein-based pulling on astral microtubules, bringing the chromosomes into position at the metaphase plate through kinetochore attachments, and separating chromosomes, in part through the activity of kinesin-based sliding of polar microtubules and dynein-based pulling of astral microtubules.

In contrast to the various functions of microtubules within the spindle, F-actin is traditionally thought to act entirely at the cell cortex during mitosis and, subsequently, at cytokinesis. Based on pharmacological studies, cortical F-actin has been shown to be required for spindle anchoring and orientation in several cultured mammalian cells (Thery et al., 2005; Toyoshima & Nishida, 2007). It was also found that myosin-10, an unconventional actin motor that can also bind microtubules (Weber et al., 2004), was required for spindle orientation (Toyoshima & Nishida, 2007). Furthermore, localization of myosin-10 to cell surface projections in cultured mammalian cells (Berg & Cheney, 2002) supported the conclusion of a cortical role for F-actin during mitosis.

Beyond cortical F-actin, several studies have reported subcortical and cytoplasmic arrays of F-actin with some involvement in mitotic processes (reviewed in Sandquist et al., 2011). In both *Xenopus* egg extracts and intact zebrafish, cytoplasmic F-actin cables were reported to form coincident with mitotic entry and disappear at the onset of interphase (Field et al., 2011). In cultured mammalian cells, Mitsushima et al. (2010) found that a bolus of F-actin forms at the onset of metaphase and revolves below the cortex. A separate study found that modulation of external adhesive forces on the

cell cortex regulates spindle orientation. This occurs through changes in the oscillating network of cytoplasmic actin described above, which then interacts dynamically with astral microtubules (Fink et al., 2011). Finally, live imaging of F-actin in *Xenopus* embryonic epithelia revealed dynamic F-actin cables extending between spindle poles and the cortex, which moved in concert with spindle rotations (Woolner et al., 2008).

While reports of subcortical and cytoplasmic F-actin have made traction in our understanding of actin during mitosis, potential roles for F-actin within the mitotic spindle are viewed with skepticism. While it is currently assumed that significant amounts of F-actin are not found within animal cell mitotic spindles, this was not always the case. In the 1970s, several groups reported on the presence of spindle F-actin in several different systems, including cultured mammalian cell lines. Spindle localization was demonstrated through electron microscopy, actin antibodies, and fluorescent heavy meromyosin—the actin filament binding portion of myosin-2 (e.g., Sanger, 1975; Fujiwara and Pollard, 1976; Schloss et al., 1977; Herman and Pollard, 1979). However, the localization of F-actin at the spindle was subsequently challenged as reflecting an artifact of sample preparation and staining with fluorescent phalloidin failed to yield significant spindle labeling (Aubin et al., 1979; Barak et al., 1981).

The motivation for re-examining F-actin localization during mitosis comes from the results of our study of myosin-10. Myosin-10 is an unconventional myosin that can bind both actin filaments and microtubules (Weber et al., 2004) and localizes to the mitotic spindle in *Xenopus* embryonic epithelial cells (Woolner et al., 2008). Furthermore, spindle length defects resulting from myosin-10 knockdown can be rescued by subsequent treatment with an actin-depolymerizing compound. This result indicated a potential functional role for F-actin in controlling spindle length. To determine what functional role F-actin has in the spindle during mitosis, the question of endogenous F-actin localization had to be addressed.

The work conducted for this thesis describes spindle-associated F-actin in an intact epithelium. Specifically, my work demonstrates the existence of F-actin cables and puncta that localize to the mitotic spindle. At the start of mitosis, actin cables and puncta increase at the spindle poles. As mitosis progresses, F-actin cables span the spindle poles and reach between spindle poles and the cortex through to anaphase. These cables appear as unbranched filaments that, like spindle-associated actin puncta, move dynamically at the spindle. In the second chapter, I employ several manipulations that disrupt F-actin to determine its function at the spindle. These results point to a formin-mediated regulation of actin at the spindle. Finally, in the third chapter I identify inverted formin like 2 (IFL2) as a nucleator of spindle F-actin. I show that IFL2 knockdown depletes spindle-associated F-actin, that full-length IFL2 rescues this phenotype, and that misregulation of IFL2 disrupts actin at the spindle.

Chapter 1

Characterization of spindle-associated F-actin

Abstract

Mitotic spindles are microtubule-based structures responsible for partitioning genetic information into each new daughter cell. The roles of microtubules and microtubule-associated proteins in this process have been well characterized, however whether or not F-actin is required—or is even present—within the spindle has long been controversial. In this work I show F-actin is present in mitotic spindles of the early *Xenopus laevis* embryo and characterize spindle-associated F-actin in the intact epithelium. I modified existing approaches for labeling F-actin to visualize actin during mitosis. Subsequent imaging of fluorescently labeled phalloidin revealed the localization of endogenous F-actin structures associated with the mitotic spindle. Specifically, F-actin puncta were detected around spindle poles, and F-actin cables were found extending between spindle poles and the cortex, and spanning the poles within the spindle. Similar localization patterns are additionally detected via isoform-specific actin antibodies. Live imaging experiments further corroborated these results and highlight the dynamic nature of actin cables as they move within and around the spindle throughout mitosis. Collectively, these results show a) that mitotic spindles in an intact vertebrate epithelia associate with a substantial amount of F-actin structures; b) that these structures form coincident with spindle assembly, and; c) suggest that spindle F-actin, separate from or in coordination with cortical F-actin, may be essential for proper mitotic spindle structure and function.

Introduction

Mitotic spindles are microtubule-based structures responsible for partitioning genetic information into each new daughter cell generated by cell division. At the start of mitosis microtubules are nucleated from each of two centrosomes that will become the spindle poles. Three distinct populations of microtubules form: the kinetochore microtubules which extend towards and attach to chromosomal kinetochores; the interpolar microtubules which extend toward the spindle midplane and overlap interpolar micrutubules from the opposite pole; and the astral microtubules which extend from each pole out towards the cortex. Each of these microtubule populations works in concert with motor proteins and microtubule-associated proteins to carry out the essential function of the mitotic spindle: precise chromosome segregation.

The roles of different microtubule populations and their associated proteins in this process have been well characterized (Gatlin & Bloom, 2010; Goshima & Scholey) while the other major cytoskeletal system, actin, is known to function together with myosin to provide the contractile strength necessary to divide the cell during cytokinesis. However, whether or not filamentous actin (F-actin) is required—or is even present—within the spindle has long been controversial. In the 1970s, several groups reported F-actin localization to mitotic spindles in a variety of cell types. Using a range of techniques including electron microscopy, fluorescent actin antibodies, and a fluorescently conjugated myosin-2 fragment as a probe for F-actin, actin was found decorating spindles in several different systems including cultured mammalian cell lines (e.g. Gawadi 1971; Sanger, 1975; Schloss et al., 1977; Fujiwara & Pollard, 1976; Cande et al., 1977; Herman & Pollard, 1979). The conclusion of these results was that F-actin and myosin may fill specific roles in the spindle such as structural support, force production for chromosomal movements, and spindle organization (Sanger, 1975; Fujiwara & Pollard, 1976; Schloss et al., 1977; Herman & Pollard, 1979). These early reports were

subsequently challenged as artifacts of sample preparation since alterations in fixation technique caused non-specific antibodies to label the spindle (Aubin et al., 1979). Further, staining cells with fluorescent phalloidin failed to label spindle-associated F-actin while cortical F-actin was robustly labeled (Barak et al., 1981). In agreement with the notion that spindle F-actin did not exist, cell-free extract systems prepared in the presence of cytochalasins (which prevent F-actin assembly) were found to allow relatively normal spindle assembly and progression (Lohka & Maller, 1985).

Considering the technical challenge of F-actin preservation during preparation for visualization it is not surprising that uncertainty over the presence and potential role of spindle F-actin remains (reviewed in Sandquist et al., 2011). For example, any attempt to detect F-actin in fixed samples results in potential loss of F-actin during permeabilization and fixation, particularly if that F-actin is labile or highly dynamic in living cells. Reports of F-actin detection in animal meiotic spindles (Schuh & Ellenberg, 2008) and plant mitotic spindles (Seagull et al., 1987) have touched on this challenge by noting that special conditions are required for preservation of F-actin in these structures. Another consideration is the high abundance of F-actin in the cortex, which may overwhelm less concentrated subcortical F-actin signal during visualization. Similarly, manipulations that disrupt F-actin generally do not discriminate between cortical and non-cortical F-actin, such that any change in spindle behavior or function following F-actin disruption is typically ascribed to loss of cortical F-actin (e.g. Théry et al., 2005; Toyoshima & Nishida, 2007).

These issues are also a problem when visualizing F-actin in living cells, especially concerning the issue of signal-to-noise ratios. Use of fluorescent monomeric actin (G-actin)—though seemingly an ideal method of labeling F-actin—often produces high levels of background fluorescence since most cellular actin is retained as a monomeric pool. Identifying F-actin structures becomes difficult at best under these

conditions. Another limitation is that high levels of fluorescent actin expression are very often toxic (e.g. Ballestrem et al., 1997). Additionally, fluorescent actin has been shown to under report certain populations of F-actin as it is poorly incorporated into formin-nucleated actin filaments (Kovar et al., 2006). Labeling F-actin in living cells with probes that bind F-actin directly, such as Lifeact (Riedl et al., 2008), UtrCH (Burkel et al., 2007), or moesin (Edwards et al., 1997) overcomes the signal-to-noise problem of fluorescent monomeric actin. However, these probes come with concerns as well, such as their potential to stabilize filaments or compete with endogenous F-actin binding proteins, which may alter filament dynamics. While these probes do not appear to under-report formin-nucleated actin filaments (Wu & Pollard, 2005), they are limited by their binding rates as any pool of actin that assembles and disassembles too quickly will not be efficiently bound. Collectively, the challenges and caveats that surround each F-actin labeling technique firmly suggest that a combination of altering techniques to preserve the largest amount of F-actin possible combined with the use of multiple visualization techniques should enable fully described F-actin populations.

In this work I describe the presence of non-cortical F-actin structures that associate with the spindle throughout mitosis in an intact epithelium. Through the use of multiple fixation and labeling techniques I characterized spindle-associated F-actin endogenously and related these findings to F-actin localization in live cells by harnessing various fluorescent markers.

Results

Modification of existing approaches for F-actin detection within fixed samples of intact epithelial cells

In order to assess the existence of spindle associated F-actin, several technical hurdles had to be surmounted. First, optimal conditions for the preservation of F-actin and microtubules had to be established for *X. laevis* embryos. For example, while microtubules benefit from post-fixation incubation in methanol, this treatment renders F-actin unrecognizable by fluorescent phalloidin, a reagent considered to be the gold standard for labeling F-actin in fixed samples. This problem is made worse by the fact that the pigment and yolk of the *Xenopus* embryo hamper fluorescence imaging, such that clearing of samples in a mixture of benzyl benzoate and benzyl alcohol is needed for optimal imaging, and this in turn requires dehydration (Klymkowsky & Hanken, 1991). Typically, methanol would be used for this dehydration step but as methanol alters the structure of F-actin, an alternate approach was necessary. I therefore tried several different fixations and dehydration approaches that avoided the use of methanol and thus permitted me to employ fluorescent phalloidin.

Second, a reliable method of labeling DNA without increasing background noise was needed. Traditional chemical DNA labels such as DAPI or propidium iodide produce relatively high background signal in the frog system. To overcome this problem, I employed injection of fluorescently tagged histone H2B mRNA, which allowed for clear DNA signal that persisted after sample preparation without negative consequences such as excessive yoke-illumination.

Third, experimental time had to be reduced from prior protocols to overcome issues with sample degradation. The standard immunofluorescence protocol for microtubule labeling in *Xenopus* embryos takes 4-5 days to execute and, based on pilot experiments, as well as reports on the instability of non-cortical F-actin in other model

systems (e.g. Schuh & Ellenberg 2008) it was apparent that this was far to long for optimal preservation of non-cortical F-actin. This challenge was overcome by development of a new, accelerated protocol that sacrifices preservation of the deeper cell layers for speed (see methods).

Detection of spindle-associated F-actin with phalloidin and characterization of an F-actin cycle

To begin characterizing the localization of endogenous F-actin relative to mitotic spindles, embryos were labeled with fluorescent phalloidin (AlexaFluor) and immunostained for α-tubulin to label microtubules. As expected, F-actin was detected robustly at the cell cortex throughout the cell cycle, culminating in the accumulation of F-actin at the cleavage furrow during telophase, just prior to cytokinesis (Figure 1a).

In addition to the cortical F-actin, several striking, internal F-actin-based structures were also observed. These include F-actin cables that extend between the spindle poles and between the spindle and the cell cortex, as well as F-actin puncta. During interphase, cables and puncta are visible in a seemingly random distribution (Figure 1a, interphase). At the start of nuclear envelope breakdown (NEB) in late G2 cells, there is an increase in these structures, centered near each microtubule organizing center (MTOC), which will become the spindle poles (Figure 1a, late G2). From prometaphase through telophase, F-actin puncta are clustered at or near each spindle pole (Figure 1a, b). These puncta decrease in size and number as mitosis is concluded (data not shown). F-actin cables also associate with the spindle for the duration of mitosis—spanning between spindle poles, spindle poles and chromosomes, and between the spindle and the cortex both at the poles and the spindle body (Figure 1a).

To verify that the observed F-actin structures were due to phalloidin labeling and not caused by signal bleed through from the anti-α-tubulin channel, I performed control

experiments lacking microtubule labeling. Embryos expressing mCherry-histone H2B were fixed and labeled with fluorescent phalloidin, then immediately imaged. This method recapitulated the F-actin localization described above (Figure 1b). The shortened timeframe between fixation and imaging often allowed for superior visualization of fine F-actin cables, further highlighting the fragile nature of these structures.

To address the possibility of phalloidin induced F-actin stabilization in mitotic cells, actin antibodies were used as an alternative to phalloidin labeling. A fluor-conjugated antibody of monomeric actin (G-actin), specifically of cytoplasmic gamma-actin (1-37::488; Hanft et al., 2006), was employed using a paraformaldehyde fixation with a methanol post-fix protocol. This antibody labeled the same actin structures—cables and puncta—associated with the mitotic spindle (Figure 1c). Similar to phallodin-labeled cells, antibody staining brightly labeled the cell cortex, as expected.

Spindle-associated F-actin is detectable by various fixation methods

To confirm F-actin localization to spindles, I used several fixation methods to preserve F-actin during mitosis. In addition to paraformaldehyde fixation either with (Figure 1c) or without (Figure 1a, 1b) a methanol post-fix, cold-acetone fixation was employed. The benefit of this method is rapid permeabilization and fixation in the absence of cross-linkers such as gluteraldehyde (see methods). However, this treatment also leaves cells brittle and susceptible to breakdown such that additional washes and antibody incubations were not feasible. To identify the location of spindles without antibody labeling, I used embryos expressing fluorescent histone H2B. In mitotic cells fixed with acetone and labeled with fluorescent-phallodin, F-actin could be detected surrounding the mitotic spindle at all stages. F-actin cables within the spindle can be readily detected (Figure 2a, arrows) while cables spanning between spindle poles and

the cortex are not as clear. This is in large part due to the formation of large vesicles in the surrounding cytoplasm, a side effect of subjecting cells to an organic solvent like acetone. As with paraformaldehyde-based methods, F-actin puncta were detectable (Figure 2a, arrowheads). Although microtubules are not visible in these cells, the localization of these puncta with respect the metaphase plate is similar to that seen in anti-tubulin labeled cells.

One additional method of labeling F-actin in fixed cells harnessed the Utrophin probe, eGFP-UtrCH (Burkel et al, 2007). This fluorescently tagged probe contains the first 261 amino acids of Utrophin, a F-actin side-binding protein. By imaging this probe after paraformaldehyde fixation, I was able to capture GFP-UtrCH localization through the entire spindle at high resolution. This is in contrast to imaging in live cells where the timing of mitosis and movement of spindles puts limitations on the resolution used. Similar to the previously described phalloidin and actin antibody labeling, GFP-UtrCH labels F-actin cables and puncta at the mitotic spindle (Figure 2b).

Variation in F-actin detection by actin antibodies

Epithelial cells express two of the six actin isoforms, cytoplasmic beta-actin (β-CYA) and gamma-actin (γ-CYA) (Vandekerckhove & Weber, 1978). Although these two isoforms vary by only 4 amino acids within the first nine residues, they have been shown to have distinct subcellular localization in several cell types (Hill & Gunning 1993; Dugina et al., 2009; Baranwal et al., 2012). To examine potential specificity in the composition of spindle-associated F-actin, I visualized mitotic actin using the γ-actin antibody 1-37, a second γ-actin antibody (mAb 2-4; Sonnemann et al., 2006), and a β-actin antibody (AC-15::FITC). As described above, the γ-actin antibody 1-37 labeled cortical actin and spindle associated cables and punta above background signal (Figure 1c). To determine the localization pattern of AC-15::FITC, embryos were first injected with a DNA marker

(mCherry-histone H2B), fixed, and labeled for microtubules (anti-α-tubulin) and β-actin. The AC-15 antibody distinctly labeled cortical actin structures while appearing mainly diffuse in the cytoplasm (Figure 3a). Close examination of cytoplasmic signal revealed small puncta near spindle poles or along microtubules extending out from the spindle (Figure 3a). F-actin cables were not readily detectable above background signal in mitotic or interphase cells. The mAb 2-4 γ-actin antibody also distinctly labeled cortical actin (Figure 3b), however non-cortical structures were undetectable above high background signal in all cells. The contrast between γ-actin antibodies mAb 2-4 and 1-37 may reflect slight differences in each antibody to bind under the sample preparation method used.

Visualization of spindle F-actin in living cells

To compliment the localization of endogenous F-actin described above, I examined F-actin localization in live cells using both fluorescently labeled monomeric actins (G-actin) and F-actin binding probes. Embryos were injected with either mCherry-α-tubulin or mCherry-histone H2B to visualize microtubules or DNA, respectively, and co-injected with each of the following constructs. Expression of eGFP-β-actin at low concentrations resulted in only diffuse cytoplasmic signal (not shown). At higher concentrations, eGFP-β-actin signal was detected diffusely in the cytoplasm and nucleus during interphase, while during mitosis it largely localized in an orb around spindles (Figure 4a). There was little to no integration of tagged β-actin into cortical actin filaments (Figure 4a). Cells expressing high levels of eGFP-β-actin also displayed mitotic defects, including a delayed metaphase-to-anaphase transition (not shown) and poor separation of chromosomes (Figure 4a).

A second fluorescently tagged monomeric actin was examined to test the possibility that F-actin cables at the mitotic spindle may be isoform-specific. Embryos co-

injected with mCherry-α-tubulin and eGFP-γ-actin displayed similar localization patters to that of eGFP-β-actin with some notable differences. Unlike β-actin, γ-actin could be visualized at points within the cell cortex (Figure 4a) and occasionally decorated spindle-associated cable structures above background signal (Figure 4a). However, localization of eGFP- γ-actin was generally similar to eGFP-β-actin as γ-actin was mainly detected in a cloud of signal that moved with the spindle from prometaphase to telophase.

Two F-actin side-binding probes were also examined in mitotic cells. The first was Lifeact-eGFP, a 17 amino acid fragment from the actin binding protein Abp140 of *Saccharomyces cerevisiae* (Riedl et al., 2008). Due to its low-affinity binding to F-actin, Lifeact-eGFP is thought to cause few perturbations in actin dynamics (Riedl et al., 2008). Expression of Lifeact-eGFP was monitored in embryos co-injected with mCherry-histone H2B (to visualize DNA). Distinct from fluorescent monomeric actin visualization described above, Lifeact-eGFP clearly decorated cortical F-actin (Figure 4b). During mitosis, bright F-actin puncta and transient cables were present (Figure 4b); however, high eGFP signal around the spindle made these difficult to observe.

As previously described in Woolner et al. (2008), the Utrohphin probe (eGFP-UtrCH; Burkel et al., 2007) decorates F-actin cables associated with the mitotic spindle. I repeated this experiment with both single eGFP- and triple eGFP- versions of this probe (3XeGFP-UtrCH). To improve the visualization of this probe, I used a combination of shortened time points (<1s versus 6s), higher resolution imaging, and took several z-series images through the spindle. This allowed the entire mitotic spindle to be imaged over time. eGFP-UtrCH bound F-actin at the cortex (Figure 4b) and decorated both F-actin puncta and cables at the spindle during mitosis (Figure 4b, 4d). Spindle-associated structures decorated by this probe were dynamic, moving with and around the spindle through to telophase.

Recently, a truncated 230-residue form of the Utrophin probe, UtrCH-230, was reported to bind nuclear F-actin in cultured cells with less filament stabilization (Belin et al., 2013). Expression of this probe during live-cell imaging initially resulted in the detection of only bright F-actin puncta with little to no signal at the cortex or along cytoplasmic F-actin structures (not shown). To examine the localization of UtrCH-230 as compared to phalloidin-labeled filaments, embryos were injected with mCherry-UtrCH-230, then fixed and labeled with 488-phalloidin. UtrCH-230 was found brightly decorating F-actin puncta (Figure 4c), however it failed to label cytoplasmic or cortical F-actin (Figure 4c). It is unclear why this probe failed to label F-actin cables in *X. laevis*.

Figure 1: F-actin localizes to mitotic spindles in the *X. laevis* embryonic epithelium

(a) Confocal micrographs of interphase and mitotic cells in the epithelium of *X. laevis* triple labeled for microtubules (anti-α-tubulin; red), F-actin (phalloidin; green), and DNA (histone H2B; blue). During interphase, F-actin is brightly labeled in the cortex while F-actin cables and puncta are detected in the cytoplasm. Beginning at prometaphase and continuing through mitosis, F-actin puncta are found near the nascent spindle poles (arrowheads, prometaphase), cables span between spindle poles and the cortex (arrows, prometaphase), and cables reach from spindle poles into the spindle (arrows, metaphase and anaphase). (b) Confocal images of mitotic cells labeled with fluorescent phalloidin in the absence of αtubulin antibodies. Arrowheads point to F-actin puncta clustered near presumptive metaphase spindle poles. F-actin cables are detectable as well (arrows, anaphase). (c) Confocal micrographs of spindles labeled with a γ-actin antibody (1-37::488). F-actin structures are noted with arrowheads (puncta) and arrows (cables). Scale bars represent 10 μm.

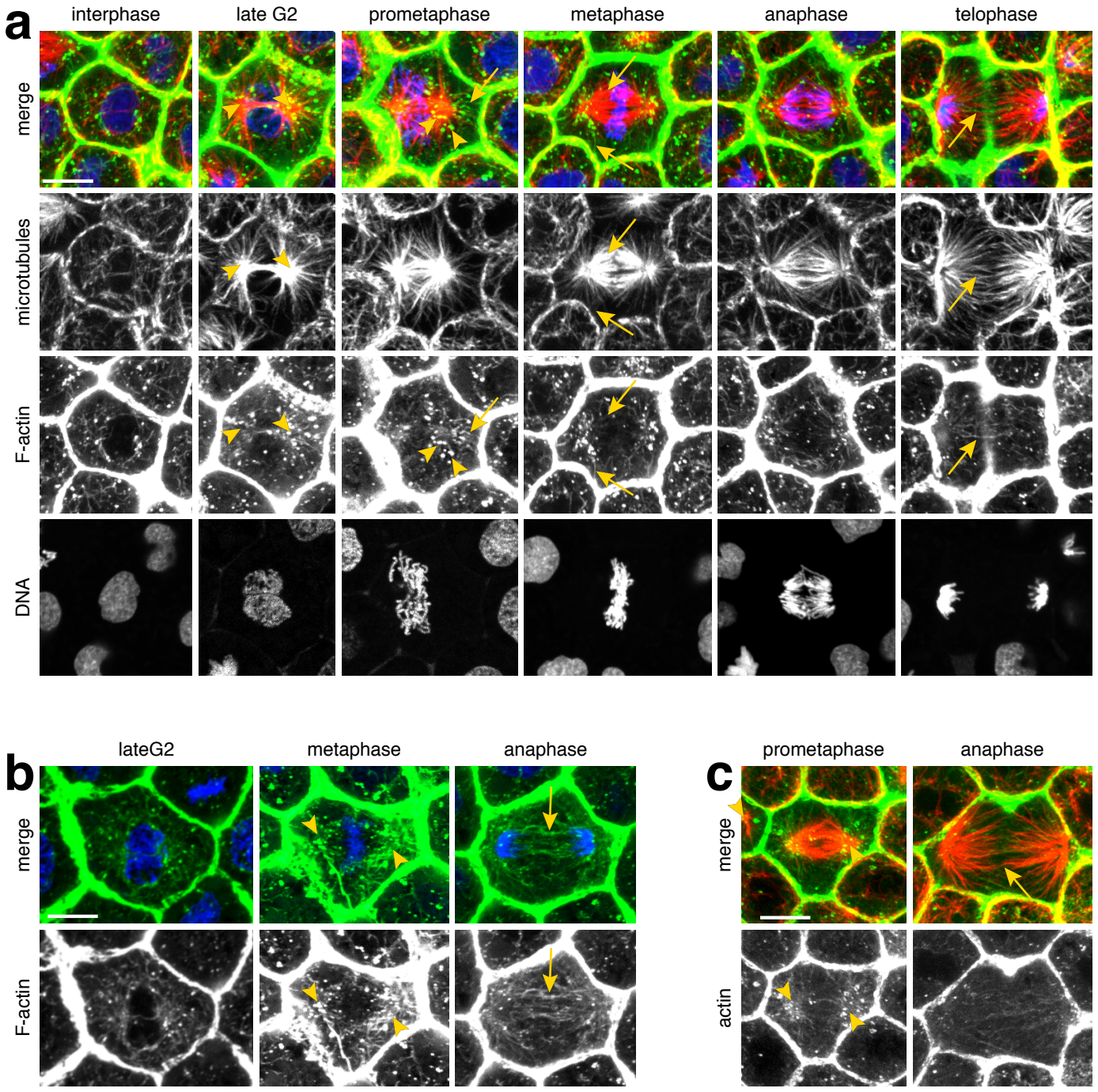
a
interphase
late G2
prometaphase
metaphase
anaphase
telophase
merge
microtubules
F-actin
DNA
b
lateG2
metaphase
anaphase
merge
F-actin
c
prometaphase
anaphase
merge
actin

Figure 2: Alternative methods of labeling F-actin in fixed cells recapitulate spindle-associated localization

(a) Confocal micrographs from embryos fixed and permeabilized with cold acetone. F-actin (phallodin, green) is detected at the cortex and in cables (arrows) within the mitotic spindle. F-actin puncta (arrowheads) are also visible above background signal. (b) Mitotic cells from embryos expressing the utrophin probe (UtrCH) which, similar to phallodin, binds actin filaments. UtrCH (green) labels spindle-associated F-actin cables (arrows) throughout mitosis. F-actin puncta are also detectable (arrowheads). Scale bars represent 10 μm.

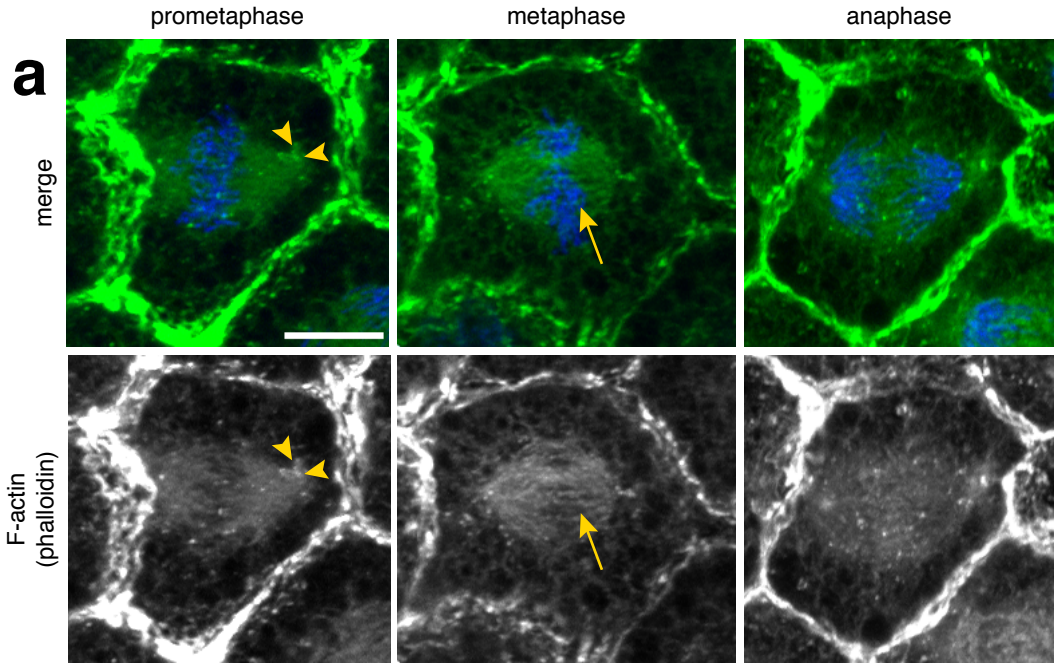
a
prometaphase
metaphase
anaphase
merge
F-actin
(phalloidin)

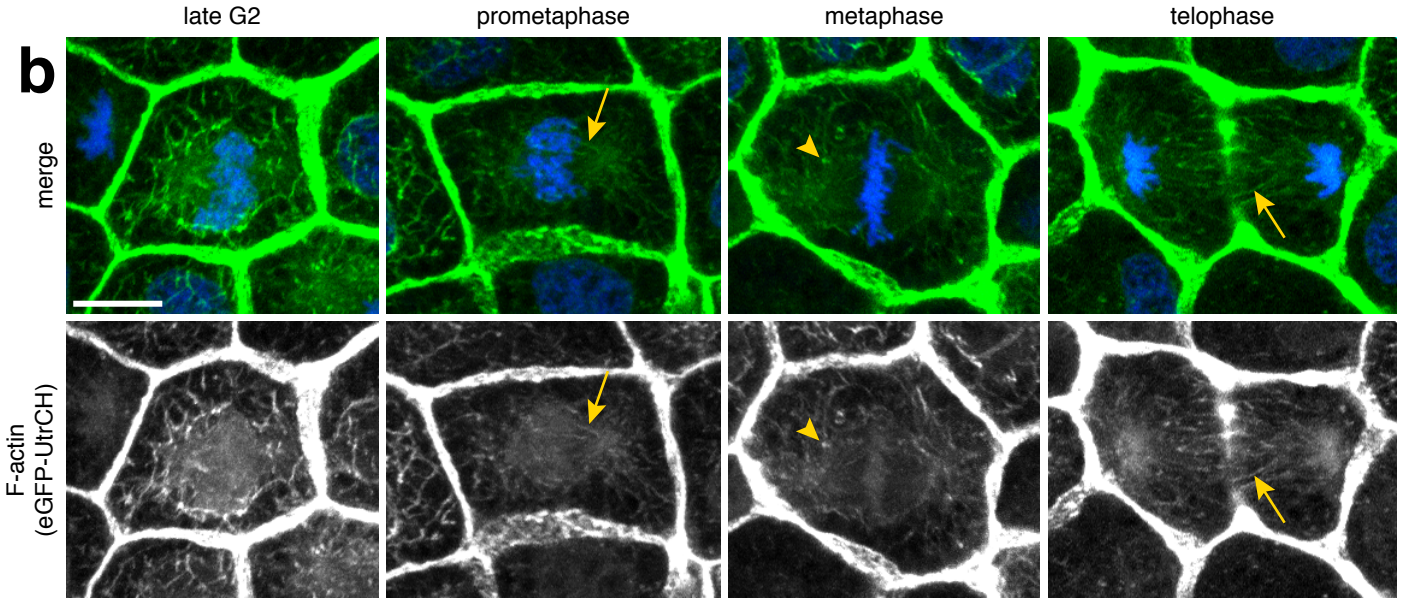
b
late G2
prometaphase
metaphase
telophase
merge
F-actin
(eGFP-UtrCH)

Figure 3: Variation in F-actin detection by isoform-specific actin antibodies

(a) Confocal micrographs of mitotic cells in the epithelium of *X. laevis* triple labeled for microtubules (anti-α-tubulin, red), β-actin (AC-15::FITC, green), and DNA (histone H2B, blue). Throughout mitosis, β-actin is clearly detected at the cortex while cytoplasmic signal is diffuse. Bright puncta of β-actin are found in close proximity with the spindle poles or associated with microtubules (arrowheads, premetaphase). Cytoplasmic F-actin cables are not detectable above background signal. (b) Confocal micrographs of cells labeled with the γ-actin antibody mAb 2-4 (green). This antibody also labels cortical actin structures and is diffuse throughout the cytoplasm. No actin puncta are decorated near presumptive spindle poles (arrowheads) and F-actin cables are not detectable within the cytoplasm. Scale bars represent 10 μm.

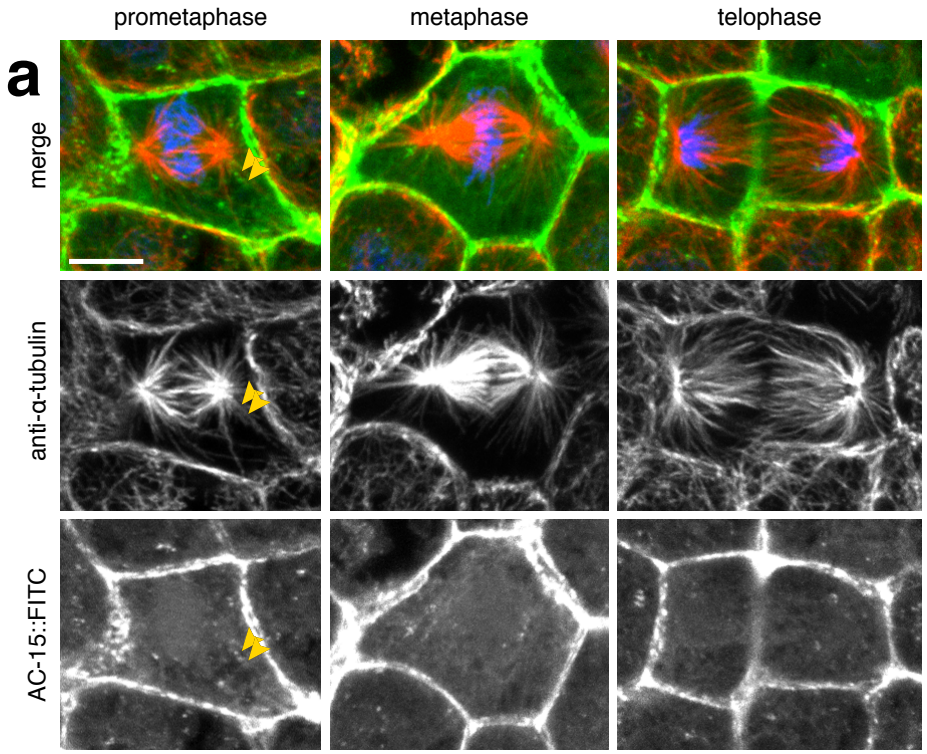
a
prometaphase
metaphase
telophase
merge
anti-α-tubulin
AC-15::FITC

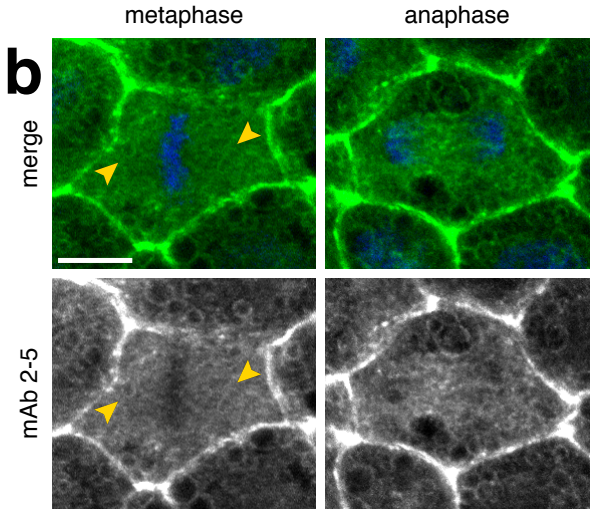
b
metaphase
anaphase
merge
mAb 2-5

Figure 4: Utrophin probe yields clearest labeling for tracking spindle-associated F-actin in live cells

Stills from live imaging of fluorescently tagged monomeric actin and probes for F-actin. Images shown are from metaphase for all panels in (a) and (b). (a) Expression of eGFP-β-actin (green) with DNA (red, mCherry-histone H2B; left panels) and eGFP-γ-actin (green) with microtubules (red, mCherry-α-tubulin; right panels). eGFP-β-actin fails to label F-actin puncta or cables and is not integrated into cortical F-actin (asterisks). eGFP-γ-actin is more efficiently integrated at the cortex (asterisks) and occasionally decorates F-actin cables above background (arrows). (b) Stills from embryos expressing the F-actin probes Lifeact-eGFP (green, left panels) and eGFP-UtrCH-261 (green, right panels). Each probe was co-imaged with mCherry-histone H2B to label DNA (red). With both of these F-actin binding probes, puncta (arrowheads) and cables (arrows) can be detected. (c) Confocal micrographs from embryos expressing UtrCH-230 (red), that were fixed and labeled with phalloidin (F-actin, green). In contrast to UtrCH-261 in (b), this truncation labels only F-actin puncta (arrowheads) and fails to label F-actin cables (arrows) or cortical F-actin (asterisks). (d) Time-lapse montage of a cell expressing eGFP-UtrCH (green) and mCherry-histone H2B (red) from NEB to metaphase. Arrows indicate actin cables spanning the spindle and arrowheads point to spindle pole at the start of mitosis. Time is shown in minutes and seconds. Scale bars represent 10 μm.

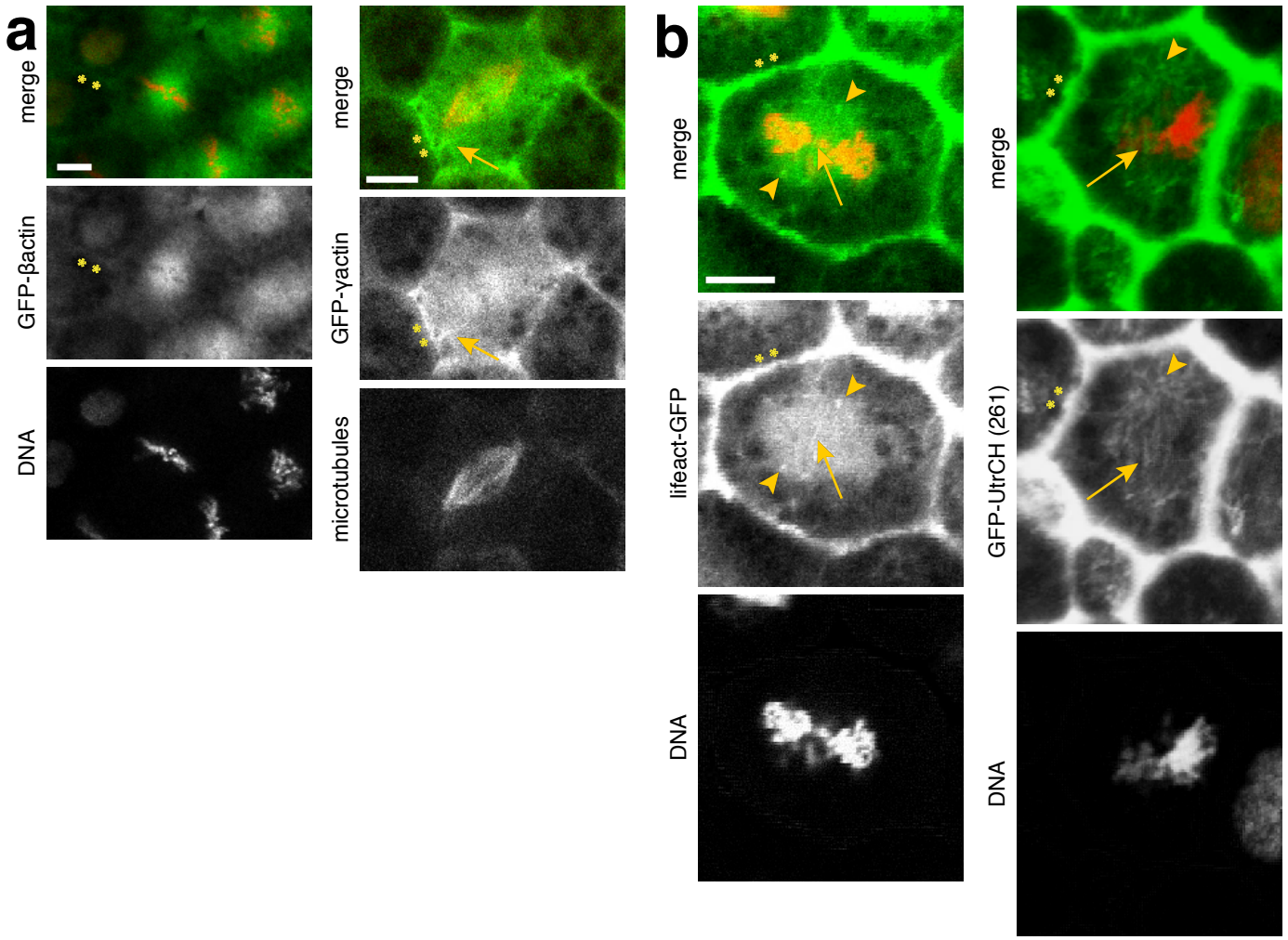
a
merge
GFP-βactin
DNA
merge
GFP-γactin
microtubules
b
merge
lifeact-GFP
DNA
merge
GFP-UtrCH (261)
DNA

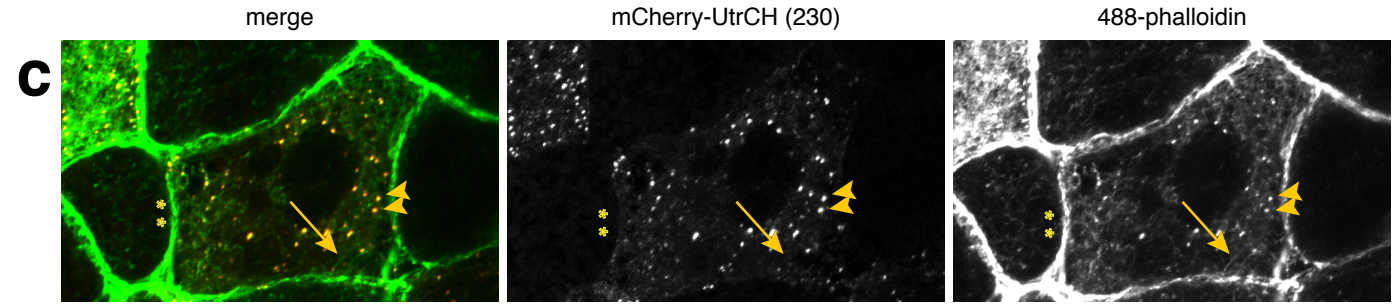
c
merge
mCherry-UtrCH (230)
488-phalloidin

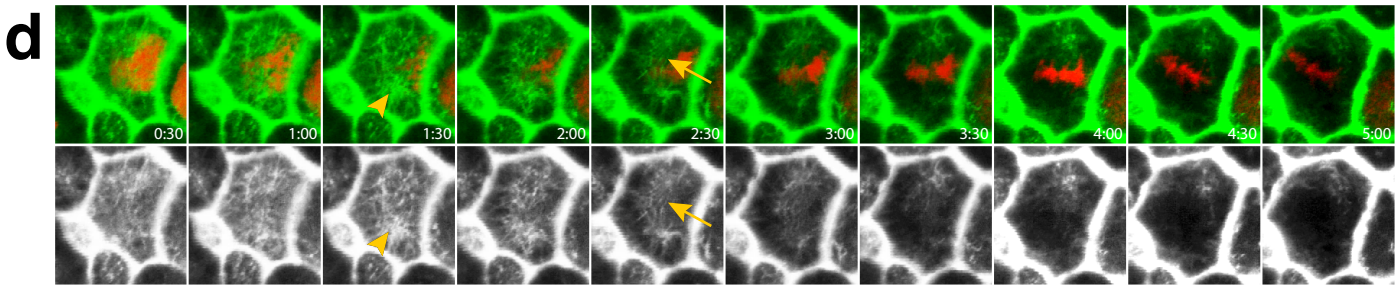
d
0:30
1:00
1:30
2:00
2:30
3:00
3:30
4:00
4:30
5:00

Figure 5: Model of changes in spindle-associated F-actin in response to various drug treatments

(a) Schematic representations of the spindle and associated F-actin structures throughout mitosis starting with a burst of F-actin polymerization at spindle poles just after NEB. At prometaphase cables are detected reaching between spindle poles and between the spindle and the cortex while F-actin puncta are found in close proximity to spindle poles. Cables and puncta remain associated with the spindle through metaphase into anaphase, with a lessening in both structures during anaphase. F-actin is depicted in green, microtubules are depicted in red, and cell outlines are depicted in gray.

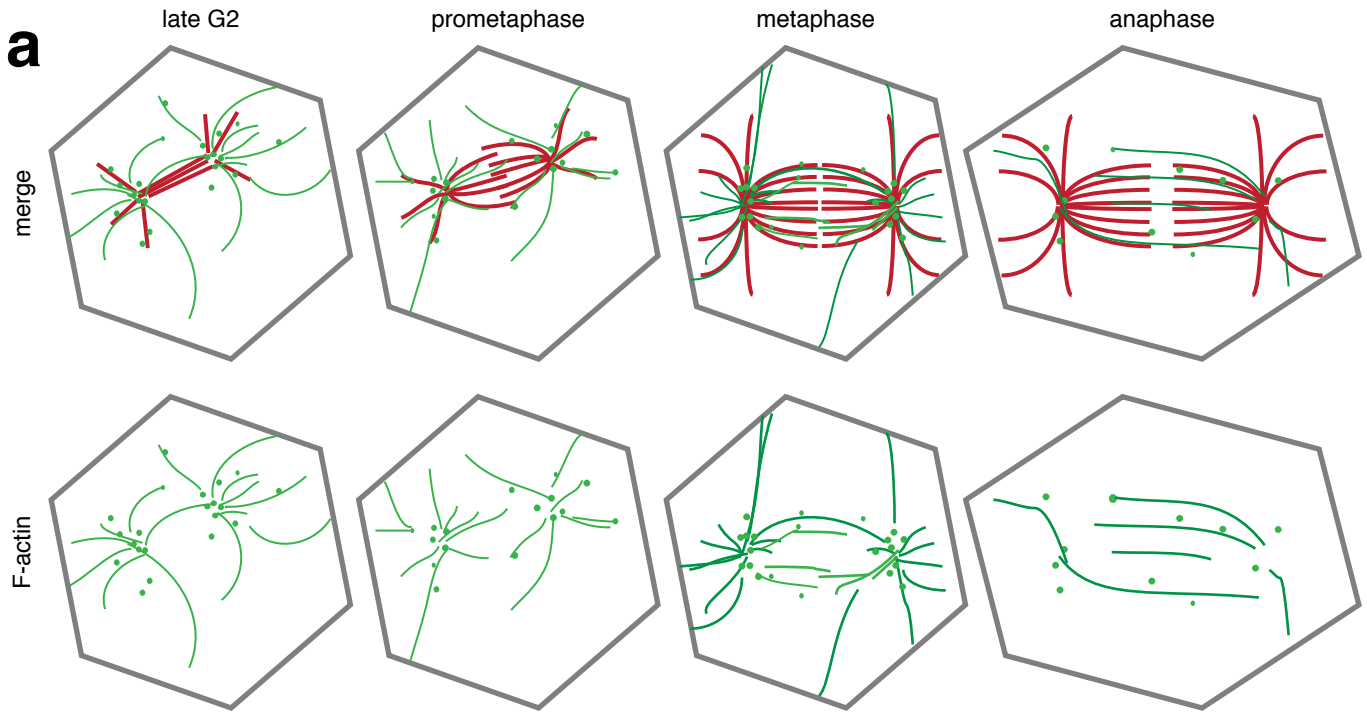
a
late G2
prometaphase
metaphase
anaphase
merge
F-actin

Discussion

In this study I developed the means to preserve and visualize non-cortical F-actin in xenopus embryonic epithelial cells using several complementary approaches. Using these methods I have demonstrated the existence of F-actin associated with the mitotic spindle and characterized changes in spindle F-actin that occur during mitotic progression. The textbook view of actin during mitosis is that it is a major component of the cell cortex and that, together with myosin, actin filaments provide the force necessary to pinch apart the cell during cytokinesis. It is not surprising that these functions of cortical actin are well characterized and studied, as there is a great deal of actin that makes up these structures. Unfortunately, one consequence of the focus on cortical F-actin is the under-characterization—or lack of characterization—of non-cortical actin during mitosis. The first, most obvious reason for this is that the striking abundance of F-actin at the cortex and within the cytokinetic ring apparatus means it is difficult to visualize non-cortical actin unless one is willing to accept saturation of the fluorescent signal at the cortex. A second reason for this under-characterization is that preservation of much the less abundant spindle actin structures (relative to cortical arrays, for example) requires special consideration during sample preparation. Finally, spindle-associated F-actin appears to be relatively dynamic in nature, and reliable preservation of dynamic actin cables is known to be a challenging endeavor (Schuh & Ellenberg, 2005; Seagull et al., 1987; Yu et al., 2006). Thus it is perhaps not surprising that non-cortical F-actin, including spindle-associated actin, has been overlooked in past studies centered around mitotic cytoskeletal processes.

Nonetheless, my results clearly indicate that such F-actin exists. Spindle-associated F-actin structures were detectable by several complimentary approaches: multiple phalloidin-based staining methods, labeling with actin antibodies, and visualization of the side-binding actin probe UtrCH in both live and fixed samples.

Collectively, these results confirm the existence of spindle F-actin in the early embryos of a vertebrate epithelium.

The localization of F-actin at the spindle during mitosis begins with an increase in actin cables coincident with nuclear envelope breakdown (NEB) (represented in Figure 5a). Fine actin cables are formed in close proximity to the nascent spindle poles and move with the poles from prometaphase into metaphase. Along with these fine actin cables, bright F-actin puncta are found at the spindle poles and within the spindle body, usually closely associated with at least one microtubule (Figure 5a). As the cell enters anaphase, both actin cables and puncta appear to decrease overall, although cables remain detectable spanning between spindle poles and between each pole and the cortex (Figure 5a). These changes in spindle F-actin during mitosis—from high polymerization at the start that decreases over time—may indicate variation in the roles filled by this actin at different stages of mitosis. This also hints at the existence of an F-actin cycle during mitosis, similar to that of microtubules. Consistent with this idea, bulk F-actin in xenopus cell extracts was reported to undergo structural alterations in response to the cell cycle (Field et al. 2011).

The localization of F-actin cables to the mitotic spindle suggests a role for actin beyond cortical stability and cytokinesis during mitosis. The close proximity of actin cables and puncta to microtubules during this process may indicate actin:microtubule cross-talk in the spindle, which has been described in a broad array of cellular functions (reviewed in Rodriguez et al. 2003). Further, the increase of F-actin during prometaphase and cables spanning between spindle poles and the cortex could be clues to the function of spindle-associated actin. For example, early in mitosis F-actin may help to stabilize the newly forming spindle, while cables that appear later may help with spindle positioning by transmitting external cues from the cell cortex to the spindle (Fink et al., 2011). F-actin cables may also contribute to determination of spindle length,

as suggested by previous that showed spindle length defects could be rescued by actin depolymerization by latrunculin A (Woolner et al., 2008).

This study establishes the endogenous localization of spindle-associated F-actin structures. More generally, my results clearly indicate that there is far more non-cortical F-actin than currently represented by the textbook view of actin during mitosis. That is, my results show that throughout the cell cycle, the cell interior has a variety of dynamic, F-actin based structures including internal cables and puncta. In contrast, the textbook view of F-actin shows it concentrated entirely in the cortex, in cell surface protrusions such as microvilli, or in large cortical structures such as stress fibers. The existence of an extensive array of non-cortical f-actin suggests that other, non-traditional roles for this polymer should be considered.

Materials & Methods

Plasmids

The mCherry-histone H2B, mCherry-α-tubulin, eGFP-UtrCH, and pCS2+3XeGFP plasmids were made as previously described (Burkel et al. 2007; Bement & Miller 2009). UtrCH was subcloned into pCS2-3XeGFP with BspE1 and Xho1. The first 630 nucleotides of UtrCH were amplified and inserted into pCS2-mCherry with BspE1 and Xho1 to generate UtrCH-230.

eGFP-N1-Lifeact was obtained from Erik Dent (University of Wisconsin) and the sequence of Lifeact-eGFP was amplified from this vector and cloned into pCS2+ using Xho1 and Xba1. eGFP-β-actin was obtained from Kevin Sonnemann (University of Wisconsin) and the β-actin sequence was amplified and cloned into pCS2-eGFP BspE1 and BglII. eGFP-γ-actin was obtained from Timothy Gomez (University of Wisconsin) and cloned into pCS2-eGFP using BamH1 and Stu1.

Embryo preparation

Adult *X. laevis* females were injected with 800 units of human chorionic gonadotropin (HCG; MP Biomedicals) into the dorsal lymph sac 1 day prior to use. Eggs were laid into 1X MMR (100 mM NaCl, 2 mM KCl, 1 mM MgCl2, and 5 mM Hepes, pH 7.4) and fertilized in vitro with macerated testes. Embryos were dejellied in 2% cysteine solution (in 0.1X MMR, pH 7.8) then rinsed five times in 1X MMR and five times in 0.1X MMR. Overnight embryo culture occured in 0.1X MMR at 17°C

mRNA preparation and embryo microinjection

All mRNA was transcribed *in vitro* using the mMessage Machine SP6 kit (Life Technologies) and reactions were purified with the RNeasy Mini Kit (Qiagen). Embryos were submerged in 0.1X MMR + 5% Ficoll (Sigma) and injected with a 5nL volume at the

2-cell stage. mCherry-histone H2B was injected at 12.5 µm/mL for both live and fixed cell imaging. For live cell imaging, mCherry-α-tubulin was injected at 25 µg/mL, GFP-β-actin and GFP-γ-actin were injected at 50 µg/mL, and Lifeact-eGFP, eGFP-UtrCH-261, and eGFP-UtrCH-230 were injected at 80 µg/mL. After microinjection, embryos were incubated in 0.1X MMR at 17°C for 18-20 hr before live imaging or processing for fixation.

Fixation and immunofluorescence

To fix for double labeling of F-actin and microtubules, embryos were briefly rinsed in 1X PBS, then dropped into a modified paraformaldehyde (PFA) solution. This consisted of a "superfix" buffer (100 mM KCl, 3 mM MgCl, 10 mM HEPES, 150 mM sucrose, pH 7.4) to which the following was added (listed in final concentrations): 3.7% PFA, 10% DMSO, 2mM EGTA, 0.2 µM paxitaxol, 0.1% gluteraldehyde, and 0.02% Triton-X-100. Flourescent phalloidin (AlexaFlour 488, Life Technologies) was added to the fix buffer at a concentration of 1:200 for same day imaging, or added to primary and secondary antibody incubations at 1:100. Embryos were incubated for 1 hr on an orbital shaker at room temperature to fix. Microtubules were labeled using mouse monoclonal anti-α-tubulin (DM1A, Sigma) at 1:20,000 and a donkey derived anti-mouse secondary was used at 1:10,000 (AlexaFluor 647, Life Technologies). Primary antibody incubations were 3 hr at room temperature while secondary incubations were overnight at 4°C.

For cold-acetone fixation, embryos were rinsed in 1X PBS, then dropped directly into acetone chilled to -20°C. Embryos were incubated for 20 m in acetone at -20°C, then rehydrated in acetone:PBS serial washes. To label F-actin, embryos were blocked in 1X PBST + 0.1% BSA (Sigma) for 10 m, then incubated in 1X PBST + 0.1% BSA with 1:200 fluorescent phalloidin for 30 m, followed by brief washes with 1X PBS alone.

Actin antibody experiments were performed using a modified version of the microtubule fixation protocol in Danilchik et al (1998). Embryos were fixed for 1 h in 3.7% PFA, 0.25% glutaraldehyde, and 0.2% Triton X-100 in a microtubule assembly buffer (80 mM K-Pipes, pH 6.8, 5 mM EGTA, 1 mM $MgCl_2$, pH 7.4). Following fixation, embryos were post-fixed in -20°C methanol for 30 m, then rehydrated with a methanol:PBS wash series. Samples were incubated for 3 hr at room temperature or overnight at 4°C with primary antibodies at the following concentrations: 1:100 mouse monoclonal anti-γ-actin 1-37::488 (gift from the Ervasti lab); 1:500 mouse monoclonal anti-β-actin AC-15::488 (Sigma); 1:100 rabbit monoclonal anti-γ-actin mAB 2-4 (gift from the Ervasti lab).

Following all fixation techniques, embryos were dehydrated using a series of isopropanol washes then cleared with Murray's Clear (2:1 benzyl alcohol, benzyl benzoate) for confocal microscopy.

Microscopy and image processing

Imaging of all fixed experiments was conducted with a 1.4 NA 60X oil immersion objective on a Nikon Eclipse Ti inverted microscope using Prairie View software (Brüker). Z-series were acquired using 0.5 μm step size and were reconstructed in Fiji. For live imaging, embryos were mounted in 0.1X MMR and imaged using a 1.0 NA 40X oil immersion or 1.4 NA 60X oil immersion objective on the Nikon Eclipse Ti microscope. Single-plane time series were captured at 2.3 s or less and processed using Fiji software. Multi-plane imaging was processed using Velocity software (PerkinElmer).

Chapter 2

Manipulation of spindle-associated F-actin

Abstract

F-actin cables and puncta associate with the mitotic spindle in the intact epithelium of *Xenopus laevis* embryos. To determine what role these actin structures play in mitotic spindle function, I employed two methods of F-actin disruption. The first method was use of various chemical inhibitors of both F-actin polymerization and of actin nucleation factors. Incubation with a low dose of the actin polymerization inhibitor latrunculin A resulted in a decrease in spindle actin structures with no apparent effect on spindle structure. Low-dose treatment with cytochalasin D, another polymerization inhibitor, caused an increase in fluorescent phalloidin signal at the spindle. There was also a significant decrease in spindle length in cytochalasin D-treated cells. Inhibition of formin family nucleation factors with a small molecule inhibitor of FH2 domains (SMIFH2) had several consequences for the cell, including a decrease in spindle-associated F-actin, decreased spindle-length, displacement of spindles from the center of cells, and chromosomal segregation defects. A second approach to disrupting spindle-associated F-actin employed the targeted expression of actin regulatory proteins to the spindle. While this approach resulted in various spindle-related phenotypes, the effects on spindle F-actin were unclear. Collectively, these results suggest that perturbation of cytoplasmic actin has an effect on the mitotic spindle and that one or more formin proteins regulate spindle-associated F-actin.

Introduction

Cellular processes in eukaryotic cells depend on cytoskeletal networks to provide the structure and force generation necessary to complete each task. The actin cytoskeleton is comprised of actin monomers (globular, G-actin) that polymerize into actin filaments (filamentous, F-actin), which can be dynamic in nature or form rigid networks, depending on the actin binding proteins interacting with it at any given time. Added to this are actin-binding proteins that provide the support necessary to generate higher order structures in cells. The formation of these structures can occur relatively rapidly in response to cellular cues (e.g. filopodia and lamellapodia) (reviewed in Blanchoin et al., 2014) or it can generate more persistent cellular structures (e.g. stereocilia and the cell cortex). The flexible nature of the actin cytoskeleton has lent itself to a wide range of cellular processes, from cell motility and cell migration (Mogilner & Keren, 2009), to multicellular and single-cell wound healing (Sonnemann & Bement, 2011), and cytokinesis (Pollard, 2010).

In addition to actin-binding proteins that direct structural formation, individual filament turnover is tightly controlled by even more actin-binding proteins. These include proteins that sequester actin monomers, nucleate or elongate filaments, cap filament ends, sever filaments, or promote their depolymerization (Lee & Dominguez, 2010). The nucleation step of actin filament formation involves generating actin dimer and trimer "nuclei" from which the new filament can grow. Nucleation is kinetically unfavorable, thus cells use factors that directly nucleate actin to both overcome this obstacle and to control the timing and location of actin filament formation (Campellone & Welch, 2011).

The first identified actin nucleator was the Arp2/3 complex, which is comprised of seven interacting proteins and is highly conserved in eukaryotic cells. Once activated, the Arp2/3 complex binds to the side of an existing actin filament and initiates assembly of a new filament at a 70° angle. Repeated binding and filament assembly by Arp2/3

generates a branched F-actin array (Goley & Welch, 2006). The entire network is disassembled starting with the oldest formed branches, allowing actin monomers to be recycled to the newer, growing barbed ends. In cells, Arp2/3 organizes branched F-actin networks in lamellapodia during cell migration (Wu et al., 2012), around endocytic structures (Duleh & Welch, 2010), and in subcortical arrays that help position the mitotic spindle in response to external cell forces (Mitsushima et al., 2010; Fink et al., 2011).

A second class of actin nucleators is the formin family proteins, characterized by their formin homology (FH) domains FH1 and FH2. Formin proteins form homodimers through FH2 domain binding. The FH2 domains together with FH1 domains can then nucleate unbranched actin filaments (Pruyne et al., 2002). Additionally, formin homodimers promote filament elongation and protect the growing filament by remaining associated with the barbed filament end, which protects filaments from capping proteins that would terminate elongation (Chesarone et al., 2010). These formin proteins fall into several different classes based on FH2 sequence divergence and function in a variety of cellular processes including filopodia formation (Pellegrin & Mellor, 2005), vesicle trafficking (e.g. Leader et al., 2002; Azoury et al., 2008), and cytokinesis (Wantanabe et al., 2010). A subset of formins is also reported to interact with microtubules directly or indirectly. These interactions have been shown to stabilize microtubules (Palazzo et al., 2001; Bartolini et al., 2008), align them with F-actin structures (Ishizaki et al., 2001), or control centrosome and spindle orientation (Andrés-Delgato et al., 2012; Lee et al., 1999). Thus, in addition to generating actin filaments, formins are ideal candidates for actin:microtubule crosstalk.

In this study, I demonstrate that actin polymerization inhibitors at low doses can disrupt spindle-associated F-actin, which, in turn, affects spindle structure and function. Chemical inhibition of a specific class of actin nucleation proteins—known as formins—also disrupts spindle-associated F-actin and mitotic events. Finally, spindle-targeted

actin biding proteins can disrupt spindle-associated F-actin, although the results of this approach are unclear. The conclusions of this work suggest that one or more formin proteins nucleate spindle-associated F-actin and may be required for proper mitotic spindle function.

Results

Effects of cell-wide F-actin disruption by actin inhibitors on mitotic spindle structure

Two approaches were used to disrupt spindle-associated F-actin. The first employed various inhibitors that widely disrupt actin filaments throughout the cell. These inhibitors include compounds that 1) bind actin monomers and block their addition into filaments (latrunculin A), 2) cap the barbed ends of F-actin (cytochalasin D), or 3) block formin-mediated actin nucleation and polymerization (SMIFH2). While each of these compounds provided information on how spindle-associated of F-actin is regulated, this particular method of disruption affects all cellular F-actin, including cortical, subcortical, and cytoplasmic structures. Because of this, I cannot separate the effects non-spindle F-actin may have on the resulting phenotypes. However, this approach was meant to provide initial clues on how spindle F-actin is regulated and how it contributes to mitotic spindle function.

The actin depolymerizing drugs latrunculin A and cytochalasin D distrupt actin filaments through distinct mechanisms. Latrunculin A binds actin monomers in direct competition with the monomer-sequestering protein profilin. This binding prevents actin monomer addition at fast-growing barbed ends, which leads to complete F-actin depolymerization over time. Embryos expressing mCherry-histone H2B were incubated in 3.5 μM latrunculinA or DMSO control for 30 min, then immediately fixed and stained for microtubules and F-actin, using anti-α-tubulin and phalloidin, respectively. As shown in Figure 1a, latruncuilin A greatly reduces cytoplasmic actin structures in both interphase and mitotic cells. There were no significant effects on spindle length (Figure 1b). Although several concentrations were tested, none were determined to affect only cytoplasmic F-actin without also creating large holes in the cortical F-actin network (not shown). Intriguingly, a concentration of 2.5 μM latrunculin A caused an increase in

spindle actin in contrast to the overall decrease in spindle F-actin at 3.5 μM (Figure 1c). This highlights how the changes in the equilibrium between actin monomers and filaments actin can have intermediate states. Freeing up new actin monomers can stimulate actin nucleators; for example, the generation of G-actin has been shown to trigger an increase in nucleation activity of the formin inverted formin 2 (INF2) (Ramabhadran et al., 2013).

In contrast to latrunculin A, cytochlasin D disrupts F-actin by binding to available barbed filament ends, directly blocking the addition of new monomers. Embryos expressing mCherry-histoneH2B were incubated in 30 μM cytochalasinD or DMSO control for 30 min, then immediately fixed and stained for microtubules and F-actin. This treatment resulted in a significant decrease in metaphase spindle length (Figure 1b) coupled with an increase in overall F-actin signal at the spindle (Figure 1b). This increase in signal intensity was due to a general increase of indistinct phalloidin signal surrounding the spindle (Figure 1a).

Inhibition of formin-mediated F-actin nucleation and polymerization severely disrupts mitotic spindles and spindle F-actin

Actin filaments self assemble rapidly, thus control of the timing and location of filament formation within cells is essential. Several mechanisms exist within cells to generate F-actin, including the Arp2/3 complex that generates branched F-actin networks and formin proteins that generate long, unbranched actin filaments. To test if either, or both of these players are responsible for the formation of spindle-associated F-actin, I used the Arp2/3 inhibitor CK666 (Nolan et al., 2009) and the pan-formin inhibitor SMIFH2 (small molecule inhibitor of FH2 domains) (Rizvi et al., 2009). Embryos incubated in high concentrations of CK666 (up to 500uM) for several hours showed no change in cellular F-actin (data not shown). Although some have reported success with

lower concentrations of this inhibitor (Sun et al., 2011; Wang et al., 2014), none of these studies were carried out using *X. laevis* embryos.

To test the possibility that one or more formins may nucleate spindle F-actin, I treated embryos with the formin inhibitor SMIFH2. As compared to controls, formin-inhibition caused negative spindle phenotypes including spindle length defects (Figure 2a, 2b). Additionally, F-actin at the spindle decreased (Figure 2b) and F-actin structures became more dispersed in the cytoplasm (Figure 2a) while cortical F-actin was largely unperturbed (Figure 2a). These results suggested severe consequences for mitosis; I therefore monitored the effects of formin-inhibition in living cells. Embryos expressing markers for microtubules (mCherry-α-tubulin) and DNA (GFP-histone H2B) were incubated in SMIFH2 or DMSO alone immediately before imaging. As cells progressed through mitosis, several defects were noted. Spindle poles, which normally separate prior to nuclear envelope breakdown (NEB) and are maintained at that distance following NEB (Rosenblatt, 2005), collapsed towards one another just after NEB in drug-treated cells (Figure 3). Cells spent more time building and establishing the metaphase spindle, slowly growing as spindle poles moved away from each other (Figure 3a). Chromosomes also failed to align at the metaphase plate (Figure 3a), however, anaphase proceeded without proper alignment, resulting in disorganized chromosomal segregation (Figure 3a).

Depolymerization of astral microtubules alters cytoplasmic F-actin distribution

Microtubule and actin networks have been shown to interact in a variety of cellular processes including neuronal growth cone pathfinding (Schaefer et al., 2002), single-cell wound healing (Mandato et al. 2003), and in cortical flow processes (Canman & Bement, 1997). To test for potential interactions between microtubules and F-actin within the spindle, I used low-dose nocodazole treatment to partially depolymerize

microtubules during mitosis. Embryos expressing fluorescent histone H2B were incubated in 5 μM nocodazole or vehicle-only control then immediately fixed and stained for microtubules (anti-α-tubulin) and F-actin (phalloidin). As expected, this concentration of nocodazole reduced astral microtubules and shortened spindle length (Figure 4b). However, this treatment also reduced total spindle-associated F-actin, and F-actin puncta were redistributed away from the spindle body (Figure 4c). F-actin puncta were found displaced from the spindle yet in close proximity with spindle poles, possibly associating with the plus-ends of depolymerized microtubules (Figure 4a)

Targeted disruption of spindle-associated F-actin

To directly perturb spindle-associated F-actin, I designed and expressed a series of constructs containing three cassettes: 1) a spindle-targeting protein or fragment to localize the construct to the spindle, 2) a negative regulator of F-actin to disrupt actin filaments and, 3) a fluorescent tag to monitor localization (Figure 5a). Each targeting protein was first tested alone to verify localization to the spindle and that they had no adverse over-expression effects. As previously described, full length CyclinB1 localized to spindle poles and along polar microtubules while a N-terminal fragment of CyclinB1 localized to the spindle midplane (Bentley et al., 2007) (Figure 5b). However, both of these were also weakly cytoplasmic during interphase. The fragment of AuroraB, which has been reported to localize to the spindle midplane (Scrittori et al., 2005), was tested. This fragment weakly associated with the spindle during mitosis and was cytoplasmic during interphase (data not shown). Finally, the microtubule-related protein TPX2 was found to be nuclear during interphase and it localized more precisely to the spindle than either CyclinB1 or AuroraB (Figure 5b). Furthermore, unlike CyclinB1, it was not degraded at the metaphase-anaphase transition. Therefore, a negative regulator of F-actin attached to TPX2 would persist at the spindle through the entirety of mitosis.

Several negative regulators of actin filament formation were targeted to the spindle using the method described above. One regulator used was capping protein, which exists as a heterodimer complex and binds to the barbed ends of actin filaments (Wear et al., 2003). This binding prevents the addition of new actin monomers to the growing end, thus blocking filament elongation. Embryos were co-injected with an untagged CyclinB1-targeted capping protein, mCherry-histone H2B and eGFP-UtrCH, then imaged live. Strikingly, expression of this fusion construct generated an abundance of short F-actin cables (Figure 6a). A consequence of this was the formation of multipolar spindles, as evident by the arrangement of chromosomes across intersecting metaphase plates (Figure 6a). The generation of short F-actin cables may represent competition for filament binding between capping protein and formin protein, as formins can compete for binding to barbed filament ends in the presence of profilin (Kovar et al., 2005), which may have exacerbated the phenotype observed here. Although this construct did not deplete spindle-associated F-actin as intended, the result does demonstrate the consequence of unregulated actin polymerization at the spindle during mitosis. Additionally, though the spindles in this experiment were clearly adversely affected, cells successfully completed cytokinetic events (Figure 6a), indicating that cystoplasmic actin was specifically affected.

Experiments were also conducted in which an unregulated gelsolin—an actin filament severing protein (Kwaitkowski et al., 1989)—was targeted to spindles via fusion to TPX2. As shown in Figure 6b, embryos expressing a fluorescent TPX2-gelsolin construct had detectable signal at both the spindle and at the cortex. Targeting of gelsolin to spindles via CyclinB1 did significantly increase the timing of mitosis, specifically the metaphase to anaphase transition (Figure 6d), however, the effects on spindle associated F-actin were unclear and need further investigation.

A second F-actin severing protein, cofilin (Arber et al., 1998), was targeted to spindles via fusion to TPX2. Expression of this GFP-tagged construct resulted in localization to nuclei during interphase and to the spindle during mitosis (Figure 6c). To optimize cofilin function, I co-expressed an untagged version of cyclase associated protein (CAP), which accelerates cofilin-mediated filament severing (Normoyle & Brieher, 2012). Embryos were injected with either a constitutively active (cofilin S3A, non-phosphorylatable) or inactive (cofilin S3D, phosphomemetic) form of cofilin (Agnew et al., 1995) fused to TPX2 (TPX2-cofilin) and mCherry-histone H2B. These experiments were difficult to interpret due to variability in expression levels and results. As shown in Figure 6c, spindles in cells expressing inactive cofilin (cofilin S3D) appear normal while cells expressing cofilin S3A + CAP have spindle defects. However, it was unclear if these defects were due to experimental parameters or general cell sickness caused by the expression of several different probes. Further work will be necessary to sort these factors out, including redesigning experiments to use different targeting means and/or alternate actin regulators (e.g. actin monomer sequestering proteins).

Figure 1: Actin depolymerizing drugs have differing effects on spindle-associated F-actin

(a) Confocal micrographs of metaphase spindles from embryos treated with DMSO (control; left), latrunculin A (center), or cytochalasin D (right). After drug incubations, embryos were fixed in paraformaldehyde and stained for F-actin (phalloidin, green) and microtubules (α-tubulin, red). Treatment with 3.5 μM latrunculin A for 30 m causes a reduction in F-actin cables. F-actin puncta structures are still weakly detectable (arrowheads). Cytochalasin D treatment (40 μM) for 30 m instead caused an increase in spindle F-actin signal, however individual structures became less distinct. DNA (mCherry-histone H2B) is labeled in blue, scale bars represent 10 μm. (b) Quantifications of spindle length as a percentage of cell length (left) and F-actin fluorescence above background (right) for all treatments. Compared to DMSO treated controls, latrunculin A had no significant effect on metaphase spindle length, while cytochalasin D caused a significant decrease in spindle length. (DMSO: n= 85, latrunculin A: n = 37, cytochalasin D: n = 14) (c) Quantification of F-actin fluorescence above background from an experiment using either 2.5 μM latrunculin A, 3.5 μM latrunculin A, or DMSO. 2.5 μM latrunchlin A results in a slight increase of total F-actin fluorescence compared to DMSO control. (DMSO: n=8, 2.5 μM: n=10, 3.5 μM: n=11) (d) Confocal micrographs of latrunculin A treated cells with asterisks indicating gaps in cortical F-actin. (* $p<0.01$, **** $p<0.0001$, ns $p>0.05$)

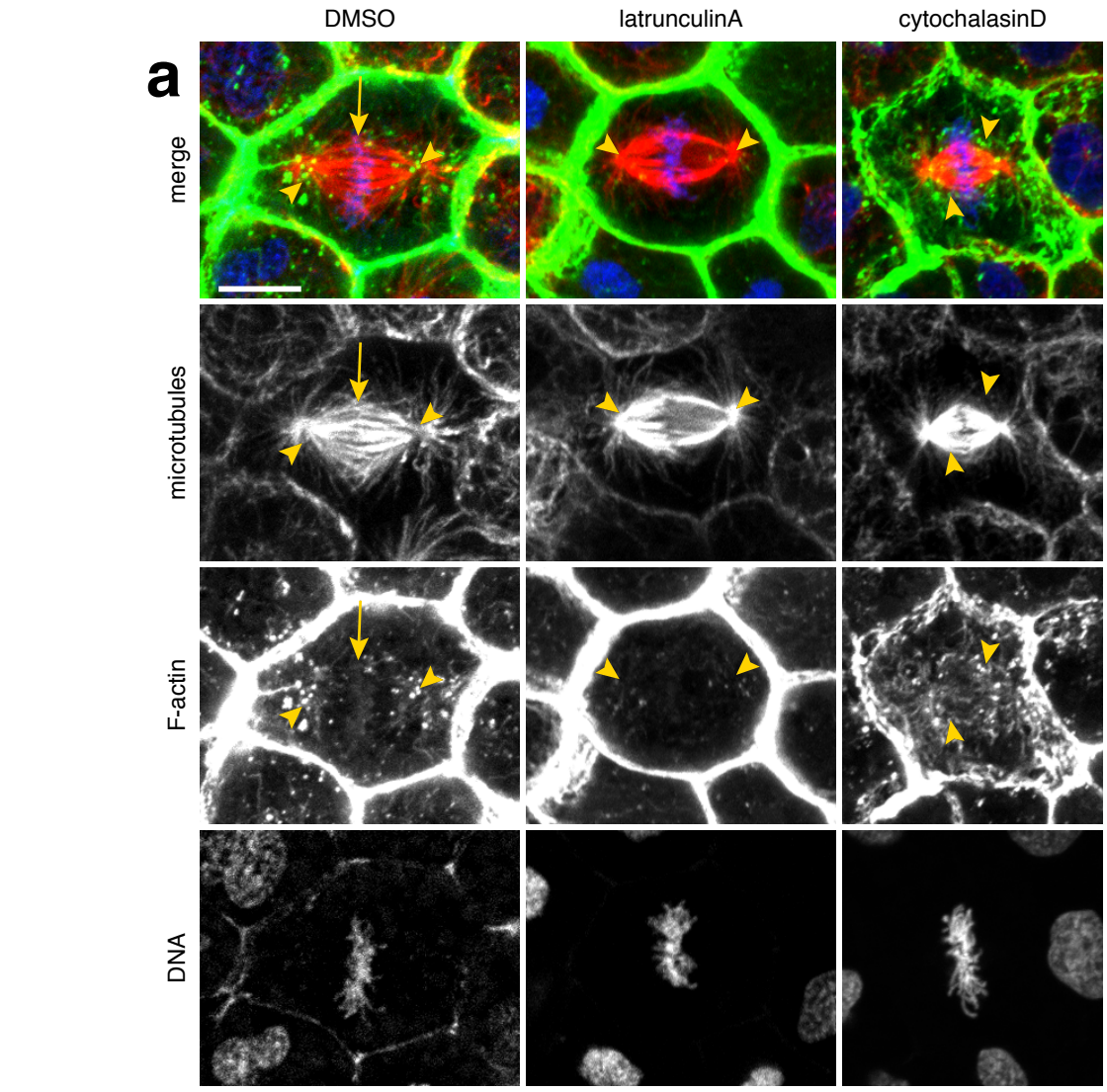
a
DMSO
latrunculinA
cytochalasinD
merge
microtubules
F-actin
DNA

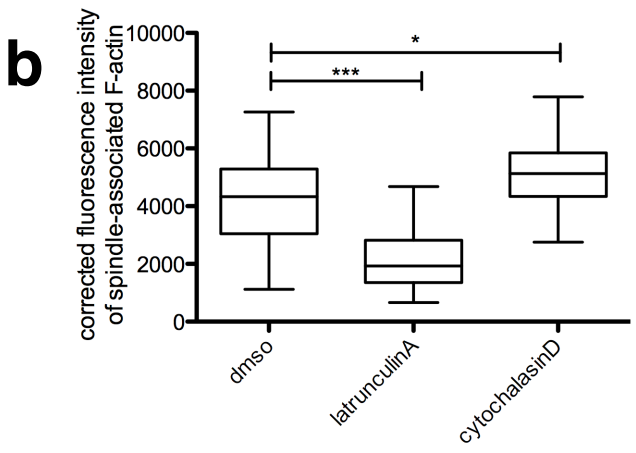
b
corrected fluorescence intensity of spindle-associated F-actin
10000
8000
6000
4000
2000
0
*
***
dmso
latrunculinA
cytochalasinD

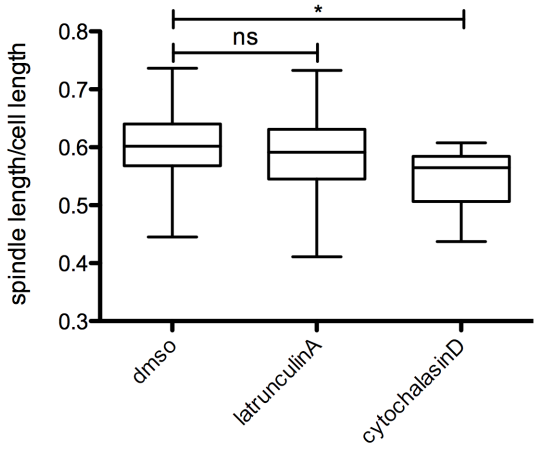
spindle length/cell length
0.8
0.7
0.6
0.5
0.4
0.3
*
ns
dmso
latrunculinA
cytochalasinD

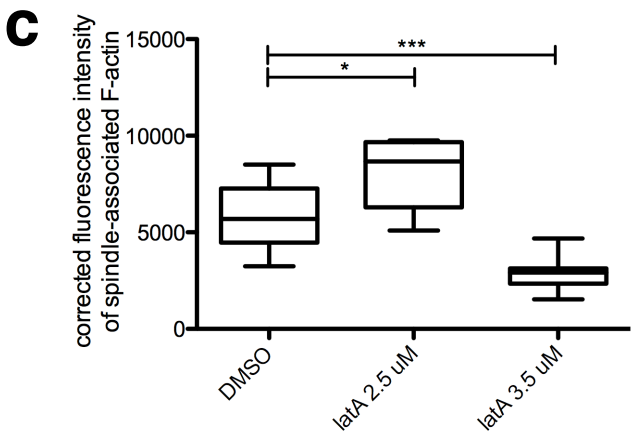
c
corrected fluorescence intensity of spindle-associated F-actin
15000
10000
5000
0
***
*
DMSO
latA 2.5 uM
latA 3.5 uM

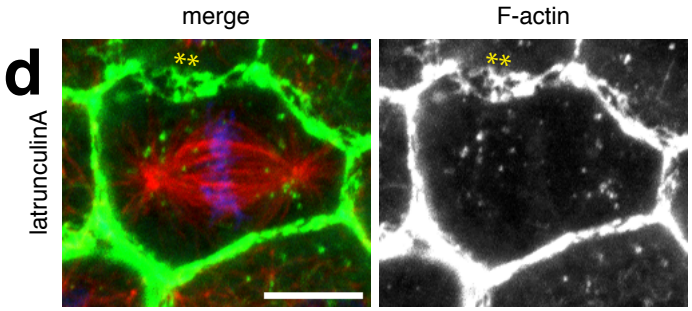
d
merge
F-actin
latrunculinA
**
**

Figure 2: The formin inhibitor SMIFH2 reduces spindle-associated F-actin and spindle length

(a) Representative images from DMSO- or SMIFH2- treated embryos of prometaphase spindles (left), metaphase spindles (center), and anaphase spindles (right). Cells are labeled for F-actin (phallodin, green), microtubules (anti-α-tubulin, red) and DNA (histone H2B, blue). Scale bar represents 10 μm. (b) Quantification of metaphase spindle length, as a percentage of cell length (left) and total F-actin fluorescence above background at the metaphase spindle (right) in DMSO and SMIFH2 treated embryos. (left DMSO: n= 92, SMIFH2: n=31; right DMSO: n=95, SMIFH2: n=48) (*** $p<0.0001$)

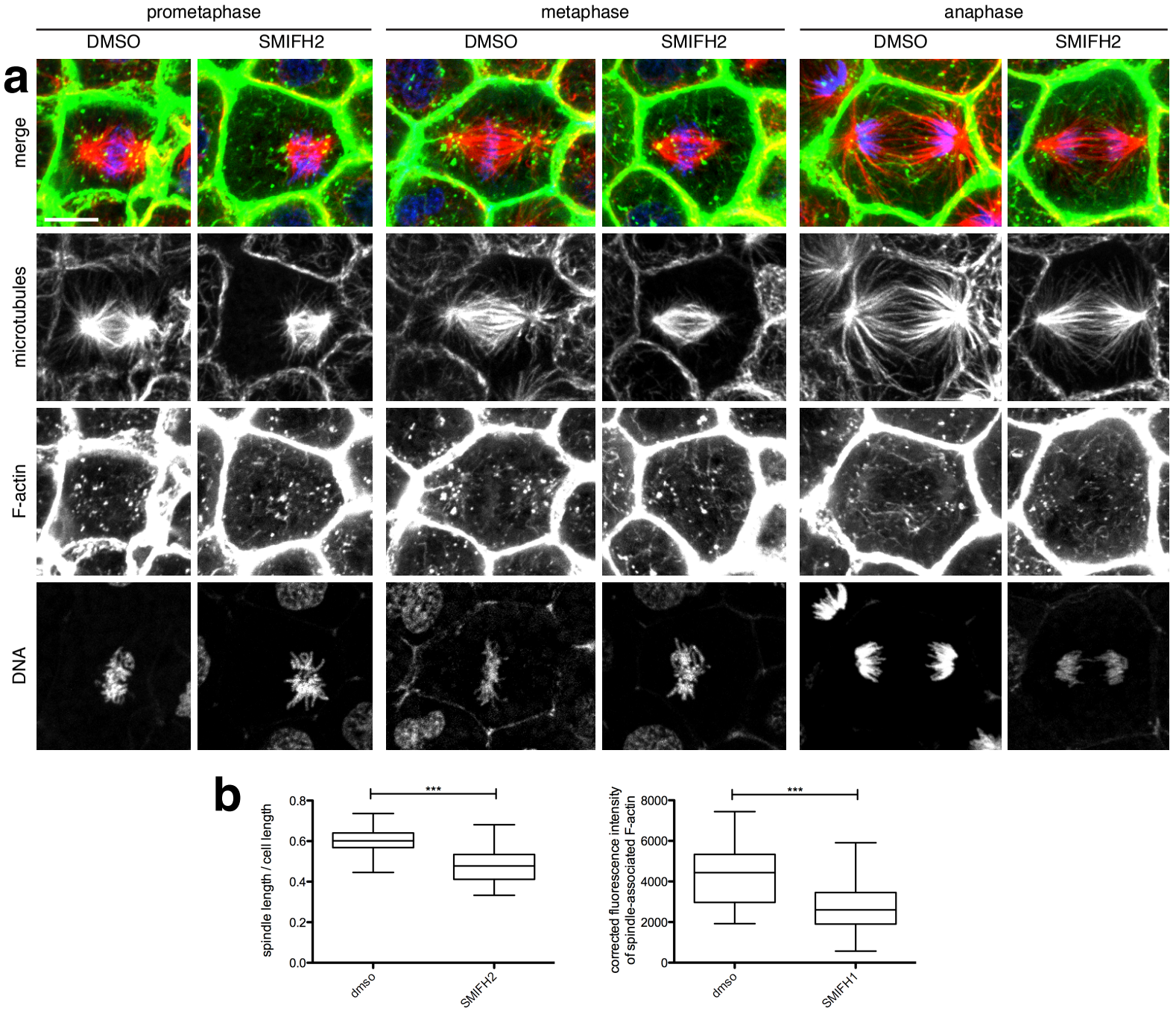
a
prometaphase
metaphase
anaphase
DMSO
SMIFH2
DMSO
SMIFH2
DMSO
SMIFH2
merge
microtubules
F-actin
DNA
b
spindle length / cell length
0.8
0.6
0.4
0.2
0.0
***
dmso
SMIFH2
corrected fluorescence intensity of spindle-associated F-actin
8000
6000
4000
2000
0
***
dmso
SMIFH1

Figure 3: Live imaging of SMIFH2-treated embryos reveals mitotic defects

(a) Timelapse montage from DMSO treated (top) and SMIFH2 treated (bottom) embryos. Arrowheads note the separation of centrosomes at NEB. (b) Quantification of the time cells spent in mitosis (from NEB to anaphase) of DMSO and SMIFH2 treated embryos. (c) Time-lapse montage of cells expressing AuroraB-3XeGFP (green) and mCherry-α-tubulin (red) that were treated with SMIFH2 (bottom) or DMSO as a control (top). Although kinetochores are not properly aligned at the metaphase plate in SMIFH2-treated cells, anaphase is triggered after a short delay. Time shown in minutes and seconds. Scale bars represent 10 μm. (DMSO: n=10, SMIFH2: n=6) (*** $p<0.0001$)

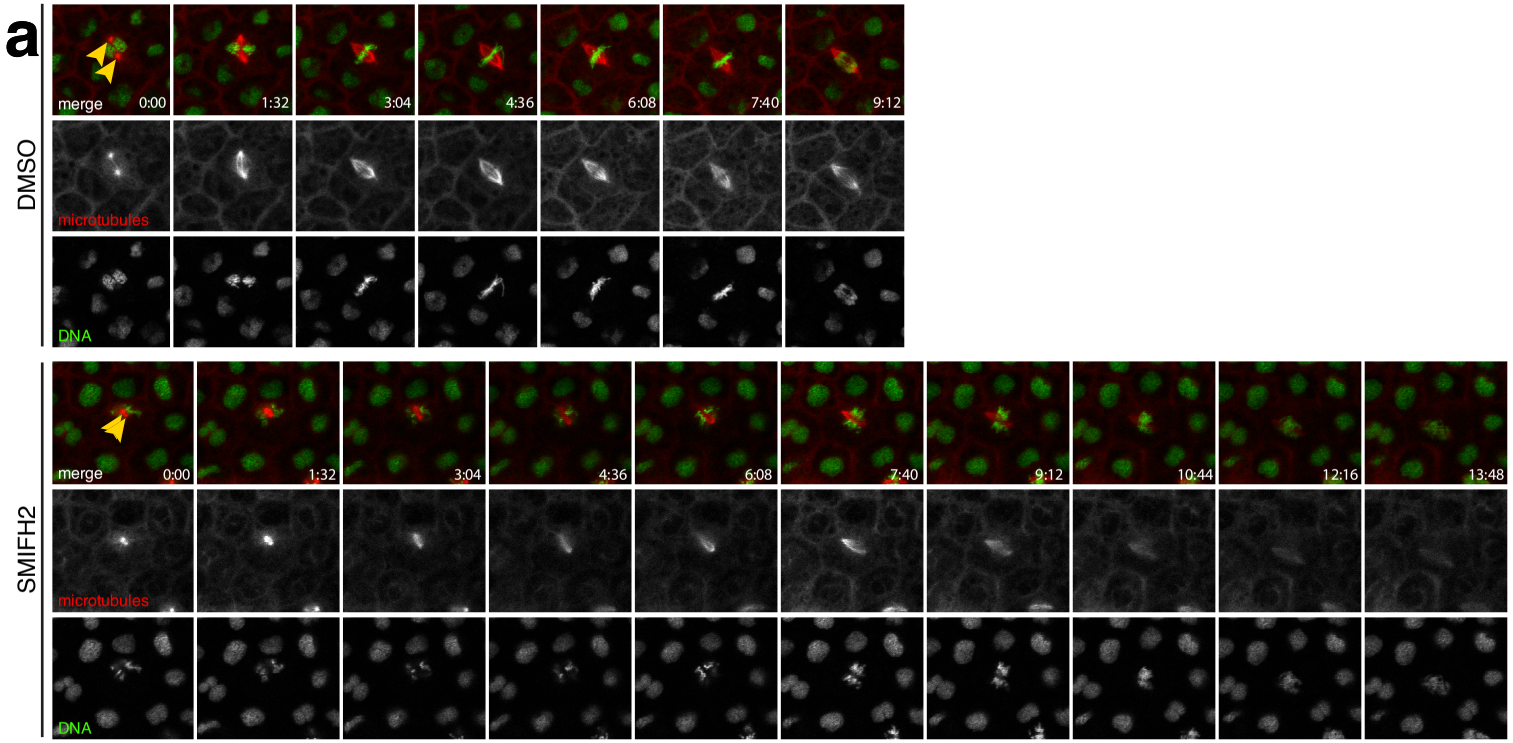
a
DMSO
merge
0:00
1:32
3:04
4:36
6:08
7:40
9:12
microtubules
DNA
SMIFH2
merge
0:00
1:32
3:04
4:36
6:08
7:40
9:12
10:44
12:16
13:48
microtubules
DNA

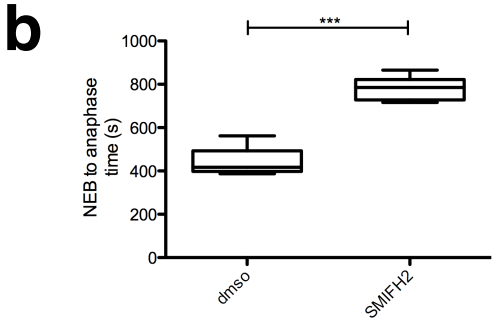
b
***
1000
800
600
400
200
0
NEB to anaphase time (s)
dmso
SMIFH2

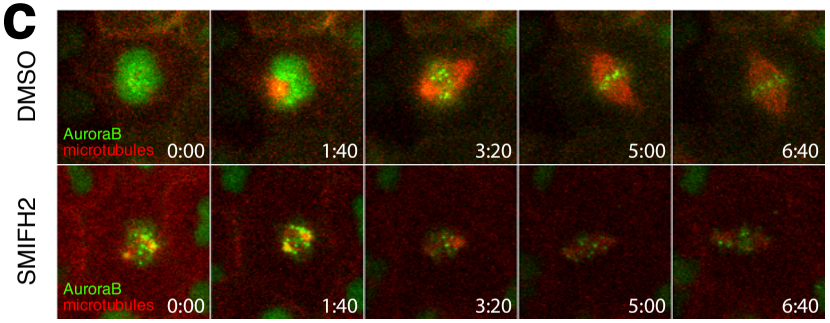
c
DMSO
AuroraB
microtubules
0:00
1:40
3:20
5:00
6:40
SMIFH2
AuroraB
microtubules
0:00
1:40
3:20
5:00
6:40

Figure 4: Comparison of the effects of F-actin and microtubule depolymerizers

(a) Confocal micrographs of metaphase spindles from embryos treated with DMSO (control), latrunculin A, SMIFH2, or nocodazole. Cells were fixed and labeled for F-actin (phalloidin, green), microtubules (anti-α-tubulin, red), and DNA (histone H2B, blue). Scale bar represents 10 μm. (b) Quantification of spindle length (left) and spindle displacement (right) during metaphase. Spindle length is represented as a percentage of cell length and spindle displacement is the distance between centroid of the cell and the metaphase spindle. (left DMSO: n=92, latrunculin A: n=53, SMIFH2: n=31, nocodazole: n=26; right DMSO: n=95, latrunculin A: n=44, SMIFH2: n=48, nocodazole: n=46) (c) Quantification of total spindle associated F-actin fluorescence (left) and spindle-associated puncta (right) at metaphase. Spindle F-actin fluorescence was determined by measuring fluorescence inside the outline of the metaphase spindle body and correcting for background signal in each image. For F-actin puncta distribution during metaphase, the total area of spindle-associated puncta was determined based on the outline of spindle bodies, then divided by the total area of visible F-actin puncta during metaphase. (left DMSO: n=85, latrunculin A: n=37, SMIFH2: n=31, nocodazole: n=45; right DMSO: n=32, latrunculin A: n=12, SMIFH2: n=18, nocodazole: n=27) (** $p<0.001$, *** $p<0.0001$, ns $p>0.05$)

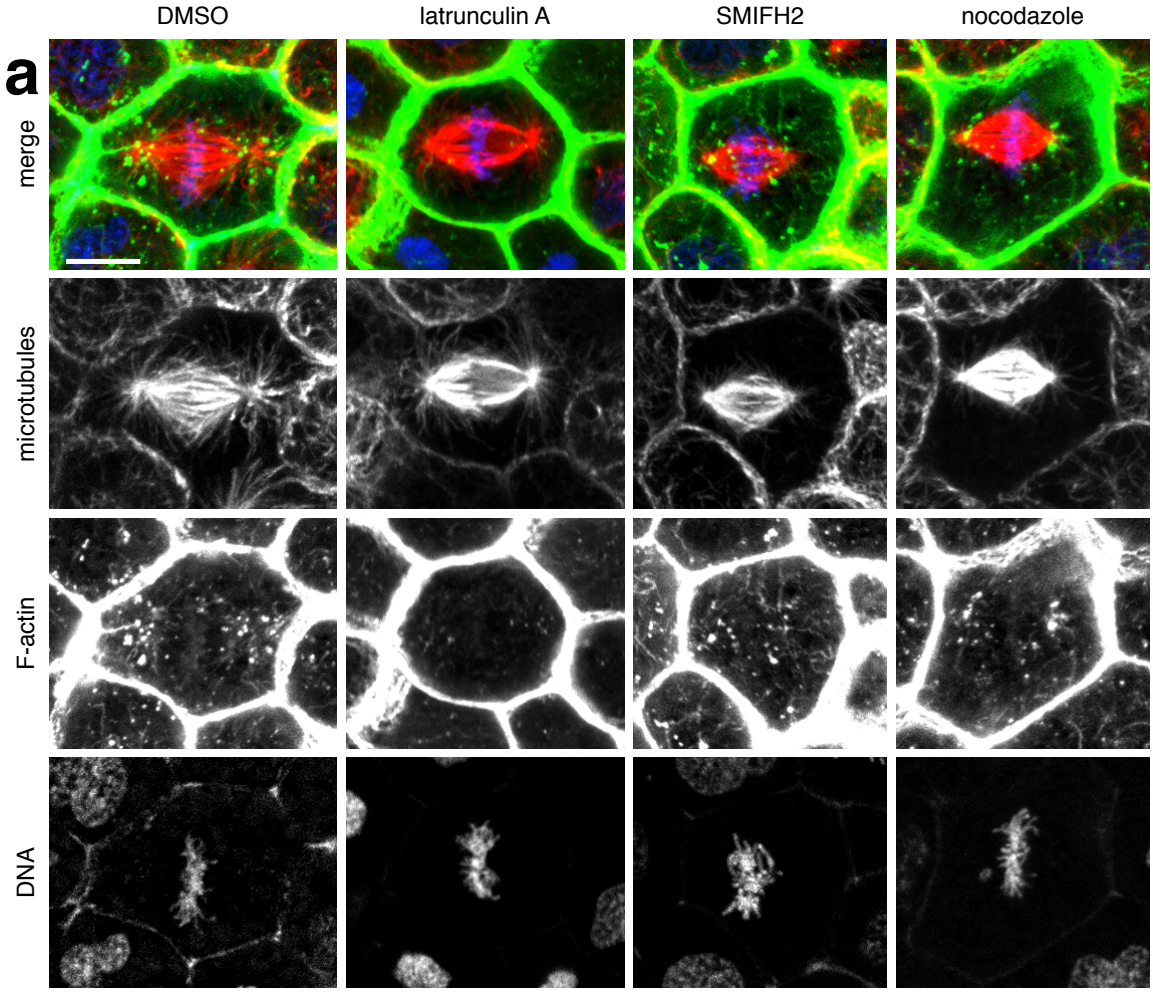
a
DMSO
latrunculin A
SMIFH2
nocodazole
merge
microtubules
F-actin
DNA

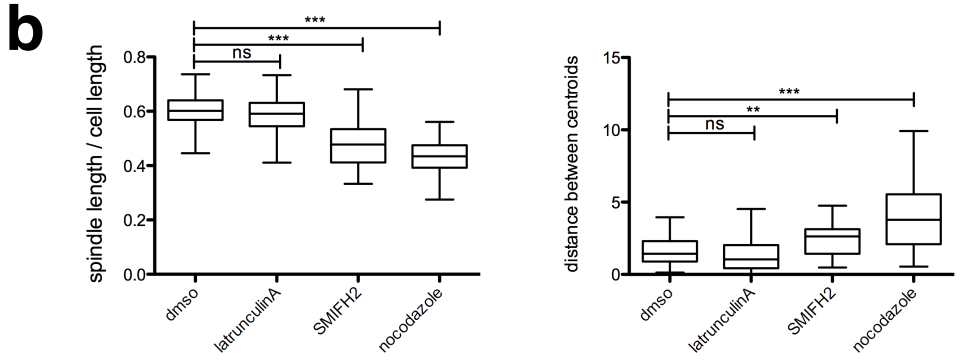
b
spindle length / cell length
0.0
0.2
0.4
0.6
0.8
***
***
ns
dmso
latrunculinA
SMIFH2
nocodazole
distance between centroids
0
5
10
15
***
**
ns
dmso
latrunculinA
SMIFH2
nocodazole

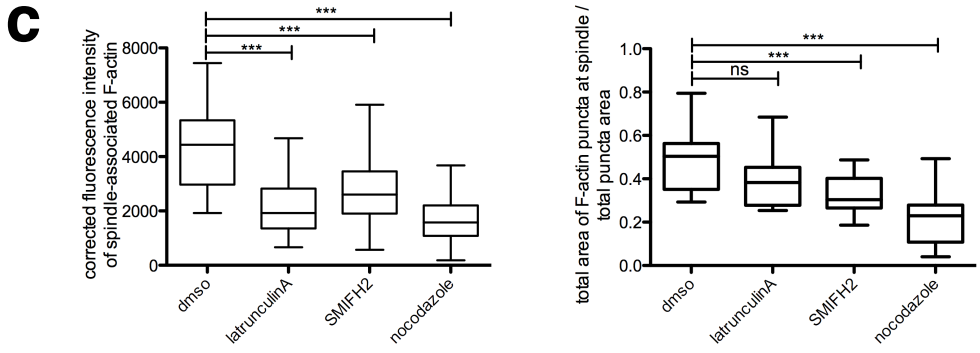
c
corrected fluorescence intensity of spindle-associated F-actin
0
2000
4000
6000
8000
***
***
***
dmso
latrunculinA
SMIFH2
nocodazole
total area of F-actin puncta at spindle / total puncta area
0.0
0.2
0.4
0.6
0.8
1.0
***
***
ns
dmso
latrunculinA
SMIFH2
nocodazole

Figure 5: Targeting actin regulators to the mitotic spindle

(a) Schematics of three targeting constructs that were generated: CyclinB1-eGFP, a fluorescently N-terminal domain of Aurora B (eGFP-ABND), and TPX2-eGFP lacking the first 241 amino acids (TPX2Δ1-241). (b) Expression of eGFP-tagged CyclinB1 in *X. laevis* at metaphase (left) and telophase (right) during live cell imaging. Dotted lines indicate the cell outline at each stage. Arrowhead indicates nearby cell that has completed cytokinesis and has degraded most of the CyclinB1-eGFP. (c) Stills taken from live cell imaging of embryos expressing eGFP-ABND (green) and mCherry-histone H2B (red). Cell outlined depicts metaphase (left) and telophase (right) expression of targeting construct. (d) Expression of TPX2(Δ1-241)-eGFP (green) and mCherry-histone H2B (red) during live cell imaging. Arrow indicates construct expression at the spindle during metaphase (left) and telophase (right). During interphase this construct is nuclear (arrowhead). Scale bars indicate 10 μm.

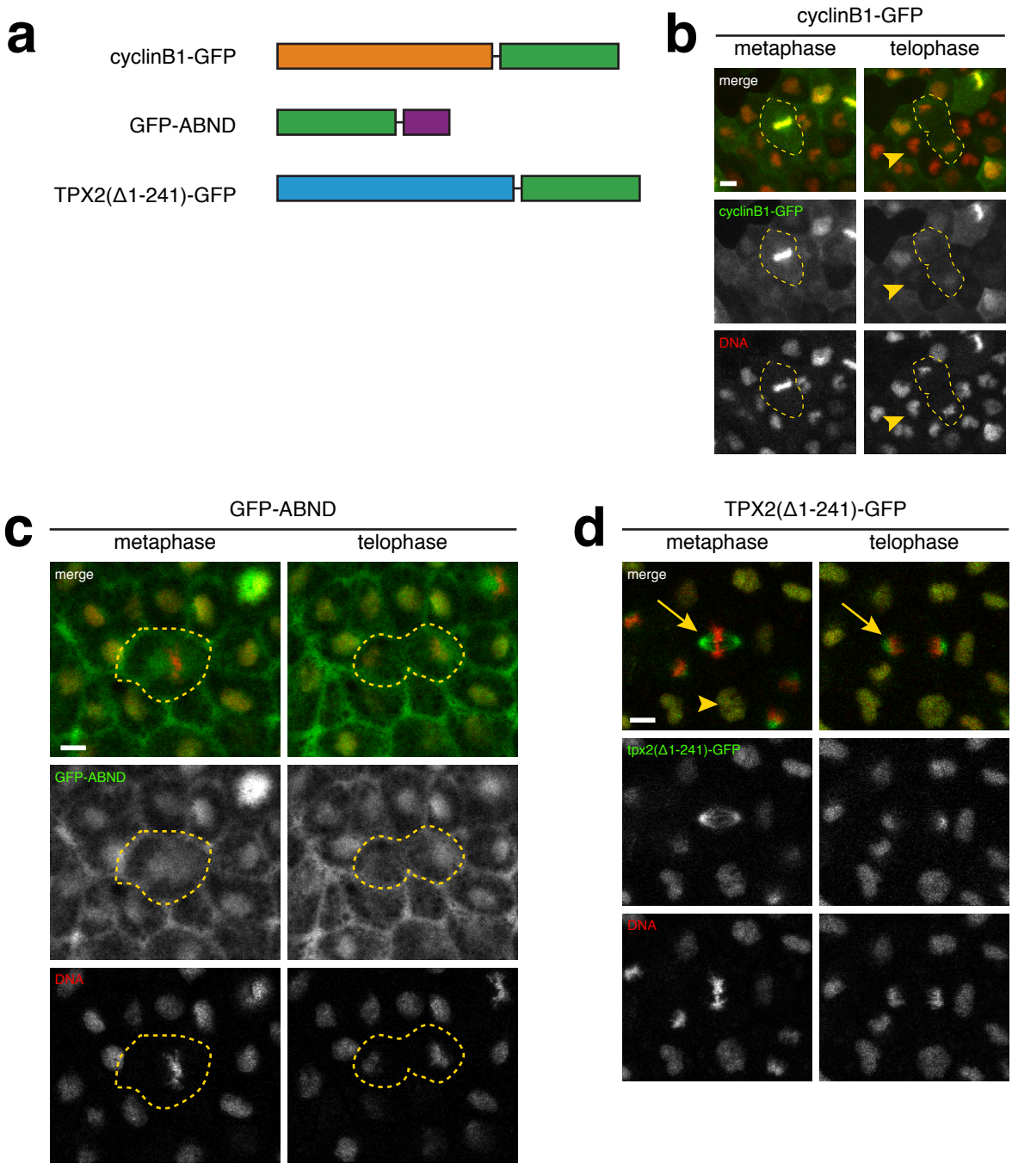
a
cyclinB1-GFP
GFP-ABND
TPX2(Δ1-241)-GFP
b
cyclinB1-GFP
metaphase
telophase
merge
cyclinB1-GFP
DNA
c
GFP-ABND
metaphase
telophase
merge
GFP-ABND
DNA
d
TPX2(Δ1-241)-GFP
metaphase
telophase
merge
tpx2(Δ1-241)-GFP
DNA

Figure 6: Effects of spindle-targeted actin regulator expression

(a) Stills from living imaging of cells expressing a CyclinB1-capping protein (CB1-CPα) fusion, eGFP-UtrCH (F-actin, green) and mCherry-histone H2B (DNA, red). Expression of this construct causes an increase in short F-actin cables, as visualized with eGFP-UtrCH (arrows) and the formation of multipolar cells. Although spindle-associated F-actin is affected by this construct, cortical F-actin appears normal and cells successfully complete cytokinesis (arrowheads). (b) Live imaging of unregulated gelsolin (gelsolin-Ca^{2+}) fused to TPX2-eGFP reveals localization to the spindle microtubules (arrow) as well as cortical structures (arrowheads). DNA (mCherry-histone H2B) is shown in red. (c) Stills from live imaging of inactive (S3D) or active (S3A) cofilin fused to TPX2 (untagged), co-injected with cyclase associated protein (CAP, untagged), mCherry-α-tubulin (microtubules, red), and eGFP-histone H2B (DNA, green). Spindles in cells expressing spindle-targeted inactive cofilin (top, arrows) appear normal, while spindles in cells expressing active cofilin (bottom, arrows) appear fragmented and chromosomes appear dispersed (arrowheads). Scale bars represent 10 μm. (d) Quantification of the length of time cells spent in mitosis in the absence (control, cyclinB1 alone) of presence of unregulated gelsolin fused to CyclinB1 (CB1-gelsolin-Ca^{2+}). Expression of CB1-gelsolin-Ca^{2+} results in increased time in mitosis (left), entirely due to an increase in the timing between metaphase and anaphase (right). (control: n=41, CB1-gelsolin-Ca^{2+}: n=53) (*** $p<0.0001$, ns $p>0.05$)

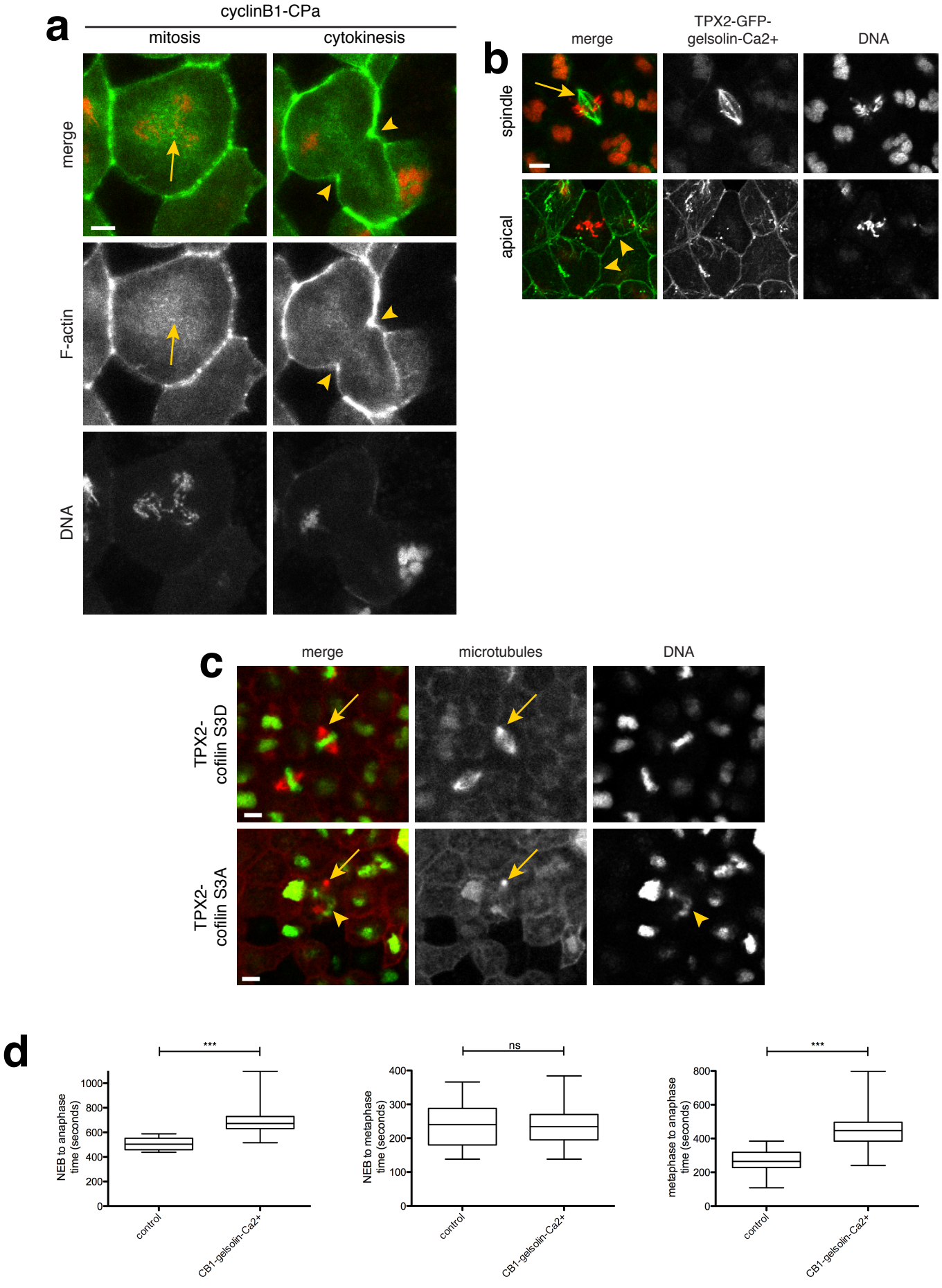
a
cyclinB1-CPa
mitosis
cytokinesis
merge
F-actin
DNA
b
merge
TPX2-GFP-gelsolin-Ca2+
DNA
spindle
apical
c
merge
microtubules
DNA
TPX2-cofilin S3D
TPX2-cofilin S3A
d
NEB to anaphase time (seconds)
***
control
CB1-gelsolin-Ca2+
NEB to metaphase time (seconds)
ns
metaphase to anaphase time (seconds)

Figure 7: Model of F-actin redistribution in response to various inhibitors

(a) Schematic representations of the metaphase spindle and associated F-actin structures in a control treatment (DMSO) versus latrunculinA (F-actin depolymerization), cytochalasin D (F-actin depolymerization), SMFH2 (formin inhibition), or nocodazole (microbutule depolymerization) treatments. Microtubules are represented in red and F-actin cables and puncta are represented in green. Cell outlines are represented in gray.

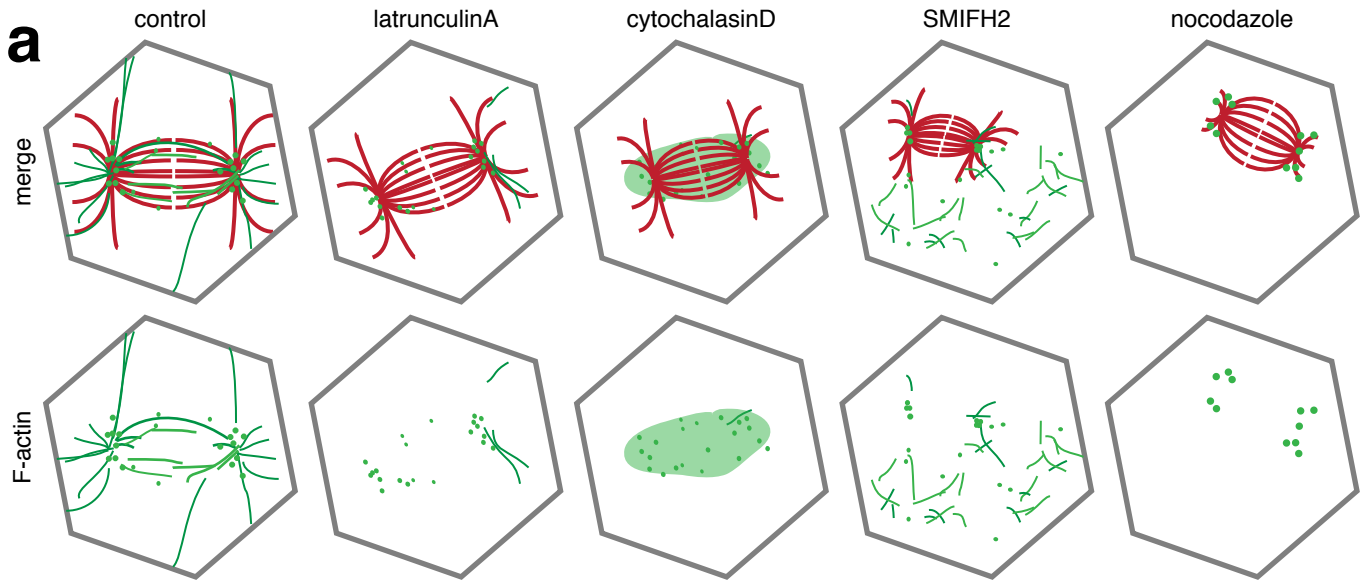
a
control
latrunculinA
cytochalasinD
SMIFH2
nocodazole
merge
F-actin

Discussion

In this work, I examined the effects of various manipulations on spindle-associated F-actin. The results of these manipulations are discussed below.

Previous studies of F-actin during mitosis have focused on the contribution of cortical F-actin to this process. Often this involves the use of actin inhibitors, which affect F-actin ubiquitously throughout the cell, or knockdown of actin regulators coupled with monitoring changes to cortical actin structures. I used two approaches to disrupt spindle-associated F-actin more specifically: 1) low-dose treatments with inhibitors of F-actin polymerization or nucleation with a close examination of changes to spindle F-actin and, 2) targeted expression of actin regulators to the mitotic spindle. The results of targeted actin disruption by the second approach are inconclusive, due to the necessity of additional controls and the lack of a demonstrated decrease in spindle-associated F-actin. However, my findings from drug treatments are discussed below.

The use of latrunculin A or cytochalasin D, two chemical inhibitors of F-actin polymerization, each uniquely affected spindle F-actin. Low-dose latrunculin A caused a loss of F-actin cables and an overall decrease in F-actin signal at the spindle (as represented in Figure 7a). In contrast, cytochalasin D treatment at low doses caused an increase in the intensity of F-actin at the spindle, though individual cables became obscured (Figure 7a), possibly indicating the presence of many short fragments of F-actin. Additionally, cytochalasin D treatment caused a decrease in spindle length while latrunculin A treatment had no significant effect. This difference may represent how these drugs differentially interact with actin. For example, the activity of endogenous actin nucleators (i.e. formins) may compete for filament end binding specifically with cytochalasin D, but not latrunculin A, which binds actin monomers. Added to this is the possibility that F-actin is playing both a positive and negative role in spindle length control, as suggested by Woolner et al. (2008). Briefly, the conclusion of this study

suggested that F-actin might promote both spindle lengthening through interactions with astral microtubules and the cell cortex, and that together with myosin10 F-actin might also have a spindle shortening function. By using this model as a guide, the results described above could be explained by disproportionate effects of low dose latrunculin A and cytochalasin D on different populations of actin filaments. That is, perhaps latrunculin A is equally affecting F-actin that contributes to spindle lengthening and spindle shortening, while cytochalasin D is having a greater effect on the F-actin that contributes to spindle lengthening. This would further indicate that the plus ends of actin filaments are involved in the spindle lengthening effect of F-actin, as a compound that specifically affects plus ends results in spindle length decrease.

To better understand how spindle actin is regulated, I used to different chemical inhibitors of actin nucleation factors. Inhibition of formin nucleation activity by SMIFH2 had several consequences for mitotic cells, including a decrease in spindle length, spindle displacement from the center of cells, and chromosome alignment errors. A close examination of F-actin localization determined that actin structures were altered as a result of formin inhibition. Spindle-associated F-actin was displaced from the spindle (represented in Figure 7a), as indicated by changes in the endogenous F-actin signal distribution, and a decrease in total F-actin fluorescence. This collection of phenotypes is likely the result of the loss of activity from more than one formin protein, as SMIFH2 does not discriminate between each of the 15 known formins. For example, the formin mDia3 helps stabilize kinetochore-microtubule connections that are necessary for proper chromosomal capture and segregation (Cheng et al., 2011). Thus the chromosome alignment defect observed in SMIFH2-treated cells may be at least partly attributed to this known function of mDia3. However, other defects including impaired metaphase spindle formation and changes in cytoplasmic and spindle F-actin organization are likely due to loss of function of potentially one or, more probably, several additional formins.

Furthermore, the severity of these results may be due to changes in both microtubule and actin networks during mitosis, as several formins have reported interactions with microtubules (Bartolini & Gunderson, 2010). To further address the possibility of actin:microtubule interactions at the spindle I treated embryos with low-dose nocodazole, a microtubule depolymerizing agent, and again examined F-actin structures. Intriguingly, disruption of spindle microtubules decreased spindle associated F-actin and caused an increase in the size of F-actin puncta (represented in Figure 7a). This indicates there is likely some level of interplay between spindle microtubules and spindle F-actin that is required for proper spindle function during mitosis.

Collectively, the results of these manipulations point to the activity of one or more formins as regulators of spindle F-actin. This is also supported by my previously described characterization of spindle-associated F-actin—i.e. that it appears as unbranched actin cables—which suggests nucleation of unbranched actin filaments, such as generated by formins.

Materials & Methods

Plasmids

The mCherry-histone H2B, mCherry-α-tubulin, eGFP-UtrCH, and pCS2+3XeGFP plasmids were made as previously described (Burkel et al., 2007; Bement & Miller, 2009). AuroraB-3XeGFP was obtained from Stacey Kigar (University of Wisconsin).

CyclinB1 was a gift from Conly Rieder (Wadsworth Center). Full-length CyclinB1 or the first 321 nucleotides were amplified and subcloned in front of eGFP in the eGFP-pCS2 vector using BamH1 and Nco1. TPX2 was also cloned in front of eGFP (BamH1/Nco1). Capping proteins (CPα, CPβ) were obtained from OpenBiosystems (Life Technologies) and cloned into pCS2 vectors with Xho1 and Xba1. Cofilin was obtained from Josh Sandquist (University of Wisconsin) and cloned into eGFP-pCS2 with EcoR1 and SnaB1. Gelsolin was obtained from OpenBiosystems (Life Technologies) and the full length protein minus a C-terminal Ca^{2+} regulatory domain was cloned into eGFP-pCS2 with BspE1 and Xho1.

Embryo preparation

Adult *X. laevis* females were injected with 800 units of human chorionic gonadotropin (HCG; MP BioMedicals) into the dorsal lymph sac 1 d prior to use. Eggs were laid into 1X MMR (100 mM NaCl, 2 mM KCl, 1 mM MgCl2, and 5 mM Hepes, pH 7.4) and fertilized in vitro with macerated testes. Embryos were dejellied in 2% cysteine solution (in 0.1X MMR, pH 7.8), and then rinsed five times in 1X MMR and five times in 0.1X MMR. Overnight embryo culture was in 0.1X MMR at 17°C.

mRNA preparation and embryo microinjection

All mRNA was transcribed *in vitro* using the mMessage Machine SP6 kit (Life Technologies) and reactions were purified with the RNeasy Mini Kit (Qiagen). Embryos

were submerged in 0.1X MMR + 5% Ficoll (Sigma) and injected with 5nL of mRNA at the 2-cell stage. eGFP- and mCherry-histone H2B was injected at 12.5 µm/mL for both live and fixed cell imaging. For live cell imaging, mCherry-α-tubulin was injected at 25 µg/mL. After microinjection, embryos were incubated in 0.1X MMR at 17°C for 18-20 hours before live imaging or processing for fixation.

Drug treatments

Embryos were incubated at room temperature using the following concentrations of each drug: 3 µM latrunculinA, 30 µM cytochalasinD, 20 µM SMIFH2, and 5 µm nocodazole in 0.1X MMR. As a control, embryos were simultaneously incubated in DMSO in 0.1X MMR at the corresponding concentration. After incubation, embryos were fixed (as described below) or dropped into 0.1X MMR, mounted on a slide and imaged live.

Fixation

To fix for F-actin labeling only or double labeling of F-actin and microtubules, embryos were briefly rinsed in 1X PBS, then dropped into a modified paraformaldehyde (PFA) solution. This consisted of a “superfix” buffer (100 mM KCl, 3 mM MgCl, 10 mM HEPES, 150 mM sucrose, pH 7.4) to which the following was added (listed in final concentrations): 3.7% PFA, 10% DMSO, 2mM EGTA, 0.2 µM paxitaxol, 0.1% gluteraldehyde, and 0.02% Triton-X-100. Flourescent phalloidin (AlexaFlour 488, Life Technologies) was added to the fix buffer at a concentration of 1:200 for same day imaging, or added to primary and secondary antibody incubations at 1:100. Embryos were incubated for 1 h on an orbital shaker at room temperature to fix. Microtubules were labeled with mouse monoclonal anti-α-tubulin (DM1A, Sigma) at a dilution of 1:20,000 and a donkey derived anti-mouse secondary was used at 1:10,000 (AlexaFluor

647, Life Technologies). Primary antibody incubations were 3 h at room temperature while secondary incubations were overnight at 4°C.

Microscopy and data analysis

Imaging of all fixed experiments was conducted with a 1.4 NA 60X oil immersion objective on a Nikon Eclipse Ti inverted microscope using Prairie View software (Brüker). Z-series were acquired using 0.5 µm step size and were reconstructed in Fiji. For live imaging, embryos were mounted in 0.1X MMR and imaged using a 1.0 NA 40X oil immersion or a 1.4 NA 60X oil immersion objective on the Nikon Eclipse Ti microscope. Single-plane time series were captured at 2.3 s or less and processed using Fiji software. Multi-plane live imaging was processed using Velocity software (PerkinElmer). Data analysis and graphing was conducted with Fiji, Microsoft Excel, and Prism 5 software. Quantitative image analysis of F-actin intensity at mitotic spindles was performed by measuring the integrated density at the spindle and using the following equation: Corrected fluorescent intensity = integrated density – (area of selected region X mean fluorescence of background readings). Five separate background regions were measured for each image and their mean fluoresce was averaged (modified from Potapova et al., 2011). CellProfiler (Carpenter et al., 2006) was used to identify spindle-associated F-actin puncta versus cytoplasmic puncta and Fiji was used quantify these results.

Chapter 3

The formin IFL2 is a nucleator of cytoplasmic F-actin during mitosis

Abstract

The mitotic spindle is made up of microtubules and microtubule-associated proteins that work in concert to drive chromosome segregation. A new study of non-cortical mitotic actin filaments (F-actin) has characterized the localization of F-actin cables and puncta at the spindle. Manipulation of these structures via inhibition of actin polymerization and nucleation has indicated a potential role for formin-mediated actin regulation. To identify formins involved in this process, I conducted a candidate localization screen. Inverted formin like 2 (IFL2), the *Xenopus laevis* homolog of human inverted formin 2 (hINF2), was found to localize to the cytoplasm during mitosis. Knockdown of IFL2 by multiple approaches resulted in a reduction of spindle-associated F-actin, suggesting IFL2 plays a role in the generation of spindle-associated F-actin. Reintroduction of full-length IFL2 into a knockdown background rescued this phenotype. To further characterize the function of IFL2 during mitosis, I conducted overexpression and dominant negative experiments. Overexpression of IFL2 resulted in the appearance of F-actin aggregates in close proximity with the spindle midplane, condensed chromosomes, and spindle poles. Dominant negative expression of the FH2 domain of IFL2 also disrupted the F-actin associated with the mitotic spindle, specifically in a disappearance of F-actin cables and an apparent increase in actin puncta at the spindle. Collectively, these results implicate IFL2 as a regulator of spindle-associated F-actin in the *X. laevis* early embryo.

Introduction

The actin cytoskeleton is regulated at several levels, including everything from monomer sequestration to the remodeling of large actin networks (reviewed in Lee & Dominguez, 2010). The formation of actin trimers—referred to as actin nucleation—is the first step in creating new actin filaments. Although unregulated actin filament polymerization is rapid and spontaneous, actin nucleation is a kinetically unfavorable process that cells overcome through the use of nucleation factors. These include the Arp2/3 complex, which nucleates branched actin networks, formin family proteins and WH2-containing proteins. Both formins and WH2-containing proteins, such as Spire, nucleate unbranched actin filaments through differing mechanisms.

Formins are the largest and most diverse class of actin nucleators, consisting of at least 15 unique members in mammals (Breitsprecher & Goode, 2013). Collectively, formins participate in a wide range of cytoskeletal processes including filapodia and lamellapodia formation (Scherinbeck et al., 2005; Yang et al., 2007), cytokinetic ring formation (Severson et al., 2002), and morphogenic movements such as gastrulation and neural tube closure (Habas et al., 2001; Lai et al., 2008). The signature feature of formin proteins is their formin homology (FH) domains, through which they interact with actin. Formin FH2 domains enable homodimer formation and the direct association of formins with barbed actin filament ends. The nearby FH1 domain can bind profilin-bound actin monomers, which allows formins to bring new monomers into close proximity with dimerized FH2 domains (Schonichen & Geyer, 2010; Cheserone et al., 2010). The activity of these two domains is responsible for the proteins' ability to nucleate and elongate filaments, and to stay associated with growing filament ends, which prevents binding of capping proteins (Zigmond et al., 2003; Kovar et al., 2005).

In addition to actin assembly activity, some formins have been characterized as functioning in actin bundling (Lew et al., 2002), actin severing and depolymerization

(Chhabra & Higgs, 2006), and microtubule binding (Gaillard et al., 2011). Thus, not only do formins contribute to actin cytoskeleton formation and reorganization, they reach beyond those roles to influence the microtubule cytoskeleton and perhaps serve as key mediators of actin:microubule cross-talk. A handful of formins have established roles in what were previously considered strictly microtubule-based processes. For example, Formin-2 nucleates actin filaments found within meiotic spindles in mouse oocytes (Schuh & Ellenberg, 2008; Azoury et al., 2008) and the formin mDia3 participates in the formation of stable kinetochore microtubule attachments through its interaction with microtubules (Cheng et al., 2011).

In this study, I report on the role of inverted formin 2-like (IFL2) in spindle-associated F-actin regulation. I show that IFL2 knockdown disrupts mitotic spindle function and decreases spindle-associated F-actin. I further show that F-actin depletion can be rescued by full length IFL2 expression.

Results

A candidate screen of actin nucleators reveals IFL2 localizes to the nucleus in interphase and is diffusely cytoplasmic during mitosis

To determine which actin nucleators may be regulating spindle-associated F-actin, I conducted a candidate screen. I assessed the localization of each candidate during mitosis using live cell imaging. Fluorescently labeled fusions were generated for four candidate proteins—three formin proteins (Daam1, fmnl-1, and IFL2) and the WH2-containing protein, Spire (Eg6) (Figure 1a). Expression of Daam1 intriguingly decorated the cytoplasm with occasional puncta near the mitotic spindle (Figure 1b), however this protein also brightly labeled the cell cortex (Figure 1b). Although the cytoplasmic localization of this protein may warrant future examination, the goal of this screen was to find candidates that solely localize to the cytoplasm. Formin-like 1 (fmnl1) expression appeared to correspond with cellular membranes, both at cell boarders and around putative vesicles (Figure 1b). The WH2-containing protein Spire—selected due to its interactions with Formin 2, which regulates meiotic spindle positioning (Leader et al., 2002)—displayed cytoplasmic localization (Figure 1b). However, this localization was reminiscent of GFP-only expression (data not shown).

One candidate, inverted formin like 2 (IFL2), localized to the nucleus in interphase and the cytoplasm during M-phase (Figure 1c). The interphase localization of IFL2 was interesting as many proteins involved in mitotic spindle formation and function are housed in the nucleus during interphase (e.g. AuroraB, TPX2, Ran GTPase). IFL2 did not clearly localize to the spindle during mitosis, which may indicate that the fluorescently-tagged version of IFL2 binds less competitively than endogenous IFL2. However, at high levels of expression, fluorescent IFL2 did aggregate specifically to structures near condensed chromosomes during mitosis (data not shown).

IFL2 knockdown decreases spindle-associated F-actin

To determine the function of IFL2, I used both morpholino and small interfering RNA (siRNA) approaches to knockdown endogenous protein levels. Translation-blocking morpholinos (MO) designed to target the 5' end of IFL2 mRNA were injected into embryos and resulting effects were monitored by both live and fixed cell imaging. As compared to controls, IFL2 MO injection resulted in a reduction of spindle-associated F-actin structures (Figure 2a, 2c). As a secondary means of IFL2 knockdown, siRNAs were designed against the mRNA sequence. Argonaut-2 was co-injected with siRNAs to activate the *X. laevis* siRNA pathway (Lund et al., 2011). Similar to morpholino injections, siRNA reduced overall F-actin structures at the spindle (Figure 2b). Quantification of F-actin fluorescence at the metaphase spindle revealed a ~50% reduction of spindle-associated F-actin when IFL2 is knocked down by morpholino or siRNA (Figure 2c).

Live cell imaging of IFL2 knockdown by morpholino also revealed mitotic defects. Embryos were injected with control or IFL2 morpholinos, and markers for microtubules (mCherry-emtb) and DNA (eGFP-histone H2B). Morphant mitotic cells displayed less spindle movement (Figure 3a). These spindles also took significantly longer to establish the metaphase spindle (NEB to metaphase) and spent less time between metaphase and anaphase (Figure 3b).

Expression of morpholino-resistant IFL2 partially rescues knockdown phenotype

To rescue IFL2 knockdown, I designed a morpholino-resistant IFL2 by site-directed mutagenesis of nucleotides bound by IFL2 MO. This mutagenesis preserved the amino acid residues to be translated but made the injected mRNA resistant to morpholino hybridization. Embryos were injected with control MO, IFL2 MO, or IFL2 MO plus gene replacement IFL2 (IFL2gr). As shown in Figure 4, expression of IFL2gr in an

IFL2 morphant background rescued the reduction in spindle-associated F-actin in fixed samples. Additionally, while cell size was increased in embryos injected with IFL2 MO (Figure 3a), expression of IFL2gr rescued this phenotype (Figure 4b).

Overexpression of IFL2 increases cytoplasmic F-actin cables and negatively impacts mitotic spindles

To assess the consequences of IFL2 overexpression, embryos were injected with untagged IFL2, mCherry-α-tubulin, and eGFP-histone H2B and monitored by live cell imaging. Compared to spindles in control cells, IFL2 overexpression caused spindles to become tethered to the cell edge (Figure 5a). This occurred due to an interaction between condensed chromosomes and the lateral cell membrane and/or cell cortex at the spindle midplane. As a consequence, chromosomes became detached during anaphase (not shown) and remained aggregated close to the cell midbody (Figure 5a). Cells from embryos expressing IFL2 and labeled for microtubules (anti-α-tubulin) reveal a reduction in spindle length and confirm the generation of multi-polar spindles (Figure 6b, 6c).

To examine the effect of IFL2 overexpression on spindle-associated F-actin, I injected embryos with untagged IFL2 and mCherry-histone H2B then fixed and labeled for F-actin. In mitotic cells overexpressing IFL2, F-actin signal was detected as bright aggregates localized near condensed chromosomes, the spindle midplane, and spindle poles (Figure 5b). F-actin cables were either absent (Figure 5b) or found in high abundance in large multipolar cells (Figure 5c). Additionally, both detached chromosomes (Figure 5b) and tethered chromosomes (Figure 5c) were observed.

Dominant-negative expression of IFL2 FH2 domain increases spindle-associated F-actin puncta and creates multipolar spindles

To further characterize IFL2 function during mitosis, I performed a dominant negative experiment by analyzing embryos expressing the FH2 domain of IFL2. Formin family proteins form homodimers through FH2-FH2 binding, thus the IFL2 FH2 domain should bind endogenous IFL2 and block its function. Without the nearby FH1 domain, IFL2 would be unable to nucleate and polymerize actin filaments, though a full length IFL2 bound to FH2 alone may still be able to interact with actin filament ends.

Embryos were injected with untagged IFL2 FH2 domain (IFL2-FH2) and mCherry-histone H2B, fixed and labeled for F-actin (phalloidin). Similar to IFL2 knockdown (Figure 2), expression of IFL2-FH2 decreased the appearance of spindle-associated actin cables (Figure 6a). Furthermore, high expression levels of IFL2-FH2 resulted in an increase in F-actin puncta at the spindle (Figure 6a, anaphase) which may indicate the presence of IFL2:IFL2-FH2 dimers bound to F-actin structures but unable to polymerize actin filaments.

Figure 1: Candidate nucleator screen reveals IFL2 localization is nuclear during interphase and cytoplasmic during M-phase

(a) Schematic representation of candidate nucleators screened: Disheveled associated activator of morphogenesis 1 (xDaam1; GenBank AAH73482), formin-like 1 (xfmnl-1; NCBI NP_001086147), Spire (xspire; NCBI NP_001086543), human inverted formin 2 (hINF2), and inverted formin like 2 (xIFL2; NCBI NP_001084562). FH1/2/3 is formin homology 1/2/3; WH2 is WASP homology 2; DAD is diaphanous autoinhibitory domain; KIND is kinase noncatalytic domain; FYVE is a zinc finger domain. (b) Stills from live cell imaging of eGFP-Daam1 (left), fmnl1-eGFP (center), and eGFP-spire (right). eGFP-Daam1 (left, green) brightly labels the cell cortex, is diffuse in the cytoplasm, and is occasionally detected in punta near the mitotic spindle (arrowheads). eGFP-fmnl1 (center, green) localizes to cell boarders and appears to outline vesicles in the cytoplasm (arrowheads). Expression of fmnl1-eGFP also generates curvatures along the apical domain of cell boarders, potentially indicating membrane localization of this protein. eGFP-Spire (right, green) is found in the cytoplasm during interphase. At NEB, eGFP-Spire is rushes into the space previously occupied by the nucleus (arrow) and appears as a cloud that tracts with the spindle (arrowhead). Microtubules (mCherry-α-tubulin) are shown in red. (c) Montage from live imaging of IFL2-3XeGFP (green) and mCherry-α-tubulin (red) depicting the rapid dispersal of IFL2-3XeGFP from the nucleus at NEB. Post NEB stills (right) show IFL2-3XeGFP is cytoplasmic during mitosis. Scale bars represent 10 μm. Time is in minutes and seconds.

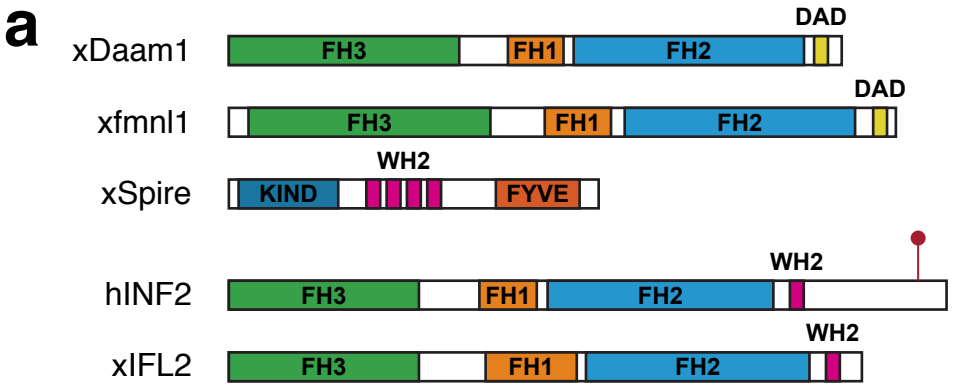
a
xDaam1
FH3
FH1
FH2
DAD
xfmnl1
FH3
FH1
FH2
DAD
xSpire
KIND
WH2
FYVE
hINF2
FH3
FH1
FH2
WH2
xIFL2
FH3
FH1
FH2
WH2

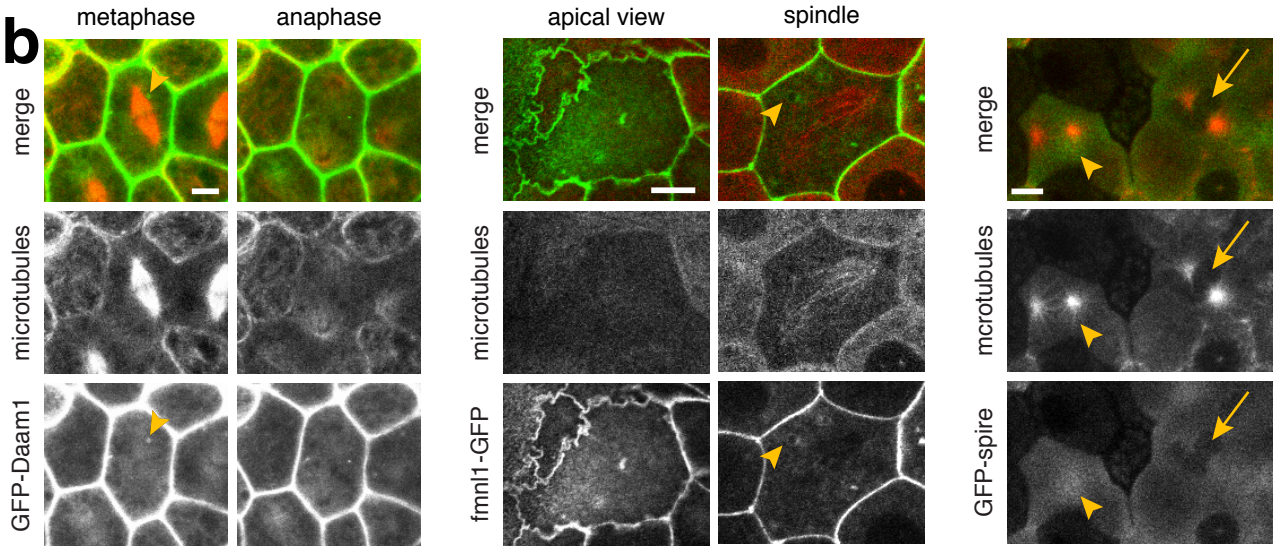
b
metaphase
anaphase
apical view
spindle
merge
microtubules
GFP-Daam1
merge
microtubules
fmnl1-GFP
merge
mcrotubules
GFP-spire

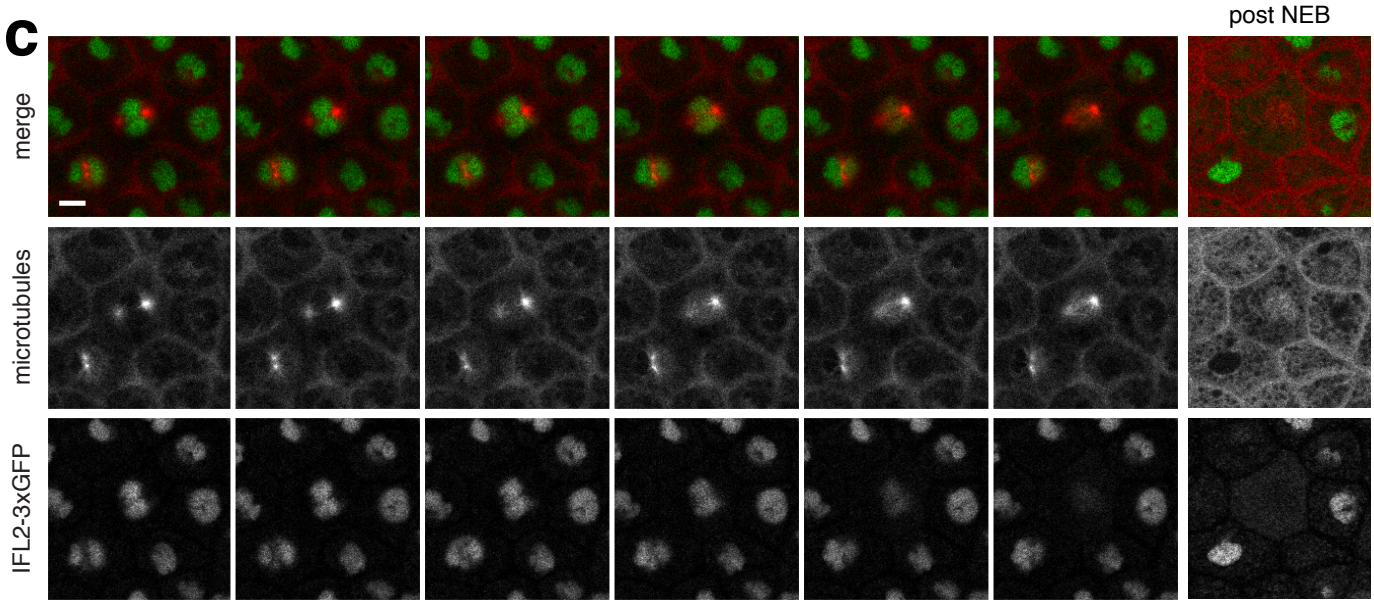
c
post NEB
merge
microtubules
IFL2-3xGFP

Figure 2: IFL2 knockdown by morpholino and siRNA reduces total spindle-associated F-actin

(a) Confocal micrographs from embryos injected with control morpholino (top) or IFL2 morpholino (bottom) then fixed and stained for F-actin (green). DNA is shown in red (mCherry-histone H2B). (b) Mitotic cells injected with control (left) or IFL2 (right) siRNA, fixed and stained for F-actin (phalloidin, green) and microtubules (anti-α-tubulin, red). Scale bars represent 10 μm. (c) Quantification of corrected fluorescence of spindle-associated F-actin during metaphase for IFL2 morpholino (top) and siRNA (bottom) experiments. (control MO: n=11, IFL2 MO: n=20; control siRNA: n=15, IFL2 siRNA: n=16) (*** $p<0.0001$)

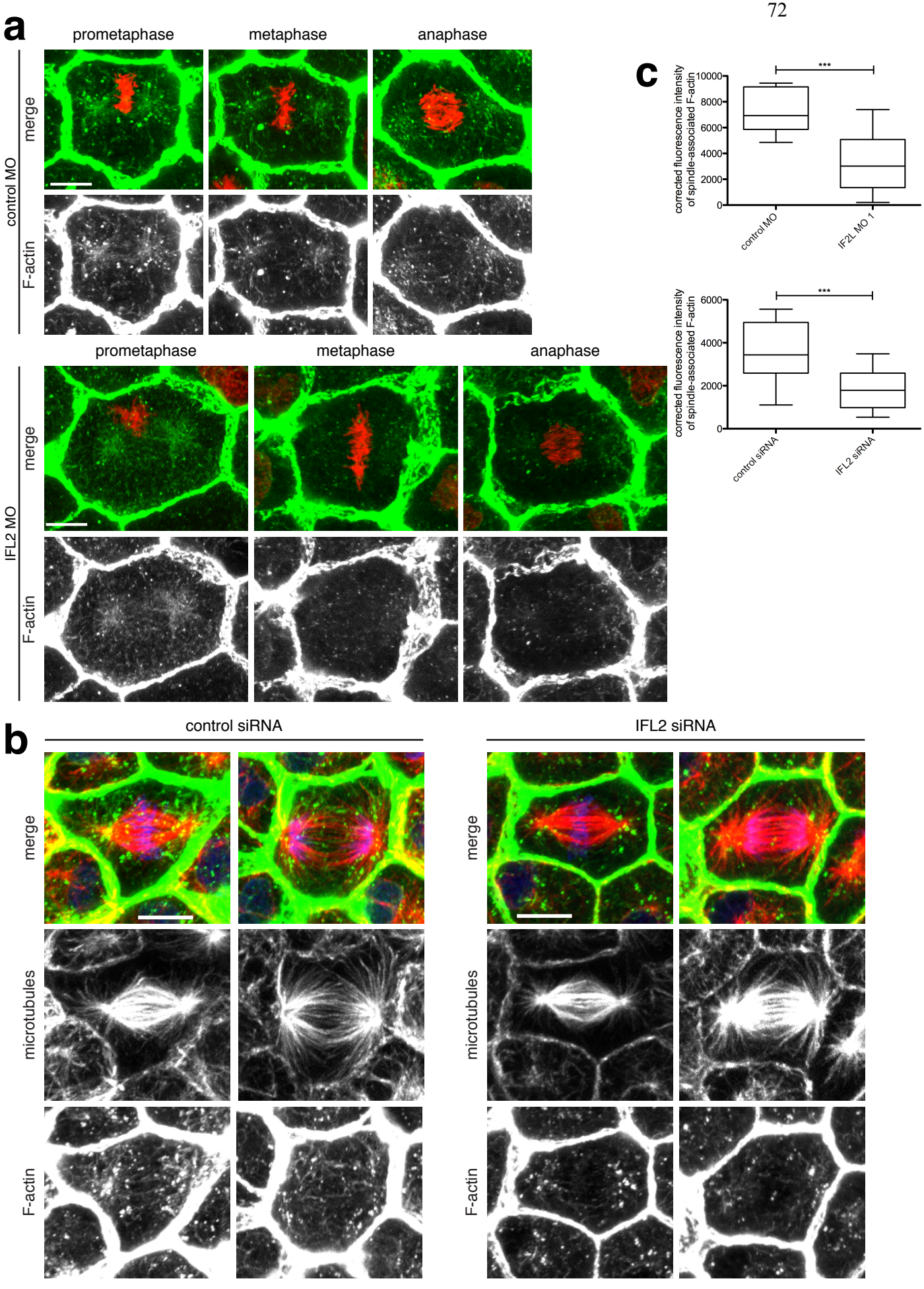
a
prometaphase
metaphase
anaphase
control MO
merge
F-actin
IFL2 MO
b
control siRNA
IFL2 siRNA
microtubules
c
corrected fluorescence intensity of spindle-associated F-actin
***
control MO
IF2L MO 1
control siRNA
IFL2 siRNA

Figure 3: IFL2 knockdown decreases spindle movements and metaphase-to-anaphase transition time

(a) Time-lapse montages of cells from embryos injected with control (top) or IFL2 (bottom) morpholinos. Arrowheads track movement of individual spindle poles. Microtubules are in red (mCherry-α-tubulin) and DNA is in green (eGFP-histone H2B). Scale bars represent 10 μm, time shown in minutes and seconds. (b) Quantification of amount of time cells spent from metaphase to anaphase in control versus IFL2 morphant embryos. (control MO: n=15, IFL2 MO: n=14) (*** $p<0.0001$)

a
control MO
IFL2 MO
merge
microtubules
0:00
0:34
1:08
1:42
2:14
2:48
3:22
3:56
4:30
5:04
5:38
6:12
6:46
7:20
7:54
8:28
9:02
9:36
10:10
10:44
11:18
11:52
12:26
13:00
b
NEB to metaphase
time (s)
metaphase to anaphase
time (s)
***
***
control MO
IFL2 MO
0
200
400
600
800
1000

Figure 4: IFL2 morphant phenotypes can be rescued by expression of a morpholino-resistant IFL2

(a) Confocal micrographs of mitotic spindles from embryos injected with control MO, IFL2 MO, or IFL2 MO plus morpholino-blind IFL2 (IFL2gr). Embryos were fixed and labeled for F-actin (phalloidin, green) and microtubules (anti-α-tubulin, red). DNA (mCherry-histon H2B) is shown in blue. Scale bars represent 10 μm. (b) Quantification of corrected fluorescence of spindle-associated F-actin during metaphase in embryos injected with control MO, IFL2 MO, and IFL2 MO + IFL2gr. (control MO: n=11, IFL2 MO: n=11, IFL2 MO + IFL2gr: n=15) (*** $p<0.0001$, ns $p>0.05$)

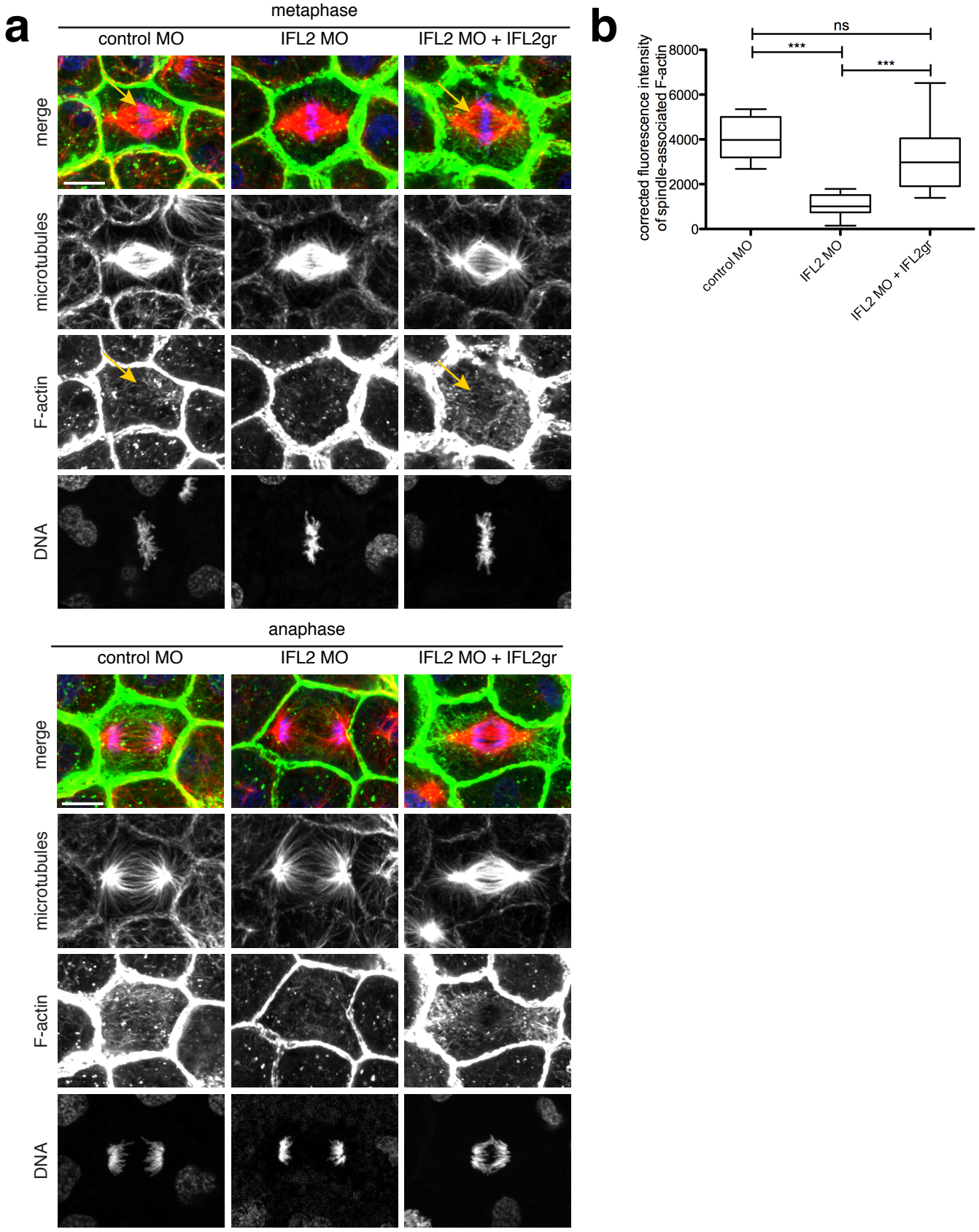
a
metaphase
control MO
IFL2 MO
IFL2 MO + IFL2gr
merge
microtubules
F-actin
DNA
anaphase
control MO
IFL2 MO
IFL2 MO + IFL2gr
merge
microtubules
F-actin
DNA
b
corrected fluorescence intensity of spindle-associated F-actin
8000
6000
4000
2000
0
ns
***
***
control MO
IFL2 MO
IFL2 MO + IFL2gr

Figure 5: Overexpression of IFL2 causes errors in chromosomal segregation and disrupts spindle-associated F-actin

(a) Montage stills from live cell imaging of control (top) versus IFL2 overexpression (bottom). Chromosomes become tethered at the cell edge (arrowheads) when IFL2 is overexpressed and tethered chromosomes are not properly segregated (telophase stills, right). Microtubules are shown in red (mCherry-α-tubulin) and DNA is shown in green (eGFP-histone H2B). Time is shown in minutes and seconds. Scale bars represent 10 μm. (b) Confocal micrographs of cells from control (left) and IFL2 overexpression (right) embryos. In contrast to the F-actin cables in control cells (arrows), IFL2 overexpression result in large F-actin aggregations (arrows) and detached chromosomes (arrowheads). (c) Large multi-polar cell with many cytoplasmic F-actin cables resulting from IFL2 overexpression. Arrowheads indicate chromosomal attachment to cell periphery. For (b) and (c), F-actin (phalloidin) is shown in green and DNA (mCherry-histone H2B) is shown in red. Scale bars indicate 10 μm.

a
control
IFL2 overexpression
merge
microtubules
DNA
0:46
1:32
2:18
3:04
3:50
4:36
5:22
6:08
6:54
7:40
8:26
telophase
b
metaphase
anaphase
control
IFL2 OE
merge
F-actin
DNA
c
IFL2 OE
merge
F-actin
DNA

Figure 6: Dominant-negative expression of FH2 domain of IFL2 disrupts spindle-associated F-actin and generates aberrant spindle phenotypes

(a) Confocal micrographs of cells from control (left) and IFL2-FH2 (right) expressing embryos. As compared to control cells, F-actin cables (arrows) are less discernable in cells expressing IFL2-FH2 (compare to IFL2-FH2 metaphase). Expression of this fragment can also cause an increase in size and number of F-actin puncta during mitosis (anaphase, arrowheads). F-actin (phalloidin) is shown in green and DNA (mCherry-histone H2B) is shown in red. (b) Control and IFL2-FH2 expressing embryos, fixed and labeled for microtubules (anti-α-tubulin, red) and DNA (mCherry-histone H2B, blue) reveal a decrease in spindle length, and the formation of multipolar spindles (right). Scale bars represent 10 μm. (c) Quantification of spindle length and multipolar spindles in control versus IFL2-FH2 expressing cells. (control: n=16, IFL2-FH2: n=16) (** $p<0.001$, *** $p<0.0001$)

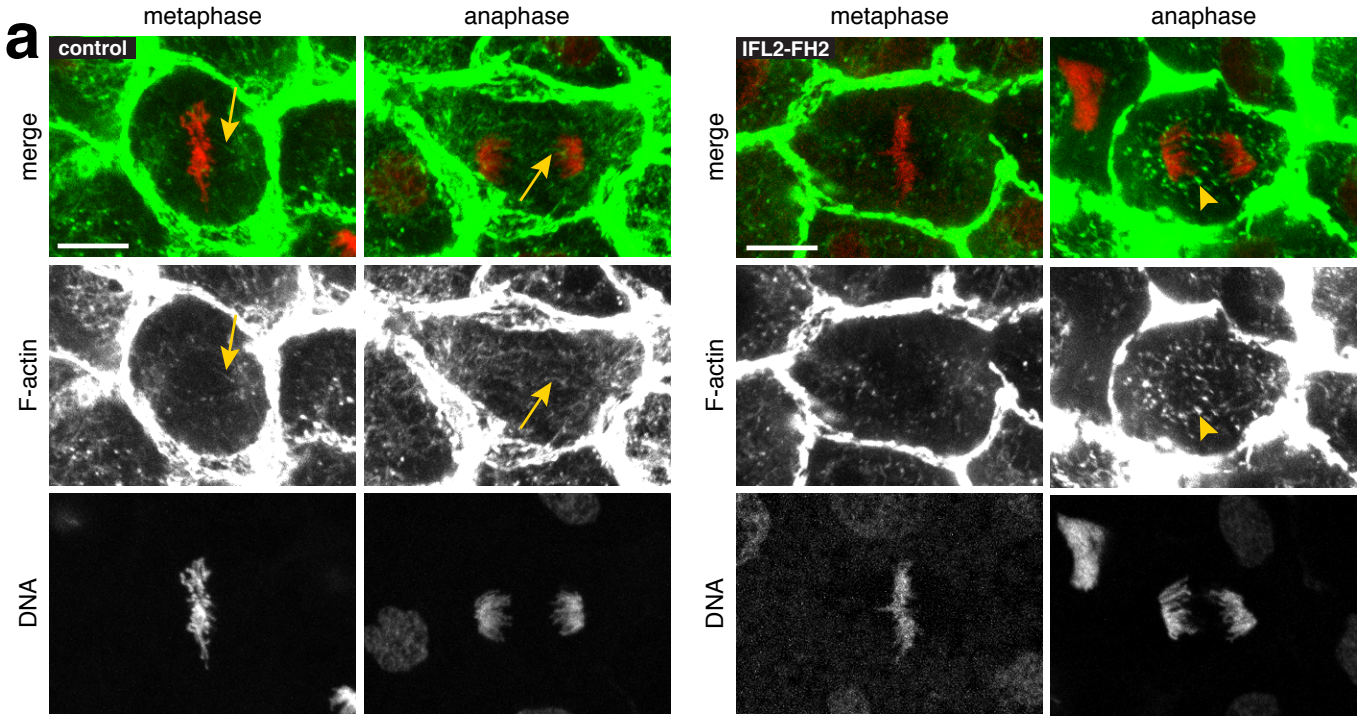
a
metaphase
anaphase
metaphase
anaphase
control
IFL2-FH2
merge
F-actin
DNA

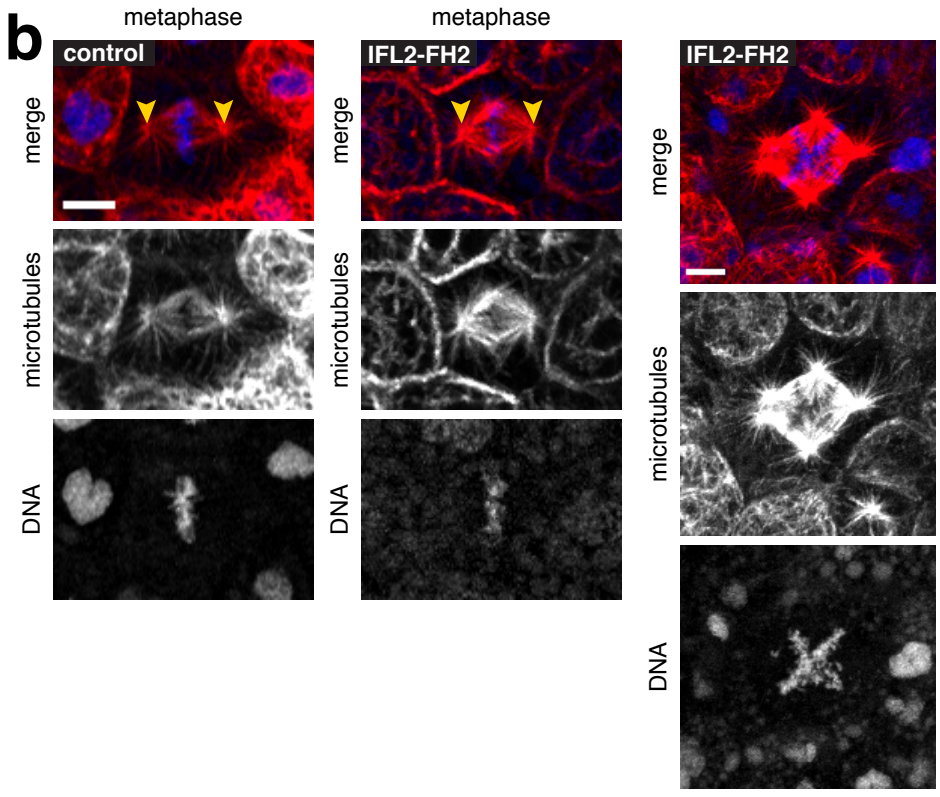
b
metaphase
metaphase
control
IFL2-FH2
IFL2-FH2
merge
microtubules
DNA

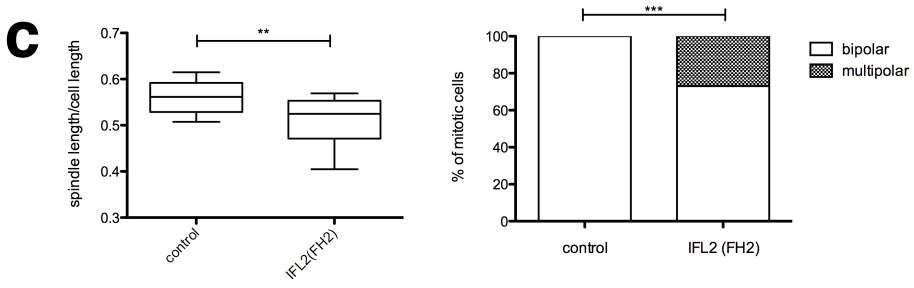
c
spindle length/cell length
0.7
0.6
0.5
0.4
0.3
**
control
IFL2(FH2)
% of mitotic cells
100
80
60
40
20
0
***
bipolar
multipolar
control
IFL2 (FH2)

Discussion

In this study, I identified inverted formin like 2 (IFL2) as a regulator of spindle-associated F-actin in the early *X. laevis* embryo. IFL2 was found to localize to the nucleus during interphase and to the cytoplasm at M-phase. As a result of IFL2 knockdown, actin was depleted at the spindle and this actin depletion was rescued by reintroducing full length IFL2 into cells. These results are described below.

Both the characterization of spindle F-actin as unbranched cables and the effect of chemical inhibitors these structures (i.e. SMIFH2 treatment) suggested that one or more formin proteins nucleate spindle F-actin. I therefore conducted a candidate screen using the localization of formin proteins as an indication of potential mitotic function. The *X. laevis* homolog of human inverted formin 2 (hINF2) localized to the nucleus during interphase and became diffusely cytoplasmic at the start of mitosis. Many factors involved in mitotic spindle function are retained in the nucleus during interphase (e.g. Ran GTPase, TPX2), so I further characterized this candidate.

The *X. laevis* homolog of human INF2—referred to in this work as inverted formin like 2 (IFL2)—shares the most sequence similarity with hINF2 out of all formins, however it differs in key details. IFL2 is 150 amino acids shorter than hINF2, and many of these make up the far C-terminal end of the protein (Figure 1a), which directs the localization of hINF2 to the endoplasmic reticulum and specific vesicle membranes (Chhabra et al., 2009). Therefore, differences in the localization of IFL2 compared to hINF2 are not surprising. IFL2 does share important similarities with hINF2, specifically in that both proteins contain a WASP-homology 2 (WH2) domain in place of a diaphanous autoinhibitory domain (DAD). In hINF2, this WH2 domain allows the protein to depolymerize F-actin in addition to its nucleation and polymerization activity (Chhabra & Higgs, 2006). Thus IFL2 is in the right place to regulate spindle F-actin, and may

additionally have the ability to both polymerize and depolymerize actin cables at the spindle.

To determine the potential involvement of IFL2 during mitosis, I conducted knockdown experiments via translation-blocking morpholinos and small interfering RNAs (siRNAs). Each of these methods resulted in a roughly 50% knockdown of spindle actin as compared to controls. I was able to rescue this F-actin depletion in IFL2 depleted cells by reintroducing the full-length protein.

To determine the consequence of unregulated IFL2 activity, I conducted overexpression experiments. These revealed that overexpression of IFL2 leads to an increase in spindle F-actin, notably in the form of large aggregations of F-actin at the spindle midplane, and near chromosomes and spindle poles. One possible explanation for this may be that F-actin builds up at sites of IFL2-mediated nucleation when protein expression is unregulated. High levels of IFL2 additionally caused chromosomal "stickiness" during mitosis, whereby large condensed chromosomes appeared stuck to the outer edges of cells. Live imaging revealed that chromosomes became tethered at the cell periphery during prometaphase and metaphase, which resulted in detached chromosomes that remained at the midbody after telophase.

Finally, to determine the consequence of IFL2 loss of function, I performed a dominant negative experiment. I made use of the fact that formins function in cells as homodimers by expressing the FH2 domain of IFL2, which should bind endogenous IFL2. This binding would block IFL2 function due to the lack of a second FH1 domain. Expression of IFL2-FH2 resulted in disruption of F-actin structures at the spindle. Specifically, F-actin cables at the spindle were reduced and bright F-actin puncta dotted the entire spindle, however cortical actin appeared unaltered. This result, similar to IFL2 overexpression, could indicate the presence of F-actin nucleation sites that become

blocked from generating cables when bound by IFL2-FH2. When active, these nucleation sites would polymerize new actin filaments as required.

Collectively, the results of this study identify IFL2 as a regulator of spindle F-actin. It is very likely that additional actin binding proteins are involved in the regulation of spindle-associated F-actin and further work could uncover these proteins and their roles.

Materials & Methods

Plasmids

The mCherry-histone H2B, mCherry-α-tubulin, eGFP-UtrCH, and pCS2+3XeGFP plasmids were made as previously described (von Dassow et al., 2009; Burkel et al., 2007; Bement & Miller, 2009). eGFP-N1-Lifeact was obtained from Erik Dent (University of Wisconsin) and the sequence of Lifeact-eGFP was amplified from this vector and cloned into pCS2+ using Xho1 and Xba1.

The following clones were obtained from OpenBiosystems (Life Technologies) and clones into eGFP-pCS2 or pCS2-eGFP with the following restriction enzymes: Daam1 was cloned with BspE1 and Xho1. Eg6/Spire was cloned using Sac1 and Xba1, Formin-like 1 (fmnl1) was cloned into pCS2-eGFP with BamH1 and Cla1. Inverted formin like 2 (IFL2) was cloned into C-terminal pCS2-3XeGFP (BamH1/Xba) and empty pCS2+ (BamH1/Xba1) for live imaging and overexpression experiments. The dominant negative IFL2-FH2 fragment was generated by amplifying nucleotides 1863-3027, and cloning this into pCS2+ with EcoR1 and Stu1.

Embryo preparation

Adult *X. laevis* females were injected with 800 units of human chorionic gonadotropin (HCG; MP BioMedicals) into the dorsal lymph sac 1 d prior to use. Eggs were laid into 1X MMR (100 mM NaCl, 2 mM KCl, 1 mM MgCl2, and 5 mM Hepes, pH 7.4) and fertilized in vitro with macerated testes. Embryos were dejellied in 2% cysteine solution (in 0.1X MMR, pH 7.8), rinsed five times in 1X MMR and five times in 0.1X MMR. Overnight embryo culture was in 0.1X MMR at 17°C

mRNA preparation and embryo microinjection

All mRNA was transcribed *in vitro* using the mMessage Machine SP6 kit (Life Technologies) and reactions were purified with the RNeasy Mini Kit (Qiagen). Embryos were submerged in 0.1X MMR + 5% Ficoll (Sigma) and injected with 5 nL of mRNA at the 2-cell stage. mCherry-histone H2B was injected at 12.5 µm/mL for both live and fixed cell imaging. For live cell imaging, mCherry-α-tubulin was injected at 25 µg/mL, Lifeact-eGFP was injected at 80 µg/mL, IFL2-3XeGFP was injected at 50 µm/mL and at 100 µm/mL for overexpression experiments. IFL2-FH2 was injected at 100 µm/mL for dominant negative experiments. After microinjection, embryos were incubated in 0.1X MMR at 17°C for 18-20 hours before live imaging or processing for fixation.

Morpholino and siRNA knockdown

An IFL2 morpholino with the sequence 5'-GGCTCCTTCCGTTAAGGACATCTTT-3' which targets the first 25 nucleotides of IFL2 coding sequence was obtained from Gene-Tools. These were injected at a needle concentration of 1-2 mM at the 2-cell stage. Morpholinos were co-injected with mCherry-histone H2B (at 25 µg/mL) to identify cells that had received morpholinos.

Four siRNAs targeting IFL2 were designed and obtained from SIgma: 1-CGUACAACUCAGAAAUGAA, 2-CCUGAAAGUGGGAAACUUU, 3-CAACUGAUGUCAAGGAGCA, 4-CCAAAUGUGAUCAAAGACA. A pool of IFL2 siRNAs 1-3 were injected at a concentration of 50 mM. These were co-injected with flag-Argonaut (at 200 µm/mL) and mCherry-histone H2B (at 25 µg/mL) to activate the siRNA pathway (Argonaut) and determine which cells had obtained siRNA treatment (histone H2B).

Fixation and immunofluorescence

To fix for double labeling of F-actin and microtubules, embryos were briefly rinsed in 1X PBS, then dropped into a modified paraformaldehyde (PFA) solution. This consisted of a “superfix” buffer (100 mM KCl, 3 mM MgCl, 10 mM HEPES, 150 mM sucrose, pH 7.4) to which the following was added (listed in final concentrations): 3.7% PFA, 10% DMSO, 2 mM EGTA, 0.2 μM paxitaxol, 0.1% gluteraldehyde, and 0.02% Triton-X-100. Fluorescent phalloidin (AlexaFlour 488, Life Technologies) was added to the fix buffer at a concentration of 1:200 for same day imaging, or added to primary and secondary antibody incubations at 1:100. Embryos were incubated for 1 h on an orbital shaker at room temperature to fix. Microtubules were labeled with 1:20,000 mouse monoclonal anti-α-tubulin (DM1A, Sigma) and a donkey derived anti-mouse secondary was used at 1:10,000 (AlexaFluor 647, Life Technologies). Primary antibody incubations were 3 h at room temperature while secondary incubations were overnight at 4°C. Following fixation, embryos were dehydrated using a series of isopropanol washes then cleared with Murray’s Clear (2:1 benzyl alcohol, benzyl benzoate) for confocal microscopy.

Microscopy and image processing

Imaging of all fixed experiments was conducted with a 1.4 NA 60X oil immersion objective on a Nikon Eclipse Ti inverted microscope using Prairie View software (Brüker). Z-series were acquired using 0.5 μm step size and were reconstructed in Fiji. For live imaging, embryos were mounted in 0.1X MMR and imaged using a 1.0 NA 40X oil immersion or a 1.4 NA 60X oil immersion objective on the Nikon Eclipse Ti microscope. Single-plane time series were captured at 2.3 s or less and processed using Fiji software. Multi-plane imaging was processed using Velocity software (PerkinElmer). Quantitative image analysis of F-actin intensity at mitotic spindles was performed by measuring the integrated density at the spindle and using the following equation:

Corrected fluorescent intensity = integrated density – (area of selected region X mean fluorescence of background readings). Five separate background regions were measured for each image and their mean fluoresce was averaged (modified from Potapova et al., 2011).

Discussion

The work conducted for this thesis was based on observations that myosin-10, an unconventional myosin that binds to actin and microtubules, localized to the mitotic spindle in the intact *Xenopus laevis* embryonic epithelium (Woolner et al., 2008). Further, myosin-10 knockdown had several consequences for the spindle including spindle pole fragmentation, loss of spindle movements, and increased spindle length. Inhibition of actin filament formation in cells with depleted myosin-10 was found to rescue spindle length defects, indicating a potential role for filamentous actin (F-actin) in mitotic spindle function (Woolner et al., 2008). A further observation was that F-actin cables could be visualized between spindle poles and the cortex via live cell imaging with the side-binding F-actin probe eGFP-UtrCH (Burkel et al., 2007). These pieces of evidence hinted at an uncharacterized role for F-actin in mitotic spindle. To address this possible role, we first required an accurate picture of the localization of endogenous F-actin during mitosis. Once established, the following questions about spindle-associated F-actin could be addressed: 1) where is F-actin with respect to the spindle?, 2) how does spindle F-actin change throughout the course of mitosis?, 3) what are the consequences of alterations to this F-actin?, and 4) what actin regulators are involved?

To address the first two questions, I investigated the localization of endogenous F-actin in fixed samples in Chapter 1. By modifying existing approaches to F-actin preservation, using appropriate controls, and employing multiple visualization techniques, I determined that F-actin does in fact localize to the mitotic spindle in the form of unbranched actin cables and F-actin puncta. These actin cables and puncta appear at the onset of prometaphase in close proximity with the spindle poles. Through metaphase and anaphase, actin cables span between poles and the cell cortex and reach inward from spindle poles towards the spindle center. Live imaging further

corroborated these results, indicating that cables and puncta move dynamically with the spindle throughout mitosis.

The presence of F-actin structures at the spindle implies an underlying functional importance. Therefore, I employed several manipulations to disrupt spindle actin in Chapter 2. Low-dose treatments with chemical inhibitors of F-actin disrupted cytoplasmic actin structures, however effects on the spindle were minor (decreased spindle length with cytochalasin D) or not apparent (i.e. latrunculin A). These results could be due to a lack of target specificity by compounds that affect all cellular actin, and thus effects on one relatively low abundance population (i.e. spindle F-actin versus cortical actin) might be obscured. The results of previous work by Woolner et al. (2008) indicated the possible influence of at least two counteracting forces on the spindle by F-actin: one that contributes to spindle shortening in coordination with myosin-10, and one that contributes to spindle lengthening independent of myosin-10. Thus, any treatment that impacts both F-actin populations equally would negate the effect of F-actin on spindle length.

A deeper consideration of the results of actin inhibition may provide clues about spindle F-actin function. Low dose cytochalasin D treatment, for example, did have a significant effect on spindle length, in contrast to latrunculin A. There are a few possible explanations for this difference. One is that differences in the composition of actin filaments could result in distinct affects by inhibitors. In a study of the distribution of β- and γ-cytoplasmic actins in fibroblasts and epithelial cells, Dugina et al. (2009) found that latrunculin A had a greater effect on γ-actin structures at the leading edge of cells while cytochalasin D inhibited the formation of β-actin stress fibers. In my investigation, only low dose latrunculin A treatment significantly reduced spindle F-actin, which could indicate these structures were composed of γ-actin monomers. Further, a γ-actin isoform specific antibody decorated actin cables and puncta at the spindle, though less robustly

than the amount visualized by phalloidin labeling. This difference is either due to the additional presence of β-actin monomers within spindle actin filaments, or actin structures at the spindle are less readily detectable by actin antibodies that bind both monomeric and filamentous actin. Another clue is that γ-actin knockdown has negative effects on microtubule stability during mitosis (Po'uha et al., 2013), which may indicate a key role for γ-actin at the spindle.

The differences in the effects of various actin polymerization inhibitors could indicate differing functions of F-actin associated with the mitotic spindle. Actin cables that reach between the spindle poles and the cell cortex may participate in maintaining spindle length, orientation, and positioning, while those that reach from spindle poles inward towards the spindle midplane may be more important for establishing and maintaining spindle length. Further, the force contributions to spindle length provided by each of these actin populations may be in opposing directions, which would fit in with the myosin-10 results described above (Woolner et al., 2008). Thus, depolymerization of both the pole-to-cortex and pole-to-pole F-actin may have little to no apparent effect on spindle length, instead affecting spindle orientation or positioning. This would explain the low-dose latrunculin A results in which spindle length was not significantly altered. Spindle position away from the cell center was also not significantly increased, although this could also be explained by less spindle movement overall. In contrast, low-dose cytochalasin D treatment increased F-actin within the spindle, and decreased spindle length. This alteration in pole-to-pole F-actin may have shifted the contributions of F-actin on spindle length towards generating shorter spindles. Alternatively, changes to this pool of F-actin may have caused defects early as the spindle was established, which then persisted through to metaphase.

Differing effects on spindle F-actin from low-dose latrunculin A and cytochalasin D could also be caused by interference of the drugs' interactions by actin binding

proteins. A filament end-binding protein, such as a capping protein or an actin nucleator, might compete with cytochalasin D for binding at barbed ends. As a result, an intermediate state of polymerization and depolymerization would occur prior to compete actin disassembly. One example of an unpredicted interaction between an actin inhibitor and a nucleation factor is that low levels of latrunculin B are reported to stimulate the processive activity of the formin mDia1 (Higashida et al., 2008).

To address the question of how spindle F-actin is regulated, I used a chemical inhibitor of formin nucleation, SMIFH2. Formin inhibition resulted in several defects in mitotic cells: spindle length was decreased, spindles were displaced, and F-actin at the spindle was reduced. In addition to a reduction in the intensity of F-actin at the spindle, actin was redistributed away from the spindle into the cytoplasm. Formins nucleate and elongate actin filaments, which would account for the general reduction of F-actin intensity. SMIFH2 blocks actin nucleation and polymerization of formins by binding the FH2 domain, however there are several formins that are reported to interact with microtubules and actin via their FH2 domain. Thus, this mechanism of formin inhibition could both block actin polymerization and displace formins from interacting with microtubules.

The results of formin inhibition suggest an interaction between actin and microtubules at the spindle. Therefore, I hypothesized that a disruption of spindle microtubules could induce changes in the associated F-actin structures. A partial microtubule depolymerization with nocodazole resulted in a reduction of spindle F-actin and the appearance of large F-actin puncta situated near the ends of astral microtubule plus ends. This fits to a model of one or more formins that can interact with microtubules and polymerize actin at the spindle.

In Chapter 3, I performed a candidate screen for nucleators of spindle F-actin based on localization studies. I preferentially examined the localization of formins based

on the results of Chapter 2, and found that the *Xenopus* homolog of human inverted formin 2 (hINF2) is cytoplasmic during mitosis. To distinguish the *Xenopus* homolog from hINF2, I refer to *Xenopus* protein as inverted formin 2 like (IFL2). Although IFL2 shares the closest homology with hINF2, there are key differences that separate them. The most apparent is that hINF2 localizes to the endoplasmic reticulum (ER) (Chhabra et al., 2006) while fluorescent IFL2 is nuclear at interphase and diffusely throughout the cytoplasm in M-phase. This difference is attributed to the lack of C-terminal residues in IFL2, which are required for the ER localization of hINF2. The formin homology (FH) 1 domain of IFL2 is also roughly 30% longer than that of hINF2. The FH1 domain binds profiln:actin complexes, bringing them close to dimerized FH2 domains so monomers can be added to the growing filament end (Paul & Pollard, 2009). The number of actin-binding polyproline repeats contained within the FH1 domain, combined with its proximity to the nearby FH2 domain, was found to alter monomer addition rates in budding yeast (Courtemache & Pollard, 2012). Thus hINF2 and IFL2 may differ in both localization pattern and actin elongation rates.

An important similarity between hINF2 and IFL2 is that both possess a WASP homology 2 (WH2) domain in place of a diaphanous autoinhibitory domain (DAD), which allows hINF2 to depolymerize actin filaments (Chhabra & Higgs, 2006). Additionally, actin monomer binding to the hINF2 WH2 domain relieves autoinhibitory interactions of the protein (Ramabhadran et al., 2013). Thus IFL2 can potentially be activated by an increase in actin monomers and depolymerize F-actin in addition to nucleating and elongating filaments.

To determine what role IFL2 has in regulating spindle F-actin, I conducted knockdown studies. Spindle-associated F-actin decreases when IFL2 is depleted, and IFL2 overexpression leads to the formation of F-actin aggregates localized near condensed chromosomes, spindle poles, and the spindle midplane. Dominant negative

expression of the FH2 domain of IFL2 also altered spindle F-actin in that actin cables were less detectable and bright actin puncta dotted the spindle. Collectively, these results indicate that IFL2 regulates spindle actin, possibly from specific nucleation sites that remain visible when IFL2 function is blocked. A recent study of the local organization of actin networks described actin nodes comprised of a formin (Daam1), myosin-2, and the actin crosslinker filamin A (Luo et al., 2013) that were proposed to assist in maintain the mechanical coherence of the cytoplasmic. The F-actin puncta uncovered by this study may represent sites of nucleation by IFL2 alone or together with other actin binding proteins. Several F-actin binding proteins and proteins associated with F-actin adhesion have been shown to localize to the mitotic spindle—including cofilin (Kaji et al., 2008), LIM Kinase (Sumi et al., 2006), cortactin (Wang et al., 2008), zyxin (Hirota et al., 2000), FAK (Park et al., 2009), and integrin kinase (Fielding et al., 2008)—and could interact with IFL2 to regulate spindle actin.

The question of why spindle F-actin exists (when microtubules already carry the weight of chromosome segregation) still remains open. In plant cells, mitotic spindle F-actin has been demonstrated using electron microscopy (Forer & Jackson, 1979), phalloidin-staining of fixed samples (Seagull et al., 1987; Traas et al., 1987; Schmit & Lambert, 1987; Yasuda et al., 2005), anti-actin antibodies (Yasuda et al., 2005), and expression of fluorescent actin binding probes (Yu et al., 2006). The summation of these studies is that at the start of mitosis the subcortical and nuclear cables disassemble and F-actin accumulates at the spindle. By metaphase, F-actin cables extend from the ends of the spindles, where they define a pole-like structure, to the chromosomes. These spindles are structurally similar to meiotic animal cells that lack centrosomes. Therefore the inclusion of F-actin within plant mitotic cells and meiotic animals cells may fill a need for additional support or tension within the spindle.

Formin-mediated filament elongation can be altered in response to tension along the filament. In the absence of profilin, filament tension decreased elongations rates while the presence of profilin increased elongation rates of the yeast formin Bni1p (Courtemache et al., 2013). A study of actin homeostasis in cultured *X. laevis* cells investigated the effects of tension on various *X. laevis* formins, including IFL2. Prior to force addition, IFL2 was detected as discrete speckles in the cytoplasm that occasionally displayed short, directional movements. After the introduction of force by micromanipulation, there was a marked increase in the total number of IFL2 speckles and an increase in the amount of directionally moving speckles (Higashida et al., 2013). Thus, IFL2 activity can be stimulated by the generation of force. Within the mitotic spindle, force generation might derive from undue strain on the structure, at which point the activation of IFL2 would provide additional support in the form of actin cables.

In conclusion, this work has revealed the existence of F-actin that associates with the mitotic spindle and puts forward IFL2 as a regulator of spindle F-actin. Further work will be necessary to identify additional regulators of spindle-associated F-actin and to determine the precise requirements for cytoplasmic and spindle F-actin during mitosis.

References

Agnew, B.J., Minamide, L.S., and Bamburg, J.R. (1995). Reactivation of phosphorylated actin depolymerizing factor and identification of the regulatory site. J Biol Chem *270*, 17582-17587.

Andrés-Delgado, L., Antón, O.M., and Alonso, M.A. (2013). Centrosome polarization in T cells: a task for formins. Front Immunol *4*, 191.

Andrés-Delgado, L., Antón, O.M., Bartolini, F., Ruiz-Sáenz, A., Correas, I., Gundersen, G.G., and Alonso, M.A. (2012). INF2 promotes the formation of detyrosinated microtubules necessary for centrosome reorientation in T cells. J Cell Biol *198*, 1025-1037.

Arber, S., Barbayannis, F.A., Hanser, H., Schneider, C., Stanyon, C.A., Bernard, O., and Caroni, P. (1998). Regulation of actin dynamics through phosphorylation of cofilin by LIM-kinase. Nature *393*, 805-809.

Aubin, J.E., Weber, K., and Osborn, M. (1979). Analysis of actin and microfilament-associated proteins in the mitotic spindle and cleavage furrow of PtK2 cells by immunofluorescence microscopy. A critical note. Exp Cell Res *124*, 93-109.

Azoury, J., Lee, K.W., Georget, V., Rassinier, P., Leader, B., and Verlhac, M.H. (2008). Spindle positioning in mouse oocytes relies on a dynamic meshwork of actin filaments. Curr Biol *18*, 1514-1519.

Ballestrem, C., Wehrle-Haller, B., and Imhof, B.A. (1998). Actin dynamics in living mammalian cells. J Cell Sci *111 (Pt 12)*, 1649-1658.

Barak, L.S., Nothnagel, E.A., DeMarco, E.F., and Webb, W.W. (1981). Differential staining of actin in metaphase spindles with 7-nitrobenz-2-oxa-1,3-diazole-phallacidin and fluorescent DNase: is actin involved in chromosomal movement? Proc Natl Acad Sci U S A *78*, 3034-3038.

Baranwal, S., Naydenov, N.G., Harris, G., Dugina, V., Morgan, K.G., Chaponnier, C., and Ivanov, A.I. (2012). Nonredundant roles of cytoplasmic β- and γ-actin isoforms in regulation of epithelial apical junctions. Mol Biol Cell *23*, 3542-3553.

Bartolini, F., and Gundersen, G.G. (2010). Formins and microtubules. Biochim Biophys Acta *1803*, 164-173.

Barton, D.A., and Overall, R.L. (2010). Cryofixation rapidly preserves cytoskeletal arrays of leaf epidermal cells revealing microtubule co-alignments between neighbouring cells and adjacent actin and microtubule bundles in the cortex. J Microsc *237*, 79-88.

Belin, B.J., Cimini, B.A., Blackburn, E.H., and Mullins, R.D. (2013). Visualization of actin filaments and monomers in somatic cell nuclei. Mol Biol Cell *24*, 982-994.

Bentley, A.M., Normand, G., Hoyt, J., and King, R.W. (2007). Distinct sequence elements of cyclin B1 promote localization to chromatin, centrosomes, and kinetochores during mitosis. Mol Biol Cell *18*, 4847-4858.

Berg, J.S., and Cheney, R.E. (2002). Myosin-X is an unconventional myosin that undergoes intrafilopodial motility. Nat Cell Biol *4*, 246-250.

Blanchoin, L., Boujemaa-Paterski, R., Sykes, C., and Plastino, J. (2014). Actin dynamics, architecture, and mechanics in cell motility. Physiol Rev *94*, 235-263.

Breitsprecher, D., and Goode, B.L. (2013). Formins at a glance. J Cell Sci *126*, 1-7.

Burkel, B.M., von Dassow, G., and Bement, W.M. (2007). Versatile fluorescent probes for actin filaments based on the actin-binding domain of utrophin. Cell Motil Cytoskeleton *64*, 822-832.

Cande, W.Z., Lazarides, E., and McIntosh, J.R. (1977). A comparison of the distribution of actin and tubulin in the mammalian mitotic spindle as seen by indirect immunofluorescence. J Cell Biol *72*, 552-567.

Canman, J.C., and Bement, W.M. (1997). Microtubules suppress actomyosin-based cortical flow in Xenopus oocytes. J Cell Sci *110 (Pt 16)*, 1907-1917.

Carpenter, A.E., Jones, T.R., Lamprecht, M.R., Clarke, C., Kang, I.H., Friman, O., Guertin, D.A., Chang, J.H., Lindquist, R.A., Moffat, J., Golland, P., and Sabatini, D.M. (2006). CellProfiler: image analysis software for identifying and quantifying cell phenotypes. Genome Biol *7*, R100.

Cheng, L., Zhang, J., Ahmad, S., Rozier, L., Yu, H., Deng, H., and Mao, Y. (2011). Aurora B regulates formin mDia3 in achieving metaphase chromosome alignment. Dev Cell *20*, 342-352.

Chesarone, M.A., DuPage, A.G., and Goode, B.L. (2010). Unleashing formins to remodel the actin and microtubule cytoskeletons. Nat Rev Mol Cell Biol *11*, 62-74.

Chhabra, E.S., and Higgs, H.N. (2006). INF2 Is a WASP homology 2 motif-containing formin that severs actin filaments and accelerates both polymerization and depolymerization. J Biol Chem *281*, 26754-26767.

Chhabra, E.S., Ramabhadran, V., Gerber, S.A., and Higgs, H.N. (2009). INF2 is an endoplasmic reticulum-associated formin protein. J Cell Sci *122*, 1430-1440.

Danilchik, M.V., Funk, W.C., Brown, E.E., and Larkin, K. (1998). Requirement for microtubules in new membrane formation during cytokinesis of Xenopus embryos. Dev Biol *194*, 47-60.

Dent, E.W., Gupton, S.L., and Gertler, F.B. (2011). The growth cone cytoskeleton in axon outgrowth and guidance. Cold Spring Harb Perspect Biol *3*.

Dugina, V., Zwaenepoel, I., Gabbiani, G., Clément, S., and Chaponnier, C. (2009). Beta and gamma-cytoplasmic actins display distinct distribution and functional diversity. J Cell Sci *122*, 2980-2988.

Duleh, S.N., and Welch, M.D. (2010). WASH and the Arp2/3 complex regulate endosome shape and trafficking. Cytoskeleton (Hoboken) *67*, 193-206.

Edwards, K.A., Demsky, M., Montague, R.A., Weymouth, N., and Kiehart, D.P. (1997). GFP-moesin illuminates actin cytoskeleton dynamics in living tissue and demonstrates cell shape changes during morphogenesis in Drosophila. Dev Biol *191*, 103-117.

Field, C.M., Wühr, M., Anderson, G.A., Kueh, H.Y., Strickland, D., and Mitchison, T.J. (2011). Actin behavior in bulk cytoplasm is cell cycle regulated in early vertebrate embryos. J Cell Sci *124*, 2086-2095.

Fink, J., Carpi, N., Betz, T., Bétard, A., Chebah, M., Azioune, A., Bornens, M., Sykes, C., Fetler, L., Cuvelier, D., and Piel, M. (2011). External forces control mitotic spindle positioning. Nat Cell Biol *13*, 771-778.

Fujiwara, K., and Pollard, T.D. (1976). Fluorescent antibody localization of myosin in the cytoplasm, cleavage furrow, and mitotic spindle of human cells. J Cell Biol *71*, 848-875.

Gaillard, J., Ramabhadran, V., Neumanne, E., Gurel, P., Blanchoin, L., Vantard, M., and Higgs, H.N. (2011a). Differential interactions of the formins INF2, mDia1, and mDia2 with microtubules. Mol Biol Cell *22*, 4575-4587.

Gaillard, J., Ramabhadran, V., Neumanne, E., Gurel, P., Blanchoin, L., Vantard, M., and Higgs, H.N. (2011b). Differential interactions of the formins INF2, mDia1, and mDia2 with microtubules. Mol Biol Cell *22*, 4575-4587.

Gatlin, J.C., and Bloom, K. (2010). Microtubule motors in eukaryotic spindle assembly and maintenance. Semin Cell Dev Biol *21*, 248-254.

Gawadi, N. (1971). Actin in the mitotic spindle. Nature *234*, 410.

Goley, E.D., and Welch, M.D. (2006). The ARP2/3 complex: an actin nucleator comes of age. Nat Rev Mol Cell Biol *7*, 713-726.

Goshima, G., and Scholey, J.M. (2010). Control of mitotic spindle length. Annu Rev Cell Dev Biol *26*, 21-57.

Gurel, P.S., Ge, P., Grintsevich, E.E., Shu, R., Blanchoin, L., Zhou, Z.H., Reisler, E., and Higgs, H.N. (2014). INF2-mediated severing through actin filament encirclement and disruption. Curr Biol *24*, 156-164.

Habas, R., Kato, Y., and He, X. (2001). Wnt/Frizzled activation of Rho regulates vertebrate gastrulation and requires a novel Formin homology protein Daam1. Cell *107*, 843-854.

Hanft, L., Rybakova, I., Patel, J., Rafael-Fortney, J., Ervasti, J. (2006). Cytoplasmic gamma-actin contributes to a compensatory remodeling response in dystrophin-deficient muscle. Proc Natl Acad Sci U S A *103*, 5385-5390.

Harris, E.S., Rouiller, I., Hanein, D., and Higgs, H.N. (2006). Mechanistic differences in actin bundling activity of two mammalian formins, FRL1 and mDia2. J Biol Chem*281*, 14383-14392.

Heimsath, E.G., and Higgs, H.N. (2012). The C terminus of formin FMNL3 accelerates actin polymerization and contains a WH2 domain-like sequence that binds both monomers and filament barbed ends. J Biol Chem *287*, 3087-3098.

Herman, I.M., and Pollard, T.D. (1979). Comparison of purified anti-actin and fluorescent-heavy meromyosin staining patterns in dividing cells. J Cell Biol *80*, 509-520.

Higashida, C., Kiuchi, T., Akiba, Y., Mizuno, H., Maruoka, M., Narumiya, S., Mizuno, K., and Watanabe, N. (2013). F- and G-actin homeostasis regulates mechanosensitive actin nucleation by formins. Nat Cell Biol *15*, 395-405.

Higashida, C., Suetsugu, S., Tsuji, T., Monypenny, J., Narumiya, S., and Watanabe, N. (2008). G-actin regulates rapid induction of actin nucleation by mDia1 to restore cellular actin polymers. J Cell Sci *121*, 3403-3412.

Hill, M.A., and Gunning, P. (1993). Beta and gamma actin mRNAs are differentially located within myoblasts. J Cell Biol *122*, 825-832.

Ishizaki, T., Morishima, Y., Okamoto, M., Furuyashiki, T., Kato, T., and Narumiya, S. (2001). Coordination of microtubules and the actin cytoskeleton by the Rho effector mDia1. Nat Cell Biol *3*, 8-14.

Klymkowsky, M.W., and Hanken, J. (1991). Whole-mount staining of Xenopus and other vertebrates. Methods Cell Bio *36*, 419-441.

Kovar, D.R., Wu, J.Q., and Pollard, T.D. (2005). Profilin-mediated competition between capping protein and formin Cdc12p during cytokinesis in fission yeast. Mol Biol Cell *16*, 2313-2324.

Kovar, D.R., Harris, E.S., Mahaffy, R., Higgs, H.N., and Pollard, T.D. (2006). Control of the assembly of ATP- and ADP-actin by formins and profilin. Cell *124*, 423-435.

Kwiatkowski, D.J., Janmey, P.A., and Yin, H.L. (1989). Identification of critical functional and regulatory domains in gelsolin. J Cell Biol *108*, 1717-1726.

Lai, S.L., Chan, T.H., Lin, M.J., Huang, W.P., Lou, S.W., and Lee, S.J. (2008). Diaphanous-related formin 2 and profilin I are required for gastrulation cell movements. PLoS One *3*, e3439.

Lancaster, O.M., and Baum, B. (2014). Shaping up to divide: Coordinating actin and microtubule cytoskeletal remodelling during mitosis. Semin Cell Dev Biol.

Leader, B., Lim, H., Carabatsos, M.J., Harrington, A., Ecsedy, J., Pellman, D., Maas, R., and Leder, P. (2002). Formin-2, polyploidy, hypofertility and positioning of the meiotic spindle in mouse oocytes. Nat Cell Biol *4*, 921-928.

Lee, L., Klee, S.K., Evangelista, M., Boone, C., and Pellman, D. (1999). Control of mitotic spindle position by the Saccharomyces cerevisiae formin Bni1p. J Cell Biol *144*, 947-961.

Lee, S.H., and Dominguez, R. (2010). Regulation of actin cytoskeleton dynamics in cells. Mol Cells *29*, 311-325.

Lew, D.J. (2002). Formin' actin filament bundles. Nat Cell Biol *4*, E29-30.

Lohka, M.J., and Maller, J.L. (1985). Induction of nuclear envelope breakdown, chromosome condensation, and spindle formation in cell-free extracts. J Cell Biol *101*, 518-523.

Lund, E., Sheets, M.D., Imboden, S.B., and Dahlberg, J.E. (2011). Limiting Ago protein restricts RNAi and microRNA biogenesis during early development in Xenopus laevis. Genes Dev *25*, 1121-1131.

Mandato, C.A., and Bement, W.M. (2003a). Actomyosin transports microtubules and microtubules control actomyosin recruitment during Xenopus oocyte wound healing. Curr Biol *13*, 1096-1105.

Mandato, C.A., and Bement, W.M. (2003b). Actomyosin transports microtubules and microtubules control actomyosin recruitment during Xenopus oocyte wound healing. Curr Biol *13*, 1096-1105.

Mandato, C.A., Weber, K.L., Zandy, A.J., Keating, T.J., and Bement, W.M. (2001). Xenopus egg extracts as a model system for analysis of microtubule, actin filament, and intermediate filament interactions. Methods Mol Biol *161*, 229-239.

Mitsushima, M., Aoki, K., Ebisuya, M., Matsumura, S., Yamamoto, T., Matsuda, M., Toyoshima, F., and Nishida, E. (2010). Revolving movement of a dynamic cluster of actin filaments during mitosis. J Cell Biol *191*, 453-462.

Mogilner, A., and Keren, K. (2009). The shape of motile cells. Curr Biol *19*, R762-771.

Nolen, B.J., Tomasevic, N., Russell, A., Pierce, D.W., Jia, Z., McCormick, C.D., Hartman, J., Sakowicz, R., and Pollard, T.D. (2009). Characterization of two classes of small molecule inhibitors of Arp2/3 complex. Nature *460*, 1031-1034.

Normoyle, K.P., and Brieher, W.M. (2012). Cyclase-associated protein (CAP) acts directly on F-actin to accelerate cofilin-mediated actin severing across the range of physiological pH. J Biol Chem *287*, 35722-35732.

Palazzo, A.F., Cook, T.A., Alberts, A.S., and Gundersen, G.G. (2001). mDia mediates Rho-regulated formation and orientation of stable microtubules. Nat Cell Biol *3*, 723-729.

Pellegrin, S., and Mellor, H. (2005). The Rho family GTPase Rif induces filopodia through mDia2. Curr Biol *15*, 129-133.

Pfender, S., Kuznetsov, V., Pleiser, S., Kerkhoff, E., and Schuh, M. (2011). Spire-type actin nucleators cooperate with Formin-2 to drive asymmetric oocyte division. Curr Biol*21*, 955-960.

Po'uha, S.T., Honore, S., Braguer, D., and Kavallaris, M. (2013). Partial depletion of gamma-actin suppresses microtubule dynamics. Cytoskeleton (Hoboken) *70*, 148-160.

Pollard, T.D. (2007). Regulation of actin filament assembly by Arp2/3 complex and formins. Annu Rev Biophys Biomol Struct *36*, 451-477.

Pollard, T.D. (2010). Mechanics of cytokinesis in eukaryotes. Curr Opin Cell Biol *22*, 50-56.

Potapova, T.A., Sivakumar, S., Flynn, J.N., Li, R., and Gorbsky, G.J. (2011). Mitotic progression becomes irreversible in prometaphase and collapses when Wee1 and Cdc25 are inhibited. Mol Biol Cell *22*, 1191-1206.

Pruyne, D., Evangelista, M., Yang, C., Bi, E., Zigmond, S., Bretscher, A., and Boone, C. (2002). Role of formins in actin assembly: nucleation and barbed-end association. Science *297*, 612-615.

Ramabhadran, V., Gurel, P.S., and Higgs, H.N. (2012). Mutations to the formin homology 2 domain of INF2 protein have unexpected effects on actin polymerization and severing. J Biol Chem *287*, 34234-34245.

Ramabhadran, V., Hatch, A.L., and Higgs, H.N. (2013). Actin monomers activate inverted formin 2 by competing with its autoinhibitory interaction. J Biol Chem *288*, 26847-26855.

Riedl, J., Crevenna, A.H., Kessenbrock, K., Yu, J.H., Neukirchen, D., Bista, M., Bradke, F., Jenne, D., Holak, T.A., Werb, Z., Sixt, M., and Wedlich-Soldner, R. (2008). Lifeact: a versatile marker to visualize F-actin. Nat Methods *5*, 605-607.

Rizvi, S.A., Neidt, E.M., Cui, J., Feiger, Z., Skau, C.T., Gardel, M.L., Kozmin, S.A., and Kovar, D.R. (2009). Identification and characterization of a small molecule inhibitor of formin-mediated actin assembly. Chem Biol *16*, 1158-1168.

Rodriguez, O.C., Schaefer, A.W., Mandato, C.A., Forscher, P., Bement, W.M., and Waterman-Storer, C.M. (2003). Conserved microtubule-actin interactions in cell movement and morphogenesis. Nat Cell Biol *5*, 599-609.

Rosenblatt, J. (2005). Spindle assembly: asters part their separate ways. Nat Cell Biol *7*, 219-222.

Sandquist, J.C., Kita, A.M., and Bement, W.M. (2011). And the dead shall rise: actin and myosin return to the spindle. Dev Cell *21*, 410-419.

Sanger, J.W. (1975). Presence of actin during chromosomal movement. Proc Natl Acad Sci U S A *72*, 2451-2455.

Schaefer, A.W., Kabir, N., and Forscher, P. (2002a). Filopodia and actin arcs guide the assembly and transport of two populations of microtubules with unique dynamic parameters in neuronal growth cones. J Cell Biol *158*, 139-152.

Schaefer, A.W., Kabir, N., and Forscher, P. (2002b). Filopodia and actin arcs guide the assembly and transport of two populations of microtubules with unique dynamic parameters in neuronal growth cones. J Cell Biol *158*, 139-152.

Schirenbeck, A., Bretschneider, T., Arasada, R., Schleicher, M., and Faix, J. (2005). The Diaphanous-related formin dDia2 is required for the formation and maintenance of filopodia. Nat Cell Biol *7*, 619-625.

Schloss, J.A., Milsted, A., and Goldman, R.D. (1977). Myosin subfragment binding for the localization of actin-like microfilaments in cultured cells. A light and electron microscope study. J Cell Biol *74*, 794-815.

Schuh, M., and Ellenberg, J. (2008). A new model for asymmetric spindle positioning in mouse oocytes. Curr Biol *18*, 1986-1992.

Schönichen, A., and Geyer, M. (2010). Fifteen formins for an actin filament: a molecular view on the regulation of human formins. Biochim Biophys Acta *1803*, 152-163.

Scrittori, L., Skoufias, D.A., Hans, F., Gerson, V., Sassone-Corsi, P., Dimitrov, S., and Margolis, R.L. (2005). A small C-terminal sequence of Aurora B is responsible for localization and function. Mol Biol Cell *16*, 292-305.

Seagull, R.W., Falconer, M.M., and Weerdenburg, C.A. (1987). Microfilaments: dynamic arrays in higher plant cells. J Cell Biol *104*, 995-1004.

Severson, A.F., Baillie, D.L., and Bowerman, B. (2002). A Formin Homology protein and a profilin are required for cytokinesis and Arp2/3-independent assembly of cortical microfilaments in C. elegans. Curr Biol *12*, 2066-2075.

Sonnemann, K.J., Fitzsimons D., Patel J.R., Liu Y., Schneider M.F., Moss R.L., Ervasti J.M. (2006). Cytoplasmic gamma-actin is not required for skeletal muscle development but its absence leads to a progressive myopathy. Dev Cell *11*, 387-397.

Sonnemann, K.J., and Bement, W.M. (2011). Wound repair: toward understanding and integration of single-cell and multicellular wound responses. Annu Rev Cell Dev Biol*27*, 237-263.

Sun, H., Schlondorff, J., Higgs, H.N., and Pollak, M.R. (2013). Inverted formin 2 regulates actin dynamics by antagonizing Rho/diaphanous-related formin signaling. J Am Soc Nephrol *24*, 917-929.

Sun, H., Schlondorff, J.S., Brown, E.J., Higgs, H.N., and Pollak, M.R. (2011a). Rho activation of mDia formins is modulated by an interaction with inverted formin 2 (INF2). Proc Natl Acad Sci U S A *108*, 2933-2938.

Sun, S.C., Wang, Z.B., Xu, Y.N., Lee, S.E., Cui, X.S., and Kim, N.H. (2011b). Arp2/3 complex regulates asymmetric division and cytokinesis in mouse oocytes. PLoS One*6*, e18392.

Thurston, S.F., Kulacz, W.A., Shaikh, S., Lee, J.M., and Copeland, J.W. (2012). The ability to induce microtubule acetylation is a general feature of formin proteins. PLoS One *7*, e48041.

Vandekerckhove, J., and Weber, K. (1978). At least six different actins are expressed in a higher mammal: an analysis based on the amino acid sequence of the amino-terminal tryptic peptide. J Mol Biol *126*, 783-802.

von Dassow, G., Verbrugghe, K.J., Miller, A.L., Sider, J.R., and Bement, W.M. (2009). Action at a distance during cytokinesis. J Cell Biol *187*, 831-845.

Wang, F., An, G.Y., Zhang, Y., Liu, H.L., Cui, X.S., Kim, N.H., and Sun, S.C. (2014). Arp2/3 complex inhibition prevents meiotic maturation in porcine oocytes. PLoS One*9*, e87700.

Watanabe, S., Ando, Y., Yasuda, S., Hosoya, H., Watanabe, N., Ishizaki, T., and Narumiya, S. (2008). mDia2 induces the actin scaffold for the contractile ring and stabilizes its position during cytokinesis in NIH 3T3 cells. Mol Biol Cell *19*, 2328-2338.

Waterman-Storer, C., Duey, D.Y., Weber, K.L., Keech, J., Cheney, R.E., Salmon, E.D., and Bement, W.M. (2000). Microtubules remodel actomyosin networks in Xenopus egg extracts via two mechanisms of F-actin transport. J Cell Biol *150*, 361-376.

Weber, K.L., and Bement, W.M. (2002). F-actin serves as a template for cytokeratin organization in cell free extracts. J Cell Sci *115*, 1373-1382.

Weber, K.L., Sokac, A.M., Berg, J.S., Cheney, R.E., and Bement, W.M. (2004). A microtubule-binding myosin required for nuclear anchoring and spindle assembly. Nature*431*, 325-329.

Woolner, S., O'Brien, L.L., Wiese, C., and Bement, W.M. (2008). Myosin-10 and actin filaments are essential for mitotic spindle function. J Cell Biol *182*, 77-88.

Wu, C., Asokan, S.B., Berginski, M.E., Haynes, E.M., Sharpless, N.E., Griffith, J.D., Gomez, S.M., and Bear, J.E. (2012). Arp2/3 is critical for lamellipodia and response to extracellular matrix cues but is dispensable for chemotaxis. Cell *148*, 973-987.

Wu, J.Q., and Pollard, T.D. (2005). Counting cytokinesis proteins globally and locally in fission yeast. Science *310*, 310-314.

Yasuda, H., Kanda, K., Koiwa, H., Suenaga, K., Kidou, S., and Ejiri, S. (2005). Localization of actin filaments on mitotic apparatus in tobacco BY-2 cells. Planta *222*, 118-129.

Yu, M., Yuan, M., and Ren, H. (2006). Visualization of actin cytoskeletal dynamics during the cell cycle in tobacco (Nicotiana tabacum L. cv Bright Yellow) cells. Biol Cell*98*, 295-306.

Zigmond, S.H., Evangelista, M., Boone, C., Yang, C., Dar, A.C., Sicheri, F., Forkey, J., and Pring, M. (2003). Formin leaky cap allows elongation in the presence of tight capping proteins. Curr Biol *13*, 1820-1823.